IMT School for Advanced Studies, Lucca

Lucca, Italy

Dynamic homogenization of composite viscoelastic materials

PhD in Institutions, Markets and Technologies
Curriculum in Computer Science and Systems Engineering

XXXI Cycle

By

Rosaria Del Toro

2018

The dissertation of Rosaria Del Toro is approved.

Program Coordinator: Prof. Rocco De Nicola, IMT Lucca

Supervisor: Prof. Marco Paggi, IMT Lucca

Supervisor: Prof. Andrea Bacigalupo, IMT Lucca

Tutor: ,

The dissertation of Rosaria Del Toro has been reviewed by:

Prof. Fabrizio Scarpa, University of Bristol

Prof, Samuel Forest, Centre des matériaux de Mines ParisTech

IMT School for Advanced Studies, Lucca

2018

Contents

List of Figures

Vita

December 13, 1990	Born, Piedimonte Matese, Italy
2015	Master Degree in Mathematics
2012	Bachelor Degree in Mathematics

Publications

R. Del Toro, A. Bacigalupo, M. Paggi (2018) Dynamic asymptotic homogenization for periodic viscoelastic materials, submitted.

Presentations

R. Del Toro, A. Bacigalupo, M. Paggi (2018) A variational-asymptotic homogenization model for the characterization of viscoelastic materials with periodic microstructure, Proc. GIMC-GM, September 13-14, 2018, Ferrara, Italy.

Abstract

A non-local dynamic homogenization technique for the analysis of a viscoelastic heterogeneous material which displays a periodic microstructure is herein proposed. The asymptotic expansion of the micro-displacement field in the transformed Laplace domain allows obtaining, from the expression of the micro-scale field equations, a set of recursive differential problems defined over the periodic unit cell. Consequently, the cell problems are derived in terms of perturbation functions depending on the geometrical and physical-mechanical properties of the material and its microstructural heterogeneities. A down-scaling relation is formulated in a consistent form, which correlates the microscopic to the macroscopic transformed displacement field and its gradients through the perturbation functions. Average field equations of infinite order are determined by substituting the down-scale relation into the micro-field equation. Based on a variational approach, the macroscopic field equations of a non-local continuum is delivered and the local and non-local overall constitutive and inertial tensors of the homogenized continuum are determined. The problem of wave propagation in case of a bi-phase layered material with orthotropic phases and axis of orthotropy parallel to the direction of layers is investigated as an example. In such a case, the local and non-local overall constitutive and inertial tensors are determined analytically and the dispersion curves obtained from the non-local homogenized model are analysed.

Chapter 1

Introduction

In this Chapter a detailed description of the thesis contents is presented. The role of viscoelastic composites in industry is analysed and particular remark is then given to the viscoelastic relation and its historical development. Finally the homogenization theory is introduced.

1.1 Structure of the thesis and motivations

In the present thesis, a dynamic asymptotic-variational homogenization method applied to a viscoelastic material with a periodic microstructure is proposed.
In Chapter 2, the field equations at the micro-scale, which describe the heterogeneous viscoelastic material, are determined in the time domain and converted into the Laplace domain, with the help of the two-sided Laplace transform. The micro-displacement field is written in terms of an asymptotic expansion in the transformed Laplace domain and its substitution into the field equations produce a sequence of recursive differential problems defined over the periodic unit cell. Then, solvability conditions are imposed to such nonhomogeneous recursive cell problems to determine the down-scaling relation, linking the microscopic transformed displacement field to the macroscopic one and its gradients through the perturbation functions. Such functions rely on the geomet-

rical and physical-mechanical properties of the material and measure the microstructural heterogeneities. Average field equations of infinite order are determined by substituting the down-scale relation into the micro-field equation. The formal solution is provided with the help of an asymptotic expansion of the transformed macro-displacement. Then the overall constitutive tensors and the overall inertial tensor related to the homogenized continuum are derived in the Laplace domain for the class of periodic viscoelastic materials, after introducing the energy-like functional in the Laplace domain. Finally, the Euler-Lagrangian differential equation at the macro-scale is determined and expressed in terms of the transformed macro-displacement and its gradients up to the fourth order.

In Chapter 3, the variational-asymptotic homogenization technique is applied to a bi-phase layered material with isotropic phases subject to periodic body forces. The solution of the homogenized problem is compared with the one established from the heterogeneous problem to verify the reliability of the proposed homogenization procedure. Finally, the problem of wave propagation and the related dispersion curves are studied. Concluding remarks complete the thesis. Viscoelastic materials can be combined with other materials to produce performing structures that are mostly employed in the aircraft sector, Fig. 1, [1]

[1] E. Cocchieri Botelho, R.A. Silva, L.C. Pardini, M.C. Rezende. A review on the development and properties of continuous fiber/epoxy/aluminum hybrid composites for aircraft structures. Mat. Res. vol.9 no.3, (2006).

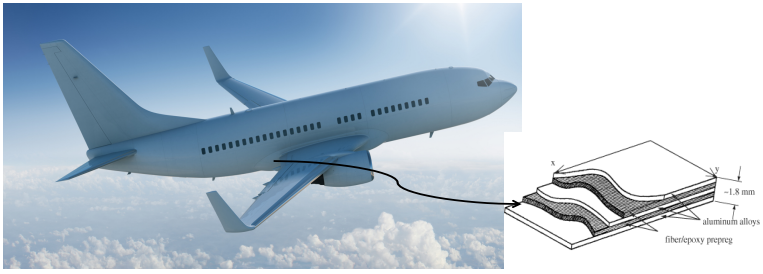

Figure 1: glare structure picked from the lower part of an airplane.

1.2 State of the art

1.2.1 Composite materials and their applications

Over the last few years, the technological progress encouraged a fast development of *composite materials*, stemming from the assemblage of two or more materials. Composites play a crucial role for various applications in civil, naval, aerospace and mechanical engineering, since they boast remarkable mechanical and physico-chemical properties even more challenging than their individual components, such as high strength, corrosion and thermal resistance, enhanced durability, light weight and ease handling. Composites usually consist of a *matrix* and a *reinforcement*. According to the type of the reiforcement, composites can be modelled as laminates (layered media), particulates or fibre reinforced. Laminates are made of plates which are sandwiched together and each plate can be a composite itself, Fig. 2, [2] Particulates consist of a host material in which small inclusions are incorporated, Fig. 3, [3]. Fibre reinforced composites include a matrix endowed with fibers, which influence the direction of the composite, Fig. 4.
Among them, the class of polymer matrix composites is very promising since they can achieve performances superior to metals with a reduced

[2]Mechanics of composite materials lab, Tel Aviv University.
[3]Scienza e Ingegneria dei Materiali: una Introduzione, Edises Napoli, 2008, p. 582.

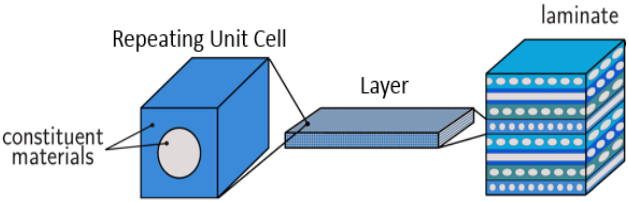

Figure 2: laminate composite.

weight. The matrix is usually a resin (epoxy or polyester) with high toughness, reinforced by fibers (glass, aramid, boron, etc.) which have very high strength. The combination of the two materials is very effective: the matrix diffuses the load among the fibers and protects them from abrasion, fracture, and damage. At the same time, the reinforcing fibres increase the overall strength and stiffness of the composite. Similarly, in laminates, the polymeric matrix is used to bond other materials together and increase the toughness of the composite, see e.g. photovoltaic modules, Paggi et al. (2016). To reduce the cost of synthetic fiber-reinforced composites and produce environmentally sustainable materials, bio-fibre-reinforced polymer composites, Dhakal et al. (2018), are very promising and are becoming increasing popular in emergent countries. The variant of hybrid composites, where synthetic and natural fiber reinforcements are mixed together offer also a possible trade-off solution. The material is said to be a composite with periodic or quasi-periodic microstructure if the heterogeneities of the reinforcement are sufficiently regular. The constitutive response of polymeric composites and their variants is that of viscoelastic materials, which exhibit creep and stress relaxation phenomena.

An intense knowledge of the behaviour of viscoelastic materials allows manufacturing devices and machinary, which can be applied to a wide range of fields, including biomedical, industrial, defence and construction. For example, graphite/epoxy composites are broadly used for space vehicles and structures thanks to their different advantages such as reduced weight, better control of thermal distortions and enhanced structural stiffness.

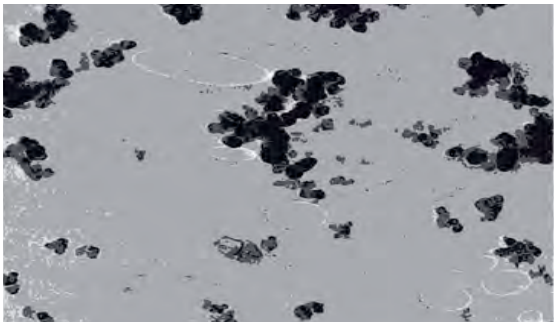

Figure 3: composite with black carbon particles.

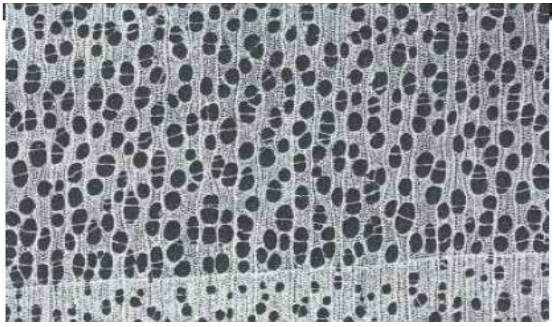

Figure 4: composite made of cellulose fibres and resinous matrix.

1.2.2 Viscoelastic relation

Historically the behaviour of viscoelastic materials has been analyzed by combining properly springs and dashpots.

Voight-Kelvin model

Among the classical models for viscoelasticity, (Skrzypek and Ganczarski (2015)), one of the most remarkable is the the *Voight-Kelvin* model, which is characterized by a linear spring element and a linear dashpot element connected in parallel, Fig. 5-(a), where the spring represents the elastic solid behavior and the dashpot describes the fluid behavior. The total stress applied to the model is subdivided into the stress applied to the spring, σ_s, and the stress applied to the dashpot ,σ_d, as

$$\sigma(t) = \sigma_s(t) + \sigma_d(t). \tag{1.1}$$

If the model undergoes a stress $\sigma(t)$, the spring and the dashpot deform by an equal amount since they are connected in parallel. Thus, the total strain $\varepsilon(t)$ is equal to the strain related to the spring ε_s and the strain related to the dashpot ε_d i.e., $\varepsilon(t) = \varepsilon_s(t) = \varepsilon_d(t)$. The stress-strain relationship for the spring and the stress-strain rate relationship for the dashpot are written as

$$\sigma_s(t) = E\varepsilon_s(t) \quad \sigma_d(t) = \eta\dot{\varepsilon}_d(t), \tag{1.2}$$

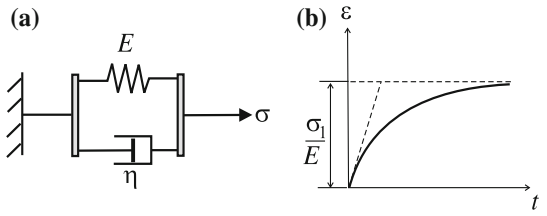

Figure 5: (a) Voigt-Kelvin model–(b) creep strain at constant stress input

where E is the spring stiffness and η is the viscosity of the material. Replacing relations (1.2) into Eq. (1.1) leads to

$$\sigma(t) = E\varepsilon_s(t) + \eta\dot{\varepsilon}_d(t). \tag{1.3}$$

Since $\varepsilon(t) = \varepsilon_s(t) = \varepsilon_d(t)$, it results

$$\sigma(t) = E\varepsilon(t) + \eta\dot{\varepsilon}(t), \tag{1.4}$$

which can be rewritten as

$$\frac{\sigma(t)}{\eta} = \frac{E}{\eta}\varepsilon(t) + \dot{\varepsilon}(t). \tag{1.5}$$

The Voight-Kelvin model is a two-parameter (E and η) viscoelastic model, described by Eq. (1.5), which links stress to strain. If a constant stress $\sigma = \sigma_1 = cost$, ($\dot{\sigma} = 0$), is applied to the model, the nonhomogeneous differential equation is retrieved

$$\frac{\sigma_1}{\eta} = \frac{E}{\eta}\varepsilon(t) + \dot{\varepsilon}(t). \tag{1.6}$$

The homogeneous equation of Eq. (1.6) is an equation of separate variables

$$\frac{\dot{\varepsilon}}{\varepsilon} = -\frac{E}{\eta}, \tag{1.7}$$

whose general integral is

$$\varepsilon(t) = CR(t)e^{\left(-\frac{E}{\eta}t\right)}. \tag{1.8}$$

By performing the variation of integration constant $CR(t)$ with initial condition $\varepsilon(0) = 0$, the solution of Eq. (1.6) is

$$\varepsilon(t) = \frac{\sigma_1}{E}\left[1 - e^{\left(-\frac{E}{\eta}t\right)}\right] \tag{1.9}$$

or

$$\varepsilon(t) = \sigma_1 CR(t), \quad CR(t) = \frac{1}{E}\left[1 - e^{\left(-\frac{E}{\eta}t\right)}\right]. \tag{1.10}$$

Function $CR(t)$ is the creep function of the Voight-Kelvin model, which identifies the response to the unitary stress σ_1. The Voight-Kelvin model does not take into account the instantaneous elasticity and so $CR(0) = 0$, Fig. 5-(b). If the model undergoes a stress $\sigma(t)$, the variation of Eq. (1.8) leads to

$$\dot{CR}(t) = \frac{1}{\eta} e^{\left(\frac{E}{\eta}t\right)} \sigma(t), \tag{1.11}$$

whose general intergral is expressed as

$$\dot{CR}(t) = CR_1 + \frac{1}{\eta} \int_0^t e^{\left(\frac{E}{\eta}\xi\right)} \sigma(\xi) d\xi. \tag{1.12}$$

Replacing Eq. (1.12) in Eq. (1.8), with initial condition $\varepsilon(0) = 0$, leads to $CR_1 = 0$ such that the solition for $\varepsilon(t)$ is

$$\varepsilon(t) = \frac{1}{\eta} e^{\left(-\frac{E}{\eta}t\right)} \int_0^t e^{\left(\frac{E}{\eta}\xi\right)} \sigma(\xi) d\xi =$$

$$= \frac{1}{\eta} \int_0^t e^{\left(-\frac{E}{\eta}(t-\xi)\right)} \sigma(\xi) d\xi. \tag{1.13}$$

The intergation by parts applied to Eq. (1.13) yields to the integral representation of the Voight-Kelvin model

$$\varepsilon(t) = \frac{\sigma(t)}{E} - \frac{1}{E} \int_0^t e^{\left(-\frac{E}{\eta}(t-\xi)\right)} \dot{\sigma}(\xi) d\xi. \tag{1.14}$$

Similarly, if the Voight-Kelvin model is subjected to a constant strain ε_1 at $t = 0$ from the initial stress level $\sigma_1 = E\varepsilon_1$, the model does not present a stress relaxation effect. In this particular case, the application of the constant strain input, ε_1, at $t = 0$, can be accomplished with an infinite initial stress response $\sigma(0) \to \infty$, such that

$$\sigma(t) = \eta\varepsilon_1 \delta(t) + E\varepsilon_1 H(t), \tag{1.15}$$

where $H(t)$ is the Heaviside unit function, describing the constant stress in the spring, followed by the infinite stress input in dashpot governed

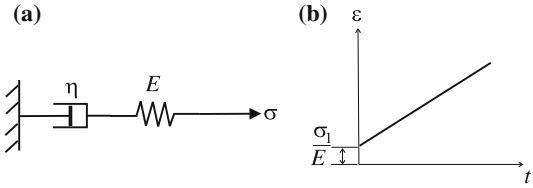

Figure 6: (a) Maxwell mechanical model–(b) creep curve under constant loading

by the δ-Dirac function. The ralaxation function in the Voight-Kelvin model is

$$G(t) = E\Big(1 + \frac{\eta}{E}\delta(t)\Big), \tag{1.16}$$

which is the response to the imposed unitary strain ε_1.

Maxwell model

The *Maxwell* model is represented by a linear elastic spring connected with a linear viscous dashpot element in series, Fig. 6-(a). If the model undergoes a stress $\sigma(t)$, which is equally applied on the spring and on the dashpot ($\sigma(t) = \sigma_s(t) = \sigma_d(t)$), the deriving strain $\varepsilon(t)$ is decomposed as $\varepsilon(t) = \varepsilon_s(t) + \varepsilon_d(t)$. By following a procedure similar to the Voight-Kelvin model, the viscoelastic behaviour is described by the following equation

$$\dot{\varepsilon}(t) = \frac{\dot{\sigma}(t)}{E} + \frac{\sigma(t)}{\eta}, \quad or \quad \sigma(t) + \frac{\eta}{E}\dot{\sigma}(t) = \eta\dot{\varepsilon}(t). \tag{1.17}$$

By performing an integration of Eq. (1.17) with $\sigma = \sigma_1 = const$, ($\dot{\sigma} = 0$), and imposing the initial condition $\varepsilon(0) = \frac{\sigma_1}{E}$, it results

$$\varepsilon(t) = \sigma_1\Big(\frac{1}{E} + \frac{1}{\eta}t\Big), \tag{1.18}$$

where the creep function for the Maxwell model is determined as

$$\varepsilon(t) = \sigma_1 CR(t), \quad CR(t) = \Big(\frac{1}{E} + \frac{1}{\eta}t\Big). \tag{1.19}$$

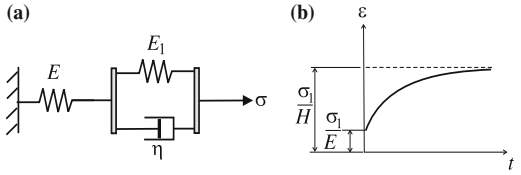

Figure 7: (a) standard model–(b) creep at constant stress input with instantaneous elastic strain built-in

If the Maxwell model undergoes a constant strain ε_1, the stress relaxation from the initial stress level $\sigma_1 = E\varepsilon_1$ at $t = 0$ to $t \to \infty$ is modelled as

$$\sigma(t) = \sigma_1 e^{\left(-\frac{Et}{\eta}\right)}, \tag{1.20}$$

where the rate of stress decrease changes from the initial $\dot{\sigma}(0) = \frac{\sigma_1 E}{\eta}$ to $\dot{\sigma}(\infty) = 0$. From Eq. (1.20), the relaxation function is $G(t) = Ee^{-\frac{E}{\eta}t}$.

Standard model

The Voight-Kelvin and the Maxwell models herein described are very intuitive, although they show strong limitations. The Voigt-Kelvin model is not able to describe the instantaneous elastic strain effect, whereas the linear creep function at constant stress input related to the Maxwell model does not confirm the experimental tests. Thus, as alternative the three-parameter *standard model* is proposed. Such a model consists of a spring element (E) and a Voight-Kelvin element (E_1, η) connected in series as depicted in Fig. 7-(a). The differential equation of the standard model is

$$\frac{\eta E}{E_1 + E}\dot{\varepsilon}(t) + \frac{E_1 E}{E_1 + E}\varepsilon(t) = \sigma(t) + \frac{\eta}{E_1 + E}\dot{\sigma}(t). \tag{1.21}$$

When a step function $\sigma = \sigma_1 = const$, ($\dot{\sigma} = 0$), is applied to the model and Eq. (1.21) is integrated with the initial condition $\varepsilon(0) = \frac{\sigma_1}{E}$, it results

$$\varepsilon(t) = \frac{\sigma_1}{E}\left[\left(1 + \frac{E}{E_1}\right) - \frac{E}{E_1}e^{\left(-\frac{E_1}{\eta}t\right)}\right], \tag{1.22}$$

where the creep function corresponding with the standard model is

$$\varepsilon(t) = \sigma_1 CR(t), \quad CR(t) = \frac{1}{E}\Big[\Big(1 + \frac{E}{E_1}\Big) - \frac{E}{E_1} e^{\Big(-\frac{E_1}{\eta}t\Big)}\Big]. \tag{1.23}$$

In Fig. 7-(b), it is represented the horizontal asymptote of $\varepsilon(t)$ curve, where the definition $\frac{1}{H} = \frac{1}{E} + \frac{1}{E_1}$ is employed. If the standard model undergoes a constant strain at $t = 0$, the stress continuously decreases from the initial level $E\varepsilon_1$ to the asymptotically approached value $H\varepsilon_1(t \to \infty)$, such that stress relaxation function of the standard model is

$$\sigma(t) = E\varepsilon_1\Big[\frac{H(t)}{E} + \Big(1 - \frac{H(t)}{E}\Big)e^{-\frac{t}{n}}\Big)\Big], \tag{1.24}$$

where $n = \frac{\eta}{E+E_1}$ and so the relaxation function is

$$G(t) = E\Big(\frac{E_1}{E+E_1} + \frac{E_1}{E+E_1} e^{-\frac{E+E_1}{\eta}}\Big). \tag{1.25}$$

Burgers model

The standard model has an horizontal asymptote (strain stabilization) for $t \to \infty$ which usually is not observed in the experiments, indeed creep strain shows an infinite increase with time. Therefore, the *Burgers model* is introduced to define such a behaviour. The model is made of the Maxwell element, (E_1, η_1), and the Voigt-Kelvin element, (E_2, η_2), connected in series, as represented in Fig. 8. The differential constitutive equation of Burgers model is written as

$$\frac{\eta_1\eta_2}{E_2}\ddot{\varepsilon}(t) + \eta_1\dot{\varepsilon}(t) = \frac{\eta_1\eta_2}{E_1E_2}\ddot{\varepsilon}(t) + \Big(\frac{\eta_1}{E_1} + \frac{\eta_1}{E_2} + \frac{\eta_2}{E_2}\Big)\dot{\sigma}(t) + \sigma(t). \tag{1.26}$$

Eq. (1.26) is a second-order linear differential equation in terms of strain and stress with constant coefficients, since it depends on the Young's moduli E_1, E_2 and the viscosity parameters η_1 and η_2. By applying a step stress input at $t = 0$ to the Burgers model, the integration of Eq. (1.26), with initial conditions $\varepsilon(0) = \frac{\sigma_1}{E}$ and $\dot{\varepsilon}(0) = \frac{\sigma_1}{\eta_1} + \frac{\sigma_1}{\eta_2}$, implies

$$\varepsilon(t) = \frac{\sigma_1}{E_1}\Big(1 + \frac{E_2}{\eta_1}t + \frac{E_1}{E_1}\Big[1 - e^{\frac{-E_2}{\eta_2}t}\Big]\Big), \tag{1.27}$$

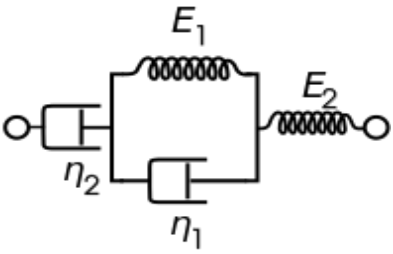

Figure 8: Burgers model

where the creep function referred to the Burgers model model is

$$\varepsilon(t) = \sigma_1 CR(t), \quad CR(t) = \frac{1}{E_1}\Big(1 + \frac{E_2}{\eta_1}t + \frac{E_1}{E_1}\Big[1 - e^{\frac{-E_2}{\eta_2}t}\Big]\Big). \tag{1.28}$$

The Boltzmann superposition principle
Let $\varepsilon(t)$ be a shear strain acting on a given material and let $\sigma(t)$ be the effect deriving from this cause. Thus, a variation in the shear strain at time t_1 produces an effect occurring at some time $t > t_1$, which can be written as (Martinez-Boza et al. (2001)):

$$\sigma(t) = G(t - t_1)\delta\sigma(t_1), \tag{1.29}$$

where $G(t-t_1)$ is the relaxation function which is a decreasing function of $(t - t_1)$. To compute the stress produced by a strain, occurring at time t_2, the incremental response of the material to the second strain is supposed to be independent on the previous one and so it results

$$\sigma(t) = G(t - t_1)\delta\sigma(t_1) + G(t - t_2)\delta\sigma(t_2). \tag{1.30}$$

In case of a series of N changes in the shear strain, taking place at a different time t_i, the cumulative stress is fromulated as

$$\sigma(t) = \sum_{i=1}^{N} G(t - t_i)\delta\varepsilon_i. \tag{1.31}$$

If the change in strain takes place continuously, the integral may raplace the sum as

$$\sigma(t) = \int_{-\infty}^{t} G(t-\tau) d\varepsilon(\tau), \tag{1.32}$$

which can be reformulated as

$$\sigma(t) = \int_{-\infty}^{t} G(t-\tau) \dot{\varepsilon}(\tau) d\tau. \tag{1.33}$$

The lower limit infers that all the strains that have taken place in the past will contribute to the effect at the current time t. The Eq. (1.33) will be used in the Chapter 2 for a 3-D case. An analogous procedure can be performed to obtain the stress in terms of the strain and the creep function,

$$\varepsilon(t) = \int_{-\infty}^{t} CR(t-\tau) \dot{\sigma}(\tau) d\tau. \tag{1.34}$$

The limitation of the classical models is due to the fact that, to obtain an acceptable approximation level, they could become too difficult to manage. The fractional derivative model allows greater flexibility, since the derivation order can vary to obtain a constitutive law suitable for the material. In the elastic solids, the stress is proportional to the zero-order derivative of the strain, whereas for the liquids the stress is proportional to the first derivative ot the strain. Thus, it is clear to suppose that for the viscoelastic materials the stress is proportional to the derivative of real order of the strain. This hypothesis led to the design of a mathematical model called Spring-Pot, whose schematic representation is shown in Fig. 9. By manipulating the kernel of Eq. (1.33) and by recalling the definition of the Caputo derivative, (Lakshmikantham et al. (2009)), of order n of a function $f(t)$, $\quad D_t^{\alpha} f(t) = \frac{1}{\Gamma(n-\alpha)} \int_{-\infty}^{t} \frac{f^n(\tau)}{(t-\tau)^{(\alpha+1-n)}} d\tau$, the governing equation of the Spring-Pot is written as

$$\sigma(t) = \frac{C_\alpha}{\Gamma(1-\alpha)} \int_{-\infty}^{t} \dot{\varepsilon}(\tau)(t-\tau)^{-\alpha} d\tau = C_\alpha D_t^{\alpha} \varepsilon(t), \quad 0 \leq \alpha \leq 1, \tag{1.35}$$

where Γ is the Gamma function and the coefficient C_α can be obtained sperimentally, (Di Paola et al.).
In Di Paola et al. (2011), it is emphasized the validity of fractional model

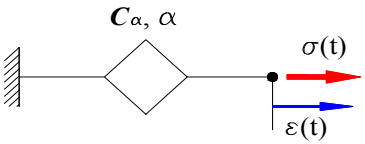

Figure 9: Spring-Pot structure.

to study viscoelastic behavior. It is proven that if relaxation test is well fitted by a power law decay, then the fractional constitutive law involving Caputo's derivative shows up. Consequently, the constitutive law is governed by a fractional differential equation. Fractional calculus is seen as an extension of the classical differential calculus and fractional operators are convolution integrals with power law kernel. There is point in observing that such a constitutive law can capture both relaxation and creep behavior just identifying only two parameters. This remark avoids the use of combining simple models as Maxwell and/or Kelvin, twhich rely on several parameters for capturing both creep and relaxation tests. Moreover, to validate the fractional model, two polymers of different chemical physical properties are tested. For each of them both relaxation and creep test are carried out, with different values of amplitudes and always the theoretical relaxation and creep functions overlap the experimental data leading to the conclusion that the fractional model can properly capture the viscoelastic behavior. In Di Paola et al. (2014), it is shown that the best fitting performed by taking or not into account the initial ramp provides very different parameters and then the constitutive law is strongly influenced by the real experimental test. It is also shown that by accounting for the effective strain (or stress) history leads to an impressive matching between experimental tests and results obtained by using Boltzmann superposition principle and power law as candidate for the best fitting procedure. As a concluding remark, it is assessed that in every experimental test the rate of the initial ramp or the time at which

the unitary (constant value of) strain (or stress) is attained must be always declared. In Ezzat et al. (2015), a simply method is introduced in the field of generalized thermo-viscoelasticity with one and two relaxation times and applied to three different problems. This method gives exact solutions in the Laplace transform domain without any assumed restrictions on either the temperature or the displacement distributions. A numerical method based on a Fourier-series expansion is used for the inversion process. The method used in the paper is applicable to a wide range of thermoelasticity problems. It can be applied to problems, which are described by the linearized Navier–Stokes equations for thermoelectric fluid, were the governing equations are coupled. Representative results for the all functions for generalized theory are distinctly different from those obtained for the coupled theory. This due to the fact that thermal waves in the coupled theory travel with an infinite speed of propagation as opposed to finite speed in the generalized case. It is clear that for small values of time the solution is localized in a finite region. This region grows with increasing time and its edge is the location of the wave front. In Colinas-Armijo et al. (2016), an approach to separate the elastic and the viscous phase in the fractional stress–strain relation is provided with the aid of an equivalent classical model (Kelvin–Voigt or Maxwell). For such equivalent model the parameters are selected by an optimization procedure. Once the parameters of the equivalent model are defined, characteristic times of fractional viscoelasticity are defined as ratio between viscosity and stiffness. In the numerical applications, three kinds of different excitations are considered, that is, harmonic, periodic, and pseudo-stochastic. It is shown that, for any periodic excitation, the equivalent models have some important features: (i) the dissipated energy per cycle at steady-state coincides with the Staverman–Schwarzl formulation of the fractional model, (ii) the elastic and the viscous coefficients of the equivalent model are strictly related to the storage and the loss modulus, respectively.

1.2.3 Homogenization models

Composites are characterized by a multiscale nature, since the size of the individual heterogenities ε is much smaller than the dimension of the entire body L i.e. $\varepsilon \leq L$. Consequently, their physical and mechanical properties can be analysed either from a macroscopic or from a microscopic standpoint. Both the approaches present several drawbacks: the macroscopic approach may not accurately capture the microscopic mechanisms and the interconnections between the various constituents. On the other side, the microscopic approach could reproduce an overwhelming quantity of information but of scarce concern. Based on the premises above, a multiscale analysis model, consisting of a synergy between the macroscopic and the microscopic approach, represents a challenging compromise to overcome the limitations of the two models.
In such a framework, the pioneering works of Maxwell, 1954; Voigt, 1889; Reuss, 1929; Rayleigh, 1871; and Einstein, 1906 envisioned the homogenization theory as a promising methodology to recognize and model the effects of the microscopic behaviour on the overall properties of materials. Furthermore, the employment of such a theory prevents the high computational costs required to tackle an heterogeneous system.
In particular, Maxwell (1954) derived the effective conductivity of a dilute particulate composite. Reuss (1929) proposed a multipole method to determine the effective electrical conductivity of a periodic array of cylinders. Rayleigh (1871) determined the effective elastic properties of a composite and Einstein (1906) found the effective viscosity of a dilute suspension of rigid spheres in a viscous fluid. Later, homogenization appoaches were devoted to problems in electrical conductivity, magnetism, electro-magnetism, thermoelasticity, porous media, fracture dynamics, fluid dynamics, as well as viscoelasticity and elasticity.
Three main classes of homogenization techniques are possible to estimate the overall static and dynamic properties of composites with periodic microstructures: the computational techniques, the asymptotic and the asymptotic-variational techniques. The basic idea of the three homogenization methods is to replace an heterogeneous material at the

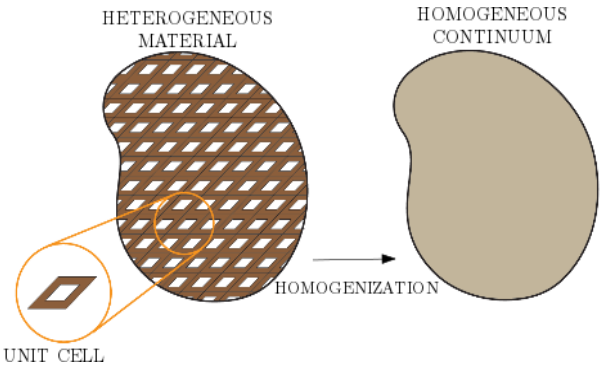

Figure 10: heterogeneous domain vs. homogeneous domain.

micro-scale with an equivalent homogenous material at the macro-scale, which can be modelled through either a *first order* (Cauchy) or a *non-local* continuum, Fig. 10, [4].

Generally, the macro-scale length stands for the dimension of the domain, whereas the micro-scale length characterizes the size of the representative volume element (RVE) or unit cell of the material, which is the smallest part of the composite containing a great number of information on the geometrical and mechanical properties at the microscopic level, Fig. 11 [5]. A first-order computational homogenization is a procedure that can be articulated in four steps (Geere et al. (2010)): (1) the RVE is isolated from the periodic domain; (2) boundary conditions at the micro-scale are provided from the macroscopic input variables and they are applied to the RVE (transition from macro to micro); (3) the macroscopic output variables are performed from the study of the deformed microstructural RVE (transition from micro to macro); (4) the (numerical)

[4] D. Bracho. Consistent Asymptotic Homogenization Method for La ice Structures Based on the Virtual Power Principle. (2016). All theses. 2546.

[5] Y.M. Shabana, N. Noda. Numerical evaluation of the thermomechanical effective properties of a functionally graded material using the homogenization method. International Journal of Solids and Structures, Vol 45, Issues 11 − 12, Pages 3494 − 3506, 2008.

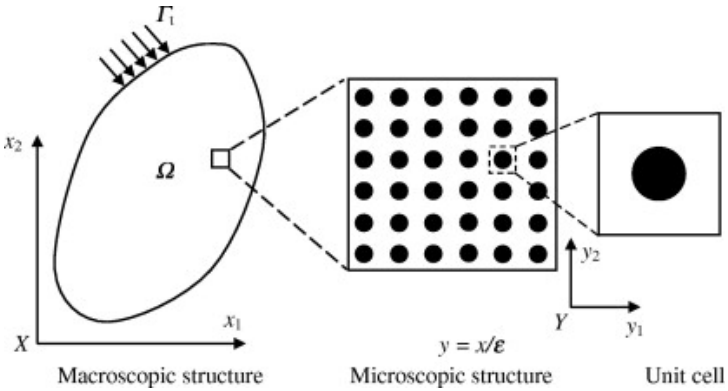

Figure 11: macroscopic, microscopic domain and unit cell.

relation between the macroscopic input and output variables are recovered.

As it is emphasized in Bacigalupo et al., 2016a; Fantoni et al., 2017; and Kouznetsova et al., 2004, a first order homogenization procedure may not take into account the size-effects and the non-local phenomena related to the micro-scale length. As a result, a first order homogenization procedure does not provide a exhaustive modelling of composites in presence of high gradients of stresses, deformations, temperature, chemical potential, heat and mass fluxes and waves dispersion. Therefore, non-local higher order homogenization techniques can be deemed as an alternative strategy. Indeed, such approaches supply constitutive relations related to an equivalent higher order continuum, embedding characteristic scale-lengths connected with the microstructural effects. The term "non-local" points out that the state of deformation at a certain point of the domain relies on the deformation in its closer points. There are three fundamental groups of non-local continua: the *multipolar*, the *micromorphic* and the *strain-gradient* continua.

Green and Rivlin (1964), proposed a continuum theory based on multipolar displacement and velocity fields subjected to multipolar body forces and surface tractions of arbitrary order. Such a theory was inspired

by a work on generalized stresses, generalized velocities, body and surface forces by Truesdell and Toupin (1960). Multipolar field variables can be found in theories concerning beams, plates and shells arising from the passage from a three-dimensional problem to a one-dimensional or a two-dimensional problem. Green and Rivlin introduced an energy balance including multipolar tractions and body forces with their work-conjugate multipolar velocities. Multipolar stresses can be derived either by applying such an energy balance to a tetrahedron or from multipolar tractions by supposing that the tractions relies linearly on the unit normal vector or on its dual. As a result, n-polar stresses are tensors of rank $n+1$. Moreover the energy balance enables to determine the local balance equations. The autors proved that an oriented domain can be seen as a special case of a multipolar continuum. Oriented domain are governed by a number of independent vectors, the so-called directors, connected to a material point of the continuum.

Eringen and Suhubu (1964), proposed a micromorphic continuum theory, which is supposed to be the most accurate top-down microscale approach. Micromorphic theory aims at predicting physical phenomena at atomic, molecular and nano level. As a consequence, a material point may have more degrees of freedom than the only three degrees of freedom in classical field theory. Despite that, the molecules that compose the internal structure of the material points withstand deformations and rotations produced by the displacements and rotations of their constituent atoms. Micromorphic theory conceives a material domain as a continuous collection of deformable particles, characterized by a proper finite size and inner structure, whereas classical continuum mechanics desccribed a material domain as a continuous collection of material points with infinitesimal size and without inner structure. In addition, Eringen considered the deformable particle as a geometric point described by some vectors, indicating the orientations and the intrinsic deformations of all the material points in the deformable particle. This is in line with the classical description where a material point in a continuum is provided with physical properties such as mass density, displacement vector, electric field, stress tensor, etc. Thus micromorphic

theory describe several physical phenomena, which otherwise cannot be described by classical field theories.
Standard continuum mechanics takes into account state functions relying only on local deformation meaures. On the other hand, strain gradient theories take place when gradients of deformation of a certain order are introduced. Non-linear elastic strain gradient continua were studied by Toupin (1964), whereas the linear elastic theory was developped by Mindlin and Eshell (1968), integrating the elastic strain energy density with the spatial gradients of the strains. By supposing that stresses and hyper-stresses are provided by the partial derivatives of the strain energy density with respect to the strains and the strain gradients, constitutive relations are obtained, whereas the Hamilton's principle provides a local equilibrium statement. Concerning with linear materials, the constitutive relations are written in terms of the elasticity tensors. In the simplest case, the stresses and the strains are associated to the fourth-order elasticity tensor, whereas hyper-stresses and strain gradients are related by a sixth-order tensor. Including the first and the second gradients of the strains, a linear second order strain gradient elasticity theory was proposed by Mindlin (1964), where sixteen material parameters are taken into account for an isotropic second order strain gradient domain. Simplified material laws were proposed by many authors, as Koiter, 1964; Kleinert, 1989; Yang et al., 2002; Aifantis, 2003; and Fleck and Hutchinson, 2001. The effective properties of two-phase composites with a linear couple-stress constitutive law for each phase have been estimated by Smyshlyaev and Fleck (1995). Such outcomes were employed to carry out the overall non-linear behaviour of the composites with a plastic strain-gradient constitutive model for the phases, (Sanchez-Palencia (1974)), and of a polycrystalline aggregate of single crystals with a strain-gradient constitutive law for each slip system. Drugan and Willis (1996), proposed a non-local effective constitutive equation for linearly elastic composites by performing the equilibrium equation with respect to stress polarization and ensemble averaging. Generally, three main classes of homogenization techniques are possible: the asymptotic techniques (Bensoussan et al., 1978; Bakhvalov

and Panasenko, 1984; Gambin and Kroner, 1989; Allaire, 1992; Meguid and Kalamkarov, 1994; Boutin, 1996; Andrianov et al., 2008; Panasenko, 2009; T.H. Tran and Bonnet, 2012; Bacigalupo, 2014), the variational-asymptotic techniques (Smyshlyaev and Cherednichenko, 2000; Smyshlyaev, 2009; Bacigalupo and Gambarotta, 2014b; Bacigalupo et al., 2014) and many identification approaches, involving the analytical (Bigoni and Drugan, 2007; Bacca et al., 2013a; Bacca et al., 2013b; Bacigalupo and Gambarotta, 2013) and the computational techniques (Forest and Sab, 1998; Kouznetsova et al., 2002; Forest, 2002; Kouznetsova et al., 2004; Kaczmarczyk et al., 2008; Yuan et al., 2008; Bacigalupo and Gambarotta, 2010; Forest and Trinh, 2011; Addessi et al., 2013; Zah and Miehe, 2013). In particular, Smyshlyaev and Cherednichenko (2000) paved the way for a combined asymptotic-variational method, based on suitable minimum functional energy. Moreover, the method guarantees the ellipticity of the higher-order homogenized equations and provides excellent approximations of the overall properties of composites.

In case of viscoelastic materials with a periodic microstructure, there are still few contributions devoted to homogenization techniques applied to this particular class of composites and three groups can be distinguished: the analytical identification techniques (Hashin, 1965; Hashin, 1970; Chen and Lakes, 1993; Masson and Zaoui, 1999; Beurthey and Zaoui, 2000; Masson et al., 2012; Meaud and Hulbert, 2013; Hoang-Duc et al., 2013); the computational techniques (Ohno et al., 2000; Haasemann and Ulbricht, 2010; Tran et al., 2011 and Q. Chen and Geng, 2017) and the asymptotic techniques (Francfort et al., 1983, Francfort and Suquet, 1986; Yi et al., 1998; Lahellec and Suquet, 2007; Suquet, 2012 and Hui and Oskay, 2013).

According to the identification analytical techniques, Hashin (1965) shows the connection between the macro- scopic elastic and viscoelastic stress-strain relations of multiphase elastic and viscoelastic media by means of the correspondence principle and some results for viscoelastic stress-strain relations of multiphase media are provided. Hashin (1970) employed the correspondence principle to derive expressions for effective com- plex moduli of viscoelastic composites. Chen and Lakes (1993) in-

vestigated the viscoelastic properties of composites to identify structures that prompt a combination of high stiffness and high loss tangent. Therefore, laminates having Voigt and Reuss structure and composite materials achieving the Hashin-Shtrikman bounds on stiffness are assessed through the correspondence principle. Masson and Zaoui (1999) analyzed a new Hill-type approach in case of rate-dependent elastoplastic heterogeneous materials. The associated linearization method reckons on an affine formulation rathen than the Hills incremental one and on the employment of the correspondence principle to derive the concentration problem. In Beurthey and Zaoui (2000), the relaxation spectra of a two-phase isotropic material whose phases are isotropic Maxwell media are analytically determined in accordance with the generalized self-consistent schemes. Such spectra show evident discrepancies that are related to the different underneath morphology, either symmetrical (polycrystal-type) or asymmetrical (composite-type). In Masson et al. (2012), an approximate self-consistent modelling is analysed to determine the effective viscoelastic response of polycrystals that shows an ageing constitutive behaviour. Meaud and Hulbert (2013) detected the effective dynamic moduli and loss factors of Reuss and Voigt composites in response to a uniaxial harmonic load. By means of the viscoelastic correspondence principle, the formulae for Reuss and Voigt composites of infinite dimensions are determined. Moreover, it is observed that the effective loss factor of a Reuss composite depends on the values of the Poisson's ratio and bulk loss factors of the constituent materials. In Hoang-Duc et al. (2013), an approximate solution for retrieving the effective behavior of linear viscoelastic heterogeneous media in the case of elastic inclusions embedded within a viscoelastic matrix is outlined. The solution in the Laplace-Carson domain is determined through the generalized self-consistent model and the simplification is determined in an explicit expression of the inverse Laplace transform.

In the context of the computational homogenization techniques, Ohno et al. (2000) dealt with an homogenization model for elastic-viscoplastic periodic materials, which allows determining the macroscopic and the microscopic stress and strain states in nonlinear time-dependent peri-

odic materials and it encompasses any problem where the history of the macro-strain and the macro-stress depends upon the time. Haasemann and Ulbricht (2010) considered a microstructure where all the constituents are linear viscoelastic. The constitutive laws at the microscale were converted into a Laplace-Carson domain, where the constitutive equations have a quite similar form to those of a linear elastic material and then a homogenization approach based on the Hill-Mandel condition was exploited. The Laplace-Carson transform associated with the application of a finite element method enables the computation of the relaxation tensor in the Laplace domain and the inverse Laplace-Carson transformation provides the material properties in the time domain. Tran et al. (2011) presented a computational homogenization method to determine the response of a linear viscoelastic heterogeneous material. The components of the relaxation tensor, which appear in the constitutive law at the macro-scale, are numerically determined in the time domain, without involving the Laplace transform. The employment of computational techniques is very attractive thanks to its simplicity, but they could not challenge dynamic problems and they could show some disadvantage in case of homogenization in micro- morphic non-local and higher-order continua (Forest and Trinh, 2011; Bacigalupo and Gambarotta, 2010a; Bacigalupo, 2014).

Concerning with the asymptotic techniques applied to viscoelastic materials, Francfort et al. (1983) developed an homogenization technique in the quasi-static framework applied to a linear viscoelastic solid. In particular, the homogenized stress field is formulated in terms of the homogenized elastic and viscous tensor components. Moreover, the expression of corresponding fourth-order kernel is derived and is proven to be symmetric and exponentially decreasing. The existence and the uniqueness of the solution related to the homogenized problem is determined by means of a fixed point method, inspired by the Cauchy-Lipschitz technique. Francfort and Suquet (1986) investigated a general theory of viscoelastic material of Kelvin-Voigt type and, in a homogenization theory framework, determined the existence and uniqueness of the solution of an initial boundary value problem in terms of displace-

ment and temperature for a bounded domain. The behavior of the displacement field is investigated when the inhomogeneities become dense in the domain. Moreover, the displacement field is found to converge (weakly) to the displacement of a body consisting of an homogeneous material which is no more of Kelvin-Voigt type but a material with fading memory. A theorem of strong convergence for the strain rate field is assessed, without any assumption on the regularity of the displacement field of the homogenized problem. This theorem allows homogenizing the mechanical dissipa- tion and finally homogenizing the energy equation. Lahellec and Suquet (2007) analyzed an approximate scheme in the time domain for deriving the effective response of linear viscoelastic composites. Suquet (2012) studied of the effective behavior of composites made of linear viscoelastic phases. Hui and Oskay (2013) proposed a second order homogenized method with multiple length scales for detecting wave propagation in a one dimensional viscoelastic composite material, by proceeding with an asymptotic expansion of the governing system of equations defined in the time domain and then recast into the Laplace domain. Srivastava and Nemat-Nasser (2014) studied the problem of reflection at the interface of a layered periodic composite and its dynamic homogenized equivalent. In particular, a two-phase composite and a three-phase composite, which exhibits negative effective properties over its second branch, is proved. Based upon the reflected energy profile of the two cases, it is observable that there are good arguments for considering the second branch of a three-phase composite as a true negative branch with negative group velocity. Through arguments of calculated reflected energy, it is observed that infinite-domain homogenization is much more applicable to finite cases of the three-phase composite than it is to the two-phase composite. In fact, the reliability of dynamic homogenization extends to most of the first branch (negligible reflection) for the three-phase composite. This is in contrast with a periodic composite without local resonance where the approximation of homogenization worsens with increasing frequency over the first branch and is demonstrably bad on the second branch. The effect of the interface location on the applicability of homogenization is also considered.

Motivated by the state-of-the-art literature on homogenization, the present study proposes a dynamic variational-asymptotic homogenization technique for the analysis of a viscoelastic material with periodic microstructure, modelled as a non-local continuum, in line with the asymptotic and variational-asymptotic methods proposed in Smyshlyaev and Cherednichenko (2000) and with the studies related to the variational principles for linear viscoelasticity in Fabrizio and Morro (1992) and Leitman (1966).

Chapter 2

Dynamic asymptotic homogenization model for periodic viscoelastic materials

In the present chapter, the asymptotic expansion of the micro- displacement field in the transformed Laplace domain allows to obtain, from the expression of the micro-scale field equations, a set of recursive differential problems defined over the periodic unit cell. Consequently, the cell problems are derived in terms of perturbation functions depending on the geometrical and physical-mechanical properties of the material and its microstructural heterogeneities. A down-scaling relation is formulated in a consistent form, which correlates the microscopic to the macroscopic transformed displacement field and its gradients through the perturbation functions. Average field equations of infinite order are determined by substituting the down-scale relation into the micro-field equation. Based on a variational approach, the macroscopic field equations of a non-local continuum are delivered and the local and non-local overall constitutive and inertial tensors of the homogenized continuum are determined. Finally, the problem of wave propagation and the re-

lated dispersion curves is studied.

2.1 Problem setting and field equation in the time domain

Let Ω be a three-dimensional viscoelastic heterogeneous material that displays a periodic microstructure. A generic point of the material is identified by the position vector $\boldsymbol{x} = x_1\boldsymbol{e}_1 + x_2\boldsymbol{e}_2 + x_3\boldsymbol{e}_3$, related to a system of coordinates with origin at point O and orthogonal base $\{\boldsymbol{e}_1, \boldsymbol{e}_2, \boldsymbol{e}_3\}$. Let $\mathcal{A} = [0, \varepsilon] \times [0, \delta\varepsilon] \times [0, \varepsilon]$ be a periodic cell with characteristic size ε. $\mathcal{A}$ is described by three orthogonal periodicity vectors $\boldsymbol{v}_1$, $\boldsymbol{v}_2$ and $\boldsymbol{v}_3$ defined as $\boldsymbol{v}_1 = d_1\boldsymbol{e}_1 = \varepsilon\boldsymbol{e}_1$, $\boldsymbol{v}_2 = d_2\boldsymbol{e}_2 = \delta\varepsilon\boldsymbol{e}_2$ and $\boldsymbol{v}_3 = d_3\boldsymbol{e}_3 = \varepsilon\boldsymbol{e}_3$. The material domain is set up by the repetition of the cell $\mathcal{A}$ in accordance with the directions of $\boldsymbol{v}_1$, $\boldsymbol{v}_2$ and $\boldsymbol{v}_3$, see Fig. 12. Since the material is $\mathcal{A}$-periodic, the micro relaxation tensor $\mathbb{G}^m(\boldsymbol{x}, t) = G^m_{ijhk}\boldsymbol{e}_i \otimes \boldsymbol{e}_j \otimes \boldsymbol{e}_h \otimes \boldsymbol{e}_k$, which depends on time and accounts for the viscoelastic effects, and the material density $\rho^m(\boldsymbol{x})$ comply with the following conditions:

$$\mathbb{G}^m(\boldsymbol{x} + \boldsymbol{v}_i, t) = \mathbb{G}^m(\boldsymbol{x}, t), \quad i = 1, 2, 3 \quad \forall \boldsymbol{x} \in \mathcal{A}, \tag{2.1}$$

$$\rho^m(\boldsymbol{x} + \boldsymbol{v}_i, t) = \rho^m(\boldsymbol{x}, t), \quad i = 1, 2, 3 \quad \forall \boldsymbol{x} \in \mathcal{A}. \tag{2.2}$$

The micro stress $\boldsymbol{\sigma}(\boldsymbol{x}, t)$ constitutive relation, which models the viscoelastic elements of the heterogeneous material, is expressed in terms of the hereditary integral, Christensen (2012):

$$\boldsymbol{\sigma}(\boldsymbol{x}, t) = \int_{-\infty}^{t} \mathbb{G}^m(\boldsymbol{x}, t - \tau)\dot{\boldsymbol{\varepsilon}}(\boldsymbol{x}, \tau)d\tau, \tag{2.3}$$

where the superscript m refers to the microscale and $\boldsymbol{\varepsilon}(\boldsymbol{x}, t) = \varepsilon_{ij}\boldsymbol{e}_i \otimes \boldsymbol{e}_j$ is the micro strain tensor. Moreover, t denotes the time coordinate and the superimposed dot indicates time derivative. The material undergoes small displacements and so the micro strain tensor is defined as $\boldsymbol{\varepsilon}(\boldsymbol{x}, t) = \frac{1}{2}(\nabla\boldsymbol{u}(\boldsymbol{x}, t) + \nabla^T\boldsymbol{u}(\boldsymbol{x}, t))$, where $\nabla\boldsymbol{u}$ is the gradient of the micro displacement $\boldsymbol{u}(\boldsymbol{x}, t)$. In the time domain, the deformation response

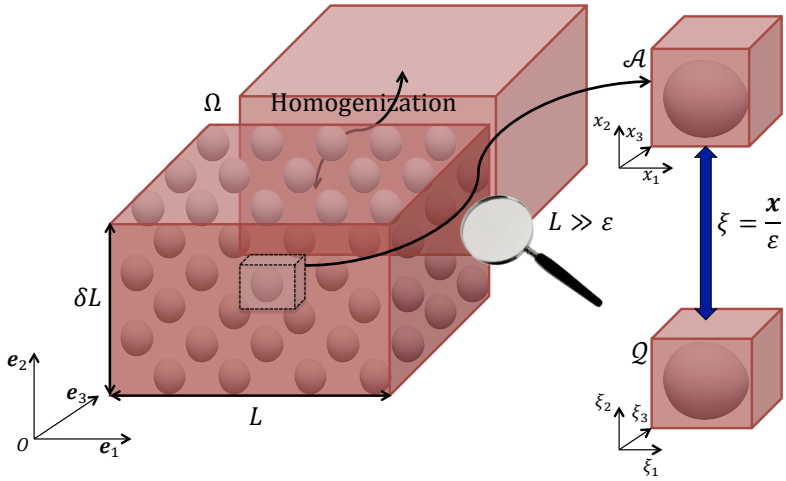

Figure 12: heterogeneous and homogeneous $3D$ domain Ω with periodic cell $\mathcal{A}$ and the corresponding nondimensional cell $\mathcal{Q}$.

of the material under dynamic loading is expressed by the momentum balance equation:

$$\nabla \cdot \boldsymbol{\sigma}(\boldsymbol{x}, t) + \boldsymbol{b}(\boldsymbol{x}, t) = \rho^m(\boldsymbol{x})\ddot{\boldsymbol{u}}(\boldsymbol{x}, t), \tag{2.4}$$

where $\boldsymbol{u}(\boldsymbol{x}, t)$ is the micro-displacement field and $\boldsymbol{b}(\boldsymbol{x}, t)$ are the body forces.

In the derivation of the theory, the heterogeneous material is supposed to be subjected to a system of $\mathcal{L}$-periodic body forces $\boldsymbol{b}(\boldsymbol{x}, t)$, with zero mean values over $\mathcal{L} = [0, L] \times [0, \delta L]$.

The structural (or macroscopic) length L is assumed to be much greater than the microstructural length ε, i.e. $L >> \varepsilon$, to allow the scales separation condition and so $\mathcal{L}$ is considered as an actual representative portion of the material. Let $\mathcal{Q} = [0, 1] \times [0, \delta]$ be the nondimensional cell reproducing the periodic microstructure. $\mathcal{Q}$ is determined by rescaling the size of the periodic cell $\mathcal{A}$ for the characteristic length ε. Accordingly, two variables are introduced to differentiate the two scales, namely the macroscopic (or slow) one, $\boldsymbol{x} \in \mathcal{A}$, which measures the slow fluctuations,

and the microscopic (or fast) variable, $\boldsymbol{\xi} = \frac{\boldsymbol{x}}{\varepsilon} \in \mathcal{Q}$, which measures the fast propagation of the signal.
Thanks to cell $\mathcal{Q}$, the properties (2.1) and (2.2) may be rewritten in terms of the microscopic variable $\boldsymbol{\xi}$ and so $\mathbb{G}^m$ and ρ^m are assumed to be $\mathcal{Q}$-periodic and defined on $\mathcal{Q}$ as

$$\mathbb{G}^m(\boldsymbol{x},t) = \mathbb{G}^m(\boldsymbol{\xi} = \boldsymbol{x}/\varepsilon, t), \quad \rho^m(\boldsymbol{x},t) = \rho^m(\boldsymbol{x}/\varepsilon, t). \tag{2.5}$$

Bearing in mind the definition of the strain tensor $\boldsymbol{\varepsilon}$, the minor simmetry of the relaxation tensor $\mathbb{G}^m$ is applied to $\dot{\boldsymbol{\varepsilon}}$ in the integral (2.3) and the substitution of Eq. (2.3) into Eq. (2.4) yields to

$$\nabla \cdot \Big[\int_{-\infty}^{t} \mathbb{G}^m\Big(\frac{\boldsymbol{x}}{\varepsilon}, t-\tau\Big) \nabla \dot{\boldsymbol{u}}(\boldsymbol{x},\tau) d\tau \Big] + \boldsymbol{b}(\boldsymbol{x},t) = \rho^m(\boldsymbol{x}) \ddot{\boldsymbol{u}}(\boldsymbol{x},t). \tag{2.6}$$

Denoting with $[[f]] = f^i(\Sigma) - f^j(\Sigma)$ the jump of the function values f at the interface Σ between two different phases i and j in the periodic cell $\mathcal{A}$, the following fully-bonded interface conditions hold

$$[[\boldsymbol{u}(\boldsymbol{x})]]|_{\boldsymbol{x}\in\Sigma} = \boldsymbol{0}, \quad \Big[\Big[\int_{-\infty}^{t} \mathbb{G}^m\Big(\frac{\boldsymbol{x}}{\varepsilon}, t-\tau\Big) \nabla \dot{\boldsymbol{u}}(\boldsymbol{x},\tau) d\tau \cdot \boldsymbol{n} \Big]\Big]\Big|_{\boldsymbol{x}\in\Sigma} = \boldsymbol{0}, \tag{2.7}$$

where $\boldsymbol{n}$ represents the outward normal to the interface Σ. Since $\mathbb{G}^m$ and ρ^m are $\mathcal{Q}$-periodic and the body forces are $\mathcal{L}$-periodic, the micro displacement depends on both the slow variable $\boldsymbol{x}$ and the fast one $\boldsymbol{\xi}$ and can be expressed as

$$\boldsymbol{u} = \boldsymbol{u}\Big(\boldsymbol{x}, \frac{\boldsymbol{x}}{\varepsilon}, t\Big).$$

2.2 Field equation in the Laplace domain

The two-sided Laplace transform of an arbitrary, real valued, time varying function, $f \in \mathbb{R}$, is defined as Paley and Wiener (1934)

$$\mathcal{L}(f(t)) = \hat{f}(s) = \int_{-\infty}^{+\infty} f(t) e^{-st} dt, \quad s \in \mathbb{C}, \tag{2.8}$$

where the Laplace argument, s, and the Laplace transform, $\hat{f}$, are complex valued (i.e. $\hat{f} : \mathbb{C} \to \mathbb{C}$). The derivative rule for the Laplace transform is provided by

$$\mathcal{L}\Big(\frac{\partial^n f(t)}{\partial t^n}\Big) = s^n \hat{f}(s), \tag{2.9}$$

and the convolution rule of f_1 and f_2 is given as

$$\mathcal{L}(f_1(t) * f_2(t)) = \mathcal{L}(f_1(t))\mathcal{L}(f_2(t)), \tag{2.10}$$

Equation (2.6) governing the periodic viscoelastic material in the time domain will be recast in the Laplace domain employing the Laplace transform (2.8), the convolution rule (2.10) and the derivative rule (2.9). Therefore, in the Laplace domain, it results

$$\nabla\cdot\Big[\mathcal{L}\Big(\mathbb{G}^m\Big(\frac{\boldsymbol{x}}{\varepsilon},t\Big)\Big)\mathcal{L}\Big(\nabla\dot{u}\Big(\frac{\boldsymbol{x}}{\varepsilon},\boldsymbol{x},t\Big)\Big)\Big]+\mathcal{L}(\boldsymbol{b}(\boldsymbol{x},t)) = \rho^m\Big(\frac{\boldsymbol{x}}{\varepsilon}\Big)\mathcal{L}\Big(\ddot{\boldsymbol{u}}\Big(\frac{\boldsymbol{x}}{\varepsilon},\boldsymbol{x},t\Big)\Big)$$

or, in other terms:

$$\nabla\cdot\Big[\hat{\mathbb{G}}^m\Big(\frac{\boldsymbol{x}}{\varepsilon},s\Big)s\nabla\hat{u}\Big(\frac{\boldsymbol{x}}{\varepsilon},\boldsymbol{x},s\Big)\Big] + \hat{\boldsymbol{b}}(\boldsymbol{x},s) = \rho^m\Big(\frac{\boldsymbol{x}}{\varepsilon}\Big)s^2\hat{\boldsymbol{u}}\Big(\frac{\boldsymbol{x}}{\varepsilon},\boldsymbol{x},s\Big), \tag{2.11}$$

where $\hat{u}$ and $\nabla\hat{u}$ represent the micro-displacement field and the gradient of the micro-displacement field converted in the Laplace domain. Moreover $\hat{\mathbb{G}}^m$ is the micro-relaxation tensor and $\hat{\boldsymbol{b}}(\boldsymbol{x},s)$ are the body forces transformed in the Laplace domain. In addition, it is convenient to consider $\hat{\mathbb{C}}^m\Big(\frac{\boldsymbol{x}}{\varepsilon},s\Big) = s\hat{\mathbb{G}}^m\Big(\frac{\boldsymbol{x}}{\varepsilon},s\Big)$.
The governing equation of the periodic viscoelastic material defined in the Laplace domain is

$$\nabla\cdot(\hat{\mathbb{C}}^m\nabla\hat{\boldsymbol{u}}) + \hat{\boldsymbol{b}} = \rho^m s^2\hat{\boldsymbol{u}}. \tag{2.12}$$

Denoting with $[[f]] = f^i(\Sigma) - f^j(\Sigma)$ the jump of the function values f at the interface Σ between two phases i and j in the periodic cell $\mathcal{A}$, the following continuity conditions hold for a perfectly bonded interface

$$[[\hat{\boldsymbol{u}}(\boldsymbol{x})]]|_{\boldsymbol{x}\in\Sigma} = \boldsymbol{0}, \quad \Big[\Big[\Big(\hat{\mathbb{C}}^m\Big(\frac{\boldsymbol{x}}{\varepsilon},s\Big)\nabla\hat{\boldsymbol{u}}\Big(\boldsymbol{x},\frac{\boldsymbol{x}}{\varepsilon},s\Big)\Big)\cdot\boldsymbol{n}\Big]\Big]\Big|_{\boldsymbol{x}\in\Sigma} = \boldsymbol{0}, \tag{2.13}$$

where $\boldsymbol{n}$ represents the outward normal to the interface Σ. Eq. (2.12), which models the periodic viscoelastic material in the Laplace domain,

shows a structure similar to the equation characterizing an elastic material, apart from the presence of the complex frequency s, which affects the constitutive tensors. Moreover, the micro-relaxation tensor $\hat{\mathbb{G}}^m$ is a general kernel that describes the behaviour and the properties of a viscoelastic material. The solution of Eq. (2.12) is too expensive from both a numerical and an analytical point of view, because the coefficients are $\mathcal{Q}$-periodic.
In order to cope with such a drawback, it is convenient to employ a nonlocal asymptotic homogenization technique to turn the heterogeneous material into an equivalent homogeneous one. Such a procedure generates equations, equivalent to (2.12), whose coefficients are not affected by oscillations and their solutions are close to those of the original equation. Moreover, the computational cost to solve (2.12) significantly reduces.
In the equivalent homogenized material, by considering a reference system $\{O, \boldsymbol{e}_1, \boldsymbol{e}_2, \boldsymbol{e}_3\}$, the macro-displacement transformed in the Laplace domain is denoted as $\hat{\boldsymbol{U}}(\boldsymbol{x}) = \hat{U}_i^M \boldsymbol{e}_i$, with respect to a point $\boldsymbol{x}$, and the transformed displacement gradiend is defined as $\nabla\hat{\boldsymbol{U}}(\boldsymbol{x}) = \frac{\partial \hat{U}_i^M}{\partial x_j} \boldsymbol{e}_1 \otimes \boldsymbol{e}_2 \otimes \boldsymbol{e}_3$.

2.3 Asymptotic expansion of the microscopic displacement

Based on the asymptotic approach developed in Smyshlyaev and Cherednichenko (2000) and Bacigalupo (2014), the micro displacement $\boldsymbol{u}$ is expressed as an asymptotic expansion in terms of the parameter ε that separates the slow $\boldsymbol{x}$ variable from the fast one $\boldsymbol{\xi} = \frac{\boldsymbol{x}}{\varepsilon}$,

$$u_h\Big(\boldsymbol{x}, \frac{\boldsymbol{x}}{\varepsilon}, t\Big) = \sum_{l=0}^{+\infty} \varepsilon^l u_h^{(l)} = u_h^{(0)}\Big(\boldsymbol{x}, \frac{\boldsymbol{x}}{\varepsilon}, t\Big) + \varepsilon u_h^{(1)}\Big(\boldsymbol{x}, \frac{\boldsymbol{x}}{\varepsilon}, t\Big) + \varepsilon^2 u_h^{(2)}\Big(\boldsymbol{x}, \frac{\boldsymbol{x}}{\varepsilon}, t\Big) +$$

$$+ \mathrm{O}(\varepsilon^3). \tag{2.14}$$

The Laplace transform (2.8) is applied to Eq. (2.14) and leads to

$$\mathcal{L}\Big(u_h\Big(\boldsymbol{x},\frac{\boldsymbol{x}}{\varepsilon},t\Big)\Big)=\sum_{l=0}^{+\infty}\varepsilon^l\hat{u}_h^{(l)}=\hat{u}_h^{(0)}\Big(\boldsymbol{x},\frac{\boldsymbol{x}}{\varepsilon},s\Big)+\varepsilon\hat{u}_h^{(1)}\Big(\boldsymbol{x},\frac{\boldsymbol{x}}{\varepsilon},s\Big)+$$

$$+\varepsilon^2\hat{u}_h^{(2)}\Big(\boldsymbol{x},\frac{\boldsymbol{x}}{\varepsilon},s\Big)+\mathrm{O}(\varepsilon^3),\tag{2.15}$$

which is equivalent to the asymptotic expansion of the micro displacement performed in the time domain. Let us consider the formula

$$\frac{D}{Dx_k}\hat{\boldsymbol{u}}\Big(\boldsymbol{x},\boldsymbol{\xi}=\frac{\boldsymbol{x}}{\varepsilon}\Big)=\Big[\frac{\partial\hat{u}_h(\boldsymbol{x},\boldsymbol{\xi})}{\partial x_k}+\frac{\partial\hat{u}_h(\boldsymbol{x},\boldsymbol{\xi})}{\partial\xi_k}\frac{\partial\xi_k}{\partial x_k}\Big]\Big|_{\boldsymbol{\xi}=\frac{\boldsymbol{x}}{\varepsilon}}=$$

$$=\Big[\frac{\partial}{\partial x_k}\hat{u}_h(\boldsymbol{x},\boldsymbol{\xi})+\frac{1}{\varepsilon}\hat{u}_{h,k}\Big]\Big|_{\boldsymbol{\xi}=\frac{\boldsymbol{x}}{\varepsilon}},\tag{2.16}$$

which introduces the macroscopic derivative $\frac{\partial}{\partial x_k}\hat{u}_h$ and the microscopic derivative $\hat{u}_{h,k}$ in the transformed Laplace domain, and let us apply it to the asymptotic expansion (2.15), leading to:

$$\frac{D}{Dx_k}\hat{\boldsymbol{u}}\Big(\boldsymbol{x},\boldsymbol{\xi}=\frac{\boldsymbol{x}}{\varepsilon}\Big)=\Big[\frac{\partial\hat{u}_h^{(0)}}{\partial x_k}+\varepsilon\frac{\partial\hat{u}_h^{(1)}}{\partial x_k}+\varepsilon^2\frac{\partial\hat{u}_h^{(2)}}{\partial x_k}+...\Big]+$$

$$+\frac{1}{\varepsilon}\Big[\hat{u}_{h,k}^0+\varepsilon\hat{u}_{h,k}^{(1)}+\varepsilon^2\hat{u}_{h,k}^{(2)}+...\Big]\Big|_{\boldsymbol{\xi}=\frac{\boldsymbol{x}}{\varepsilon}}.\tag{2.17}$$

The asymptotic technique searches for the solution of Eq. (2.12) as a decomposition in increasing powers of the microscopic lenght ε. To this purpose, the replacement of the asymptotic expansion (2.15) into the microscopic field equation (2.12) in the Laplace domain and the rearrangement of the terms with equal power ε yield the asymptotic field equation

$$\varepsilon^{-2}\Big(\hat{C}_{ijhk}^m\hat{u}_{h,k}^{(0)}\Big)_{,j}+\varepsilon^{-1}\Big[\Big(\hat{C}_{ijhk}^m\Big(\frac{\partial\hat{u}_h^{(0)}}{\partial x_k}+\hat{u}_{h,k}^{(1)}\Big)\Big)_{,j}+\frac{\partial}{\partial x_j}\Big(\hat{C}_{ijhk}^m\hat{u}_{h,k}^{(0)}\Big)\Big]+$$

$$+\varepsilon^0\Big[\Big(\hat{C}_{ijhk}^m\Big(\frac{\partial\hat{u}_h^{(1)}}{\partial x_k}+\hat{u}_{h,k}^{(2)}\Big)\Big)_{,j}+\frac{\partial}{\partial x_j}\Big(\hat{C}_{ijhk}^m\Big(\frac{\partial\hat{u}_h^{(0)}}{\partial x_k}+\hat{u}_{h,k}^{(1)}\Big)\Big)+\hat{b}_i-\rho^m s^2u_h^{(0)}\Big]+$$

$$\varepsilon\Big[\Big(\hat{C}^m_{ijhk}\Big(\frac{\partial \hat{u}^{(2)}_h}{\partial x_k}+\hat{u}^{(3)}_{h,k}\Big)\Big)_{,j}+\frac{\partial}{\partial x_j}\Big(\hat{C}^m_{ijhk}\Big(\frac{\partial \hat{u}^{(1)}_h}{\partial x_k}+\hat{u}^{(2)}_{h,k}\Big)\Big)-\rho^m s^2\hat{u}^{(1)}_h\Big]+$$

$$+\mathrm{O}(\varepsilon^2)\Big]\Big|_{\boldsymbol{\xi}=\frac{\boldsymbol{x}}{\varepsilon}}=0. \tag{2.18}$$

Interface conditions (2.13) are rephrased with respect to the fast variable $\boldsymbol{\xi}$ since the micro displacement $\hat{u}_h(\boldsymbol{x},\boldsymbol{\xi})$ is supposed to be $\mathcal{Q}-$periodic with respect to $\boldsymbol{\xi}$ and smooth in the slow variable $\boldsymbol{x}$. Indicating with Σ_1 the interface between two different phases in the unit cell $\mathcal{Q}$ and considering the asymptotic expansion (2.15) of the micro displacement, interface conditions read

$$\Big[\Big[\hat{u}^{(0)}_h\Big]\Big]\Big|_{\boldsymbol{\xi}\in\Sigma_1}+\varepsilon\Big[\Big[\hat{u}^{(1)}_h\Big]\Big]\Big|_{\boldsymbol{\xi}\in\Sigma_1}+\varepsilon^2\Big[\Big[\hat{u}^{(2)}_h\Big]\Big]\Big|_{\boldsymbol{\xi}\in\Sigma_1}+...=0 \tag{2.19}$$

$$\frac{1}{\varepsilon}\Big[\Big[\Big(\hat{C}^m_{ijhk}\hat{u}^{(0)}_{h,k}\Big)n_j\Big]\Big]\Big|_{\boldsymbol{\xi}\in\Sigma_1}+\varepsilon^0\Big[\Big[\Big(\hat{C}^m_{ijhk}\Big(\frac{\partial \hat{u}^{(0)}_h}{\partial \hat{x}_k}+\hat{u}^{(1)}_{h,k}\Big)\Big)n_j\Big]\Big]\Big|_{\boldsymbol{\xi}\in\Sigma_1}+$$

$$+\varepsilon\Big[\Big[\Big(\hat{C}^m_{ijhk}\Big(\frac{\partial \hat{u}^{(1)}_h}{\partial \hat{x}_k}+\hat{u}^{(2)}_{h,k}\Big)\Big)n_j\Big]\Big]\Big|_{\boldsymbol{\xi}\in\Sigma_1}+$$

$$+\varepsilon^2\Big[\Big[\Big(\hat{C}^m_{ijhk}\Big(\frac{\partial \hat{u}^{(2)}_h}{\partial \hat{x}_k}+\hat{u}^{(3)}_{h,k}\Big)\Big)n_j\Big]\Big]\Big|_{\boldsymbol{\xi}\in\Sigma_1}+...+=0.$$

Recursive differential problems and their solutions

The asymptotic field equation (2.18) produces a set of recursive differential problems that determine sequentially the solutions $\hat{u}^0$, $\hat{u}^1$... In particular, at the order ε^{-2}, the differential problem, which stems from problem (2.18), is

$$\Big(\hat{C}^m_{ijhk}\hat{u}^{(0)}_{h,k}\Big)_{,j}=f^{(0)}_i(\boldsymbol{x}), \tag{2.20}$$

with interface conditions

$$\Big[\Big[\hat{u}^{(0)}_h\Big]\Big]\Big|_{\boldsymbol{\xi}\in\Sigma_1}=0\quad\Big[\Big[\Big(\hat{C}^m_{ijhk}\hat{u}^{(0)}_{h,k}\Big)n_j\Big]\Big]\Big|_{\boldsymbol{\xi}\in\Sigma_1}=0.$$

The solvabiliy condition of this differential problem, in the class of $\mathcal{Q}-$periodic solutions $\hat{u}_h^{(0)}$, implies that $f_i^{(0)}(\boldsymbol{x}) = 0$ and so the differential problem (2.20) develops in the form

$$\left(\hat{C}^m_{ijhk}\hat{u}^{(0)}_{h,k}\right)_{,j} = 0. \tag{2.21}$$

The solution results to be

$$\hat{u}_h^{(0)}(\boldsymbol{x}, \boldsymbol{\xi}, s) = \hat{U}_h^M(\boldsymbol{x}, s), \tag{2.22}$$

where $\hat{U}_h^M(\boldsymbol{x}, s)$ is the transformed macroscopic displacement that does not depend on the microstructure.

Bearing in mind the solution (2.22), the differential problem from (2.18), at the order ε^{-1}, is

$$\left(\hat{C}^m_{ijhk}\hat{u}^{(1)}_{h,k}\right)_{,j} + \hat{C}^m_{ijhk,j}\frac{\partial \hat{U}_h^M}{\partial x_k} = f_i^{(1)}(\boldsymbol{x}), \tag{2.23}$$

since $\hat{U}^M_{h,k} = 0$. Its interface conditions are

$$\left[\left[\hat{u}_h^{(1)}\right]\right]\Big|_{\boldsymbol{\xi}\in\Sigma_1} = 0 \quad \left[\left[\left(\hat{C}^m_{ijhk}\left(\hat{u}^{(1)}_{h,k} + \frac{\partial \hat{U}_h^M}{\partial x_k}\right)\right)n_j\right]\right]\Big|_{\boldsymbol{\xi}\in\Sigma_1} = 0.$$

Similarly, the solvability condition in the class of $\mathcal{Q}-$periodic functions ensures that

$$f_i^{(1)}(\boldsymbol{x}) = \langle \hat{C}^m_{ijhk,j}\rangle \frac{\partial \hat{U}_h^{(M)}}{\partial x_k}, \tag{2.24}$$

where $\langle(\cdot)\rangle = \frac{1}{|\mathcal{Q}|}\int_{\mathcal{Q}}(\cdot)d\boldsymbol{\xi}$ and $|\mathcal{Q}| = \delta$. Moreover, the $\mathcal{Q}$-periodicity of the components $\hat{C}^m_{ijhk}$ and the divergence theorem entail $f_i^{(1)}(\boldsymbol{x}) = 0$ and the differential problem

$$\left(\hat{C}^m_{ijhk}\hat{u}^{(1)}_{h,k}\right)_{,j} + \hat{C}^m_{ijhk,j}\frac{\partial \hat{U}_h^M}{\partial x_k} = 0, \quad \forall \frac{\partial \hat{U}_h^M}{\partial x_k} \tag{2.25}$$

has the following solution

$$\hat{u}_h^{(1)}(\boldsymbol{x}, \boldsymbol{\xi}, s) = N^{(1,0)}_{hpq_1}(\boldsymbol{\xi})\frac{\partial \hat{U}_p^M}{\partial x_{q_1}}, \tag{2.26}$$

where $N^{(1,0)}_{hpq_1}$ is the perturbation function, which depends on the fast variable $\boldsymbol{\xi}$. The perturbation functions are supposed to have zero mean over the unit cell $\mathcal{Q}$ and so $N^{(1,0)}_{hpq_1}$ complies with the normalization condition

$$\langle N^{(1,0)}_{hpq_1} \rangle = \frac{1}{|\mathcal{Q}|} \int_{\mathcal{Q}} N^{(1,0)}_{hpq_1}(\boldsymbol{\xi}) d\boldsymbol{\xi} = 0. \tag{2.27}$$

Furthermore, the perturbation functions exclusively depend on the geometry and on the mechanical properties of the microstructure. The differential problem at the order ε^0 is

$$\Big(\hat{C}^m_{ijhk}\Big(\frac{\partial \hat{u}^{(1)}_h}{\partial x_k} + \hat{u}^{(2)}_{h,k}\Big)\Big)_{,j} + \frac{\partial}{\partial x_j}\Big(\hat{C}^m_{ijhk}\Big(\frac{\partial \hat{u}^{(0)}_h}{\partial x_k} + \hat{u}^{(1)}_{h,k}\Big)\Big) - \rho^m s^2 \hat{u}^{(0)}_i = f^{(2)}_i(\boldsymbol{x}), \tag{2.28}$$

with interface conditions

$$\Big[\Big[\hat{u}^{(2)}_h\Big]\Big]\Big|_{\boldsymbol{\xi}\in\Sigma_1} = 0 \quad \Big[\Big[\Big(\hat{C}^m_{ijhk}\Big(\frac{\partial \hat{u}^{(1)}_h}{\partial \hat{x}_k} + \hat{u}^{(2)}_{h,k}\Big)\Big) n_j\Big]\Big]\Big|_{\boldsymbol{\xi}\in\Sigma_1} = 0.$$

Considering the solutions (2.22) and (2.26) of the differential problems at the order ε^{-2} and ε^{-1}, respectively, the differential problem (2.28) is turned into

$$\Big(\hat{C}^m_{ijhk}\hat{u}^{(2)}_{h,k}\Big)_{,j} + \Big(\Big(\hat{C}^m_{ijhk}N^{(1,0)}_{hpq_1}\Big)_{,j} + \hat{C}^m_{ijhq_1} + \Big(\hat{C}^m_{ijhk}N^{(1,0)}_{hpq_1,k}\Big)\Big)\frac{\partial^2 \hat{U}^M_p}{\partial x_{q_1}\partial x_j} +$$

$$- \rho^m s^2 \hat{U}^M_i = f^{(2)}_i(\boldsymbol{x}), \tag{2.29}$$

with interface conditions

$$\Big[\Big[\hat{u}^{(2)}_h\Big]\Big]\Big|_{\boldsymbol{\xi}\in\Sigma_1} = 0, \quad \Big[\Big[\Big(\hat{C}^m_{ijhk}\Big(\hat{u}^{(2)}_{h,k} + N^{(1,0)}_{hpq_1}\frac{\partial^2 \hat{U}^M_p}{\partial x_{q_1}\partial x_k}\Big)\Big) n_j\Big]\Big]\Big|_{\boldsymbol{\xi}\in\Sigma_1} = 0.$$

Again, solvability condition of differential problem (2.29) in the class of $\mathcal{Q}-$periodic functions and the divergence theorem lead to

$$f^{(2)}_i(\boldsymbol{x}) = \langle \hat{C}^m_{ijhq_1} + \hat{C}^m_{ijhk}N^{(1,0)}_{hpq_1,k}\rangle \frac{\partial^2 \hat{U}^M_p}{\partial x_{q_1}\partial x_j} - \langle \rho^m \rangle s^2 \hat{U}^M_i \tag{2.30}$$

and, consequentely, the solution of the differential problem at the order ε^0 is

$$\hat{u}_h^{(2)}(\boldsymbol{x},\boldsymbol{\xi},s) = N^{(2,0)}_{hpq_1q_2}\frac{\partial^2 \hat{U}_p^M}{\partial x_{q_1}\partial x_{q_2}} + N^{(2,2)}_{hp}s^2 U_p^M, \tag{2.31}$$

where $N^{(2,2)}_{hp}$ is the perturbation function depending on the parameter s.

Higher order recursive differential problems

The recursive differential problems are established at the order ε, ε^2, $\varepsilon^{2\tilde{w}-1}$ and $\varepsilon^{2\tilde{w}}$, with $\tilde{w} \in \mathbb{Z}$ and $\tilde{w} \geq 2$ and they are helpful to formulate the cell problems.
Taking account of the solutions (2.26) and (2.31) related to the differential problems at the order ε^{-1} and ε^0, respectively, the differential problem at the order ε, stemmed from equation (2.18), is

$$\begin{aligned}
&\left(\hat{C}^m_{ijhk}\hat{u}^{(3)}_{h,k}\right)_{,j} + \left(\left(\hat{C}^m_{ikhj}N^{(2,0)}_{hpq_1q_2}\right)_{,k} + \hat{C}^m_{ikhj}N^{(2,0)}_{hpq_1q_2,j} + \right.\\
&\left. + \left(\hat{C}^m_{ijhq_2}N^{(1,0)}_{hpq_1}\right)\right)\frac{\partial^3 \hat{U}_p^M}{\partial x_{q_1}\partial x_{q_2}\partial x_k} + \\
&+ \left[\left(\hat{C}^m_{ijhq_1}N^{(2,2)}\right)_{,j} + \hat{C}^m_{iq_1hj}N^{(2,2)}_{hp,j} - \rho^m N^{(1,0)}_{ipq_1}\right]s^2\frac{\partial \hat{U}_p^M}{\partial x_{q_1}} = f_i^{(3)}(\boldsymbol{x}),
\end{aligned} \tag{2.32}$$

with interface conditions

$$\left[\left[\hat{u}^{(3)}_h\right]\right]\Big|_{\boldsymbol{\xi}\in\Sigma_1} = 0, \tag{2.33}$$

$$\left[\left[\left(\hat{C}^m_{ijhk}\left(\hat{u}^{(3)}_{h,k} + N^{(2,0)}_{hpq_1q_2}\frac{\partial^3 \hat{U}_p^M}{\partial x_{q1}\partial x_{q2}\partial x_k} + N^{(2,2)}s^2\frac{\partial \hat{U}_p^M}{\partial x_{q_1}}\right)\right)n_j\right]\right]\Big|_{\boldsymbol{\xi}\in\Sigma_1} = 0.$$

The solvability condition of differential problem (2.32) in the class of $\mathcal{Q}-$periodic functions and the divergence theorem provide

$$f_i^{(3)}(\boldsymbol{x}) = \left\langle \hat{C}^m_{ikhj}N^{(2,0)}_{hpq_1q_2,j} + \left(\hat{C}^m_{ikhq_2}N^{(1,0)}_{hpq_1}\right)\right\rangle\frac{\partial^3 \hat{U}_p^M}{\partial x_{q_1}\partial x_{q_2}\partial x_k} +$$

$$+\left\langle \hat{C}^m_{iq_1hj}N^{(2,2)}_{hp,j}-\rho^m N^{(1,0)}_{ipq_1}\right\rangle s^2\frac{\partial \hat{U}^M_p}{\partial x_{q_1}}, \tag{2.34}$$

and consequentely the solution of the differential problem at the order ε is

$$\hat{u}^{(3)}_h(\boldsymbol{x},\boldsymbol{\xi},s)=N^{(3,0)}_{hpq_1q_2q_3}\frac{\partial^3\hat{U}^M_p}{\partial x_{q_1}\partial x_{q_2}\partial x_{q_3}}+N^{(3,2)}_{hpq_1}s^2\frac{\partial\hat{U}^M_p}{\partial x_{q_1}}. \tag{2.35}$$

Considering the solutions (2.31) and (2.35) related to the differential problems at the order ε^0 and ε, respectively, the differential problem at the order ε^2, derived from equation (2.18), is

$$\left(\hat{C}^m_{ijhk}\hat{u}^{(4)}_{h,k}\right)_{,j}+\left(\left(\hat{C}^m_{ikhj}N^{(3,0)}_{hpq_1q_2q_3}\right)_{,k}+\hat{C}^m_{iq_3hk}N^{(2,0)}_{hpq_1q_2}+\right.$$

$$\left.+\left(\hat{C}^m_{ikhj}N^{(3,0)}_{hpq_1q_2q_3,j}\right)\right)\frac{\partial^4\hat{U}^M_p}{\partial x_{q_1}\partial x_{q_2}\partial x_{q_3}\partial x_k}+$$

$$+\left[\left(\hat{C}^m_{ijhq_2}N^{(3,2)}_{hpq_1}\right)_{,j}+\hat{C}^m_{iq_2hq_1}N^{(2,2)}_{hp}+\hat{C}^m_{iq_2hk}N^{(3,2)}_{hpq_1,k}-\rho^m N^{(2,0)}_{ipq_1q_2}\right]s^2\frac{\partial\hat{U}^M_p}{\partial x_{q_1}}+$$

$$-\rho^m N^{(2,2)}_{ip}s^4\hat{U}^M_p=f^{(4)}_i(\boldsymbol{x}), \tag{2.36}$$

with interface conditions

$$\left[\left[\hat{u}^{(4)}_h\right]\right]\Big|_{\boldsymbol{\xi}\in\Sigma_1}=0, \tag{2.37}$$

$$\left[\left[\left(\hat{C}^m_{ijhk}\left(\hat{u}^{(4)}_{h,k}+N^{(3,0)}_{hpq_1q_2q_3}\frac{\partial^4\hat{U}^M_p}{\partial x_{q1}\partial x_{q2}\partial x_{q3}\partial x_k}+N^{(2,2)}s^2\frac{\partial\hat{U}^M_p}{\partial x_{q_1}}+\right.\right.\right.$$

$$\left.\left.\left.+N^{(3,2)}_{hpq_1}s^2\frac{\partial^2\hat{U}^M_p}{\partial x_{q_1}\partial x_k}\right)\right)n_j\right]\right]\Big|_{\boldsymbol{\xi}\in\Sigma_1}=0.$$

The solvability condition of differential problem (2.36) in the class of $\mathcal{Q}-$periodic functions and the divergence theorem yield

$$f^{(4)}_i(\boldsymbol{x})=\left\langle\left(\hat{C}^m_{iq_3hk}N^{(2,0)}_{hpq_1q_2}+\hat{C}^m_{ikhj}N^{(3,0)}_{hpq_1q_2q_3,j}\right)\right\rangle\frac{\partial^4\hat{U}^M_p}{\partial x_{q_1}\partial x_{q_2}\partial x_{q_3}\partial x_k}+$$

$$+\Big\langle \hat{C}^m_{iq_2hq_1} N^{(2,2)}_{hp} + \hat{C}^m_{iq_2hk} N^{(3,2)}_{hpq_1,k} - \rho^m N^{(2,0)}_{ipq_1q_2} \Big\rangle s^2 \frac{\partial \hat{U}^M_p}{\partial x_{q_1}} - \langle \rho^m N^{(2,2)}_{ip} \rangle s^4 \hat{U}^M_p, \tag{2.38}$$

and the solution of the differential problem at the order ε^2 reads

$$\hat{u}^{(4)}_h(\boldsymbol{x}, \boldsymbol{\xi}, s) = N^{(4,0)}_{hpq_1q_2q_3q_4} \frac{\partial^4 \hat{U}^M_p}{\partial x_{q_1} \partial x_{q_2} \partial x_{q_3} \partial x_{q_4}} + N^{(4,2)}_{hpq_1q_2} s^2 \frac{\partial^2 \hat{U}^M_p}{\partial x_{q_1} \partial x_{q_2}} +$$

$$+ N^{(4,4)}_{hp} s^4 \hat{U}^M_p. \tag{2.39}$$

The generic recursive differential problem of the odd order $\varepsilon^{2\tilde{w}-1}$, with $\tilde{w} \in \mathbb{Z}$ and $\tilde{w} \geq 2$, is

$$(\hat{C}^m_{ijhk} u^{(2\tilde{w}+1)}_{h,k})_j + \frac{1}{2\tilde{w}+1} \sum_{P^*(q)} \Big[\Big(\hat{C}^m_{ijhq_{2\tilde{w}+1}} N^{(2\tilde{w},0)}_{hpq_1 \dots q_{2\tilde{w}}} \Big)_{,j} +$$

$$+ \hat{C}^m_{iq_{2\tilde{w}+1}hj} N^{(2\tilde{w},0)}_{hpq_1 \dots q_{2\tilde{w}},j} + \hat{C}^m_{iq_{2\tilde{w}+1}hq_{2\tilde{w}}} N^{(2\tilde{w}-1,0)}_{hpq_1 \dots q_{2\tilde{w}-1}} \Big] \frac{\partial^{2\tilde{w}+1} \hat{U}^M_p}{\partial x_{q_1} \dots \partial x_{q_{2\tilde{w}+1}}} +$$

$$+ \frac{1}{2\tilde{w}-1} \sum_{P^*(q)} \Big[\Big(\hat{C}^m_{ijhq_{2\tilde{w}-1}} N^{(2\tilde{w},2)}_{hpq_1 \dots q_{2\tilde{w}-2}} \Big)_{,j} + \hat{C}^m_{iq_{2\tilde{w}-1}hq_{2\tilde{w}-2}} N^{(2\tilde{w}-1,2)}_{hpq_1 \dots q_{2\tilde{w}-3}} +$$

$$+ \hat{C}^m_{iq_{2\tilde{w}-1}hj} N^{(2\tilde{w},2)}_{hpq_1 \dots q_{2\tilde{w}-2},j} - \rho^m N^{(2\tilde{w}-1,0)}_{ipq_1 \dots q_{2\tilde{w}-1}} \Big] \frac{\partial^{2\tilde{w}-1} \hat{U}^M_p}{\partial x_{q_1} \dots \partial x_{q_{2\tilde{w}-1}}} s^2 +$$

$$+ \sum_{n=1}^{n=\tilde{w}-1} (1-\delta_{1n}) \frac{1}{2\tilde{w}-2n+1} \sum_{P^*(q)} \Big[\Big(\hat{C}^m_{ijhq_{2\tilde{w}+1-2n}} N^{(2\tilde{w},2n)}_{hpq_1 \dots q_{2\tilde{w}-2n}} \Big)_{,j} +$$

$$+ \hat{C}^m_{iq_{2\tilde{w}+1-2n}hq_{2\tilde{w}-2n}} N^{(2\tilde{w}-1,2n)}_{hpq_1 \dots q_{2\tilde{w}-1-2n}} + \hat{C}^m_{iq_{2\tilde{w}+1-2n}hj} N^{(2\tilde{w},2n)}_{hpq_1 \dots q_{2\tilde{w}-2n},j} +$$

$$- \rho^m N^{(2\tilde{w}-1,2n-2)}_{ipq_1 \dots q_{2\tilde{w}+1-2n}} \Big] \frac{\partial^{2\tilde{w}+1-2n} \hat{U}^M_p}{\partial x_{q_1} \dots \partial x_{q_{2\tilde{w}+1-2n}}} s^{2n} +$$

$$+\Big[\Big(\hat{C}^m_{ijhq_1}N^{(2\tilde{w},2n)}_{hp}\Big)_{,j}+\hat{C}^m_{iq_1hk}N^{(2\tilde{w},2\tilde{w})}_{hp,k}-\rho^m N^{(2\tilde{w}-1,2\tilde{w}-2)}_{ipq_1}\Big]\frac{\partial\hat{U}^m_p}{\partial x_{q_1}}s^{2\tilde{w}}=$$

$$=\frac{1}{2\tilde{w}+1}\sum_{P^*(q)}\langle\hat{C}^m_{iq_{2\tilde{w}+1}hj}N^{(2\tilde{w})}_{hpq_1...q_{2\tilde{w}},j}+$$

$$+\hat{C}^m_{iq_{2\tilde{w}+1}hq_{2\tilde{w}}}N^{(2\tilde{w}-1)}_{hpq_1...q_{2\tilde{w}-1}}\rangle\frac{\partial^{2\tilde{w}+1}\hat{U}^M_p}{\partial x_{q_1}...\partial x_{q_{2\tilde{w}+1}}}+$$

$$+\frac{1}{2\tilde{w}-2}\sum_{P^*(q)}\langle\hat{C}^m_{iq_{2\tilde{w}-1}hq_{2\tilde{w}-2}}N^{(2\tilde{w}-1,2)}_{hpq_1...q_{2\tilde{w}-3}}+\hat{C}^m_{iq_{2\tilde{w}-1}hj}N^{(2\tilde{w},2)}_{hpq_1...q_{2\tilde{w}-2},j}+$$

$$-\rho^m N^{(2\tilde{w}-1)}_{ipq_1...q_{2\tilde{w}-1}}\rangle\frac{\partial^{2\tilde{w}-1}\hat{U}^M_p}{\partial x_{q_1}...\partial x_{q_{2\tilde{w}-1}}}s^2+$$

$$+\sum_{n=1}^{n=\tilde{w}-1}(1-\delta_{1n})\frac{1}{2\tilde{w}-2n+1}\sum_{P^*(q)}\langle\hat{C}^m_{iq_{2\tilde{w}+1-2n}hq_{2\tilde{w}-2n}}N^{(2\tilde{w}-1,2n)}_{hpq_1...q_{2\tilde{w}-1-2n}}+$$

$$+\hat{C}^m_{iq_{2\tilde{w}+1-2n}hj}N^{(2\tilde{w},2n)}_{hpq_1...q_{2\tilde{w}-2n},j}-\rho^m N^{(2\tilde{w}-1,2n-2)}_{ipq_1...q_{2\tilde{w}+1-2n}}\rangle\frac{\partial^{2\tilde{w}+1-2n}\hat{U}^M_p}{\partial x_{q_1}...\partial x_{q_{2\tilde{w}+1-2n}}}s^{2n}+$$

$$+\langle\hat{C}^m_{iq_1hk}N^{(2\tilde{w},2\tilde{w})}_{hp,k}-\rho^m N^{(2\tilde{w}-1,2\tilde{w}-2)}_{ipq_1}\rangle\frac{\partial\hat{U}^m_p}{\partial x_{q_1}}s^{2\tilde{w}} \tag{2.40}$$

and their interface conditions are

$$\Big[\Big[\hat{u}^{(2\tilde{w}+1)}_h\Big]\Big]\Big|_{\boldsymbol{\xi}\in\Sigma_1}=0 \tag{2.41}$$

and

$$\Big[\Big[\Big(\hat{C}^m_{ijhk}\hat{u}^{(2\tilde{w}+1)}_{h,k}+\frac{1}{2\tilde{w}+1}\sum_{P^*(q)}\Big(\hat{C}^m_{ijhq_{2\tilde{w}+1}}N^{(2\tilde{w},0)}_{hpq_1...q_{2\tilde{w}}}\Big)\frac{\partial^{2\tilde{w}+1}\hat{U}^M_p}{\partial x_{q_1}...\partial x_{q_{2\tilde{w}+1}}}+$$

$$+\frac{1}{2\tilde{w}-1}\sum_{P^*(q)}\Big(\hat{C}^m_{ijhq_{2\tilde{w}-1}}N^{(2\tilde{w},2)}_{hpq_1\dots q_{2\tilde{w}-2}}\Big)\frac{\partial^{2\tilde{w}-1}\hat{U}^M_p}{\partial x_{q_1}\dots\partial x_{q_{2\tilde{w}-1}}}s^2+$$

$$+\sum_{n=1}^{n=\tilde{w}-1}(1-\delta_{1n})\frac{1}{2\tilde{w}-2n+1}\times$$

$$\times\sum_{P^*(q)}\Big(\hat{C}^m_{ijhq_{2\tilde{w}+1-2n}}N^{(2\tilde{w},2n)}_{hpq_1\dots q_{2\tilde{w}-2n}}\Big)\frac{\partial^{2\tilde{w}+1-2n}\hat{U}^M_p}{\partial x_{q_1}\dots\partial x_{q_{2\tilde{w}+1-2n}}}s^{2n}+$$

$$+\hat{C}^m_{ijhq_1}N^{(2\tilde{w},2\tilde{w})}_{hp}\frac{\partial\hat{U}^M_p}{\partial x_{q_1}}s^{2\tilde{w}}\Big)n_j\Big]\Big]\Big|_{\boldsymbol{\xi}\in\Sigma_1}=0.$$

The generic recursive differential problem of the even order $\varepsilon^{2\tilde{w}}$ is

$$(\hat{C}^m_{ijhk}u^{(2\tilde{w}+2)}_{h,k})_j+\frac{1}{2\tilde{w}+2}\sum_{P^*(q)}\Big[\Big(\hat{C}^m_{ijhq_{2\tilde{w}+2}}N^{(2\tilde{w}+1)}_{hpq_1\dots q_{2\tilde{w}+1}}\Big)_{,j}+$$

$$+\hat{C}^m_{iq_{2\tilde{w}+2}hj}N^{(2\tilde{w}+1)}_{hpq_1\dots q_{2\tilde{w}+1},j}+\hat{C}^m_{iq_{2\tilde{w}+2}hq_{2\tilde{w}+1}}N^{(2\tilde{w})}_{hpq_1\dots q_{2\tilde{w}}}\Big]\frac{\partial^{2\tilde{w}+2}\hat{U}^M_p}{\partial x_{q_1}\dots\partial x_{q_{2\tilde{w}+2}}}+$$

$$+\frac{1}{2\tilde{w}}\sum_{P^*(q)}\Big[\Big(\hat{C}^m_{ijhq_{2\tilde{w}}}N^{(2\tilde{w}+1,2)}_{hpq_1\dots q_{2\tilde{w}-1}}\Big)_{,j}+\hat{C}^m_{iq_{2\tilde{w}}hq_{2\tilde{w}-1}}N^{(2\tilde{w},2)}_{hpq_1\dots q_{2\tilde{w}-2}}+$$

$$+\hat{C}^m_{iq_{2\tilde{w}}hj}N^{(2\tilde{w}+1,2)}_{hpq_1\dots q_{2\tilde{w}-1},j}-\rho^m N^{(2\tilde{w})}_{ipq_1\dots q_{2\tilde{w}}}\Big]\frac{\partial^{2\tilde{w}}\hat{U}^M_p}{\partial x_{q_1}\dots\partial x_{q_{2\tilde{w}}}}s^2+$$

$$+\sum_{n=1}^{n=\tilde{w}-1}(1-\delta_{1n})\frac{1}{2^{2\tilde{w}-2n+2}}\sum_{P^*(q)}\Big[\Big(\hat{C}^m_{ijhq_{2\tilde{w}-2n+2}}N^{(2\tilde{w}+1,2n)}_{hpq_1\dots q_{2\tilde{w}-2n+1}}\Big)_{,j}+$$

$$+\hat{C}^m_{iq_{2\tilde{w}-2n+2}hq_{2\tilde{w}+1-2n}}N^{(2\tilde{w},2n)}_{hpq_1\dots q_{2\tilde{w}-2n}}+\hat{C}^m_{iq_{2\tilde{w}+2-2n}hj}N^{(2\tilde{w}+1,2n)}_{hpq_1\dots q_{2\tilde{w}+1-2n},j}+$$

$$- \rho^m N^{(2\tilde{w},2n-2)}_{ipq_1...q_{2\tilde{w}+2-2n}}\Big]\frac{\partial^{2\tilde{w}+2-2n}\hat{U}^M_p}{\partial x_{q_1}...\partial x_{q_{2\tilde{w}+2-2n}}}s^{2n}+$$

$$+\frac{1}{2}\Big[\Big(\hat{C}^m_{ijhq_2}N^{(2\tilde{w}+1,2\hat{w})}_{hpq_1}\Big)_{,j}+\hat{C}^m_{iq_2hq_1}N^{(2\tilde{w},2\tilde{w})}_{hp}+\hat{C}^m_{iq_2hj}N^{(2\tilde{w}+1,2\tilde{w})}_{hpq_1,j}+$$

$$- \rho^m N^{(2\tilde{w},2\tilde{w}-2)}_{ipq_1q_2}+\hat{C}^m_{ijhq_1}N^{(2\tilde{w}+1,2\hat{w})}_{hpq_2}\Big)_{,j}+$$

$$+\hat{C}^m_{iq_1hq_2}N^{(2\tilde{w},2\tilde{w})}_{hp}+\hat{C}^m_{iq_1hj}N^{(2\tilde{w}+1,2\tilde{w})}_{hpq_2,j}- \rho^m N^{(2\tilde{w},2\tilde{w}-2)}_{ipq_2q_1}\Big]\frac{\partial^2\hat{U}^m_p}{\partial x_{q_1}\partial x_{q_2}}s^{2\tilde{w}}+$$

$$- \rho^m N^{(2\tilde{w},2\tilde{w})}_{ip}\hat{U}^M_p s^{2\tilde{w}}=\frac{1}{2\tilde{w}+2}\sum_{P^*(q)}\langle\hat{C}^m_{iq_{2\tilde{m}+2}hj}N^{(2\tilde{w}+1)}_{hpq_1...q_{2\tilde{w}+1},j}$$

$$+\hat{C}^m_{iq_{2\tilde{w}+2}hq_{2\tilde{w}+1}}N^{(2\tilde{w})}_{hpq_1...q_{2\tilde{w}}}\rangle\frac{\partial^{2\tilde{w}+2}\hat{U}^M_p}{\partial x_{q_1}...\partial x_{q_{2\tilde{w}+2}}}+$$

$$+\frac{1}{2\tilde{w}}\sum_{P(q)}\langle\hat{C}^m_{iq_{2\tilde{w}}hq_{2\tilde{w}-1}}N^{(2\tilde{w},2)}_{hpq_1...q_{2\tilde{w}-2}}+$$

$$+\hat{C}^m_{iq_{2\tilde{w}}hj}N^{(2\tilde{w}+1,2)}_{hpq_1...q_{2\tilde{w}-1},j}- \rho^m N^{(2\tilde{w})}_{ipq_1...q_{2\tilde{w}}}\rangle\frac{\partial^{2\tilde{w}}\hat{U}^M_p}{\partial x_{q_1}...\partial x_{q_{2\tilde{w}}}}s^2+$$

$$+\sum_{n=1}^{n=\tilde{w}-1}(1-\delta_{1n})\frac{1}{2\tilde{w}-2n+2}\sum_{P^*(q)}\langle\hat{C}^m_{iq_{2\tilde{w}-2n+2}hq_{2\tilde{w}+1-2n}}N^{(2\tilde{w},2n)}_{hpq_1...q_{2\tilde{w}-2n}}+$$

$$+\hat{C}^m_{iq_{2\tilde{w}+2-2n}hj}N^{(2\tilde{w}+1,2n)}_{hpq_1...q_{2\tilde{w}+1-2n},j}- \rho^m N^{(2\tilde{w},2n-2)}_{ipq_1...q_{2\tilde{w}+2-2n}}\rangle\frac{\partial^{2\tilde{w}+2-2n}\hat{U}^M_p}{\partial x_{q_1}...\partial x_{q_{2\tilde{w}+2-2n}}}s^{2n}+$$

$$+\frac{1}{2}\Big[\Big(\hat{C}^m_{iq_2hq_1}N^{(2\tilde{w},2\tilde{w})}_{hp}+\hat{C}^m_{iq_2hj}N^{(2\tilde{w}+1,2\tilde{w})}_{hpq_1,j}- \rho^m N^{(2\tilde{w},2\tilde{w}-2)}_{ipq_1q_2}+$$

$$+\hat{C}^m_{iq_1hq_2}N^{(2\tilde{w},2\tilde{w})}_{hp}+\hat{C}^m_{iq_1hj}N^{(2\tilde{w}+1,2\tilde{w})}_{hpq_2,j}-\rho^m N^{(2\tilde{w},2\tilde{w}-2)}_{ipq_2q_1}\Big]\frac{\partial^2\hat{U}^m_p}{\partial x_{q_1}\partial x_{q_2}}s^{2\tilde{w}}+$$

$$-\langle\rho^m N^{(2\tilde{w},2\tilde{w})}_{ip}\rangle\hat{U}^M_p s^{2\tilde{w}}, \tag{2.42}$$

and their interface conditions are

$$\Big[\Big[\hat{u}^{(2\tilde{w}+2)}_h\Big]\Big]\Big|_{\boldsymbol{\xi}\in\Sigma_1}=0 \tag{2.43}$$

and

$$\Big[\Big[\Big(\hat{C}^m_{ijhk}\hat{u}^{(2\tilde{w}+2)}_{h,k}+\frac{1}{2\tilde{w}+2}\sum_{P^*(q)}\Big(\hat{C}^m_{ijhq_{2\tilde{w}+2}}N^{(2\tilde{w}+1,0)}_{hpq_1\ldots q_{2\tilde{w}}+1}\Big)\frac{\partial^{2\tilde{w}+2}\hat{U}^M_p}{\partial x_{q_1}\ldots\partial x_{q_{2\tilde{w}+2}}}+$$

$$+\frac{1}{2\tilde{w}}\sum_{P^*(q)}\Big(\hat{C}^m_{ijhq_{2\tilde{w}}}N^{(2\tilde{w}+1,2)}_{hpq_1\ldots q_{2\tilde{w}-1}}\Big)\frac{\partial^{2\tilde{w}}\hat{U}^M_p}{\partial x_{q_1}\ldots\partial x_{q_{2\tilde{w}}}}s^2+$$

$$+\sum_{n=1}^{n=\tilde{w}-1}(1-\delta_{1n})\frac{1}{2\tilde{w}-2n+2}\sum_{P^*(q)}\Big(\hat{C}^m_{ijhq_{2\tilde{w}-2n+2}}N^{(2\tilde{w}+1,2n)}_{hpq_1\ldots q_{2\tilde{w}-2n+1}}\Big)X$$

$$X\frac{\partial^{2\tilde{w}+2-2n}\hat{U}^M_p}{\partial x_{q_1}\ldots\partial x_{q_{2\tilde{w}+2-2n}}}s^{2n}+$$

$$+\frac{1}{2}\Big[\Big(\hat{C}^m_{ijhq_2}N^{(2\tilde{w}+1,2\tilde{m})}_{hpq_1}+\hat{C}^m_{ijhq_1}N^{(2\tilde{w}+1,2\tilde{w})}_{hpq_2}\Big)\frac{\partial^2\hat{U}^M_p}{\partial x_{q_1}\partial x_{q_2}}s^{2\tilde{w}}\Big]\Big)n_j\Big]\Big]\Big|_{\boldsymbol{\xi}\in\Sigma_1}=0. \tag{2.44}$$

2.4 Cell problems and perturbation functions

In the previous section, the solutions $\hat{u}^{(0)}_h$, $\hat{u}^{(1)}_h$, $\hat{u}^{(2)}_h$, ... have been established. Such solutions are employed to formulate the cell problems, which are classified according to the even power of the parameter s.

Cell problems related to s^0

The substitution of solution (2.26) into problem (2.25) leads to the following cell problem at the order ε^{-1}

$$\left(\hat{C}^m_{ijhk} N^{(1,0)}_{hpq_1,k}\right)_{,j} + \hat{C}^m_{ijpq_1,j} = 0, \tag{2.45}$$

with interface conditions derived in terms of the perturbation function $N^{(1,0)}_{hpq_1,k}$

$$\left[\left[N^{(1,0)}_{ipq_1}\right]\right]\Big|_{\boldsymbol{\xi}\in\Sigma_1} = 0 \quad \left[\left[\left(\hat{C}^m_{ijhk}\left(N^{(1,0)}_{hpq_1,k} + \delta_{hp}\delta_{kq_1}\right)\right)n_j\right]\right]\Big|_{\boldsymbol{\xi}\in\Sigma_1} = 0, \tag{2.46}$$

where δ_{hp} and δ_{kq_1} are the Kronecker delta functions. Once the perturbation function $N^{(1,0)}_{hpq_1,k}$ has been determined, and thanks to equation (2.29) and its solution (2.31), the cell problem at the order ε^0 is derived and the symmetrized version with respect to indices q_1 and q_2 is

$$\left(\hat{C}^m_{ijhk} N^{(2,0)}_{hpq_1q_2,k}\right)_{,j} + \frac{1}{2}\Big[\left(\hat{C}^m_{ikhq_2} N^{(1,0)}_{hpq_1}\right)_{,k} + \hat{C}^m_{iq_2pq_1} + \left(\hat{C}^m_{iq_2hk} N^{(1,0)}_{hpq_1,k}\right) +$$

$$+ \left(\hat{C}^m_{ikhq_1} N^{(1,0)}_{hpq_2}\right)_{,k} + \hat{C}^m_{iq_1pq_2} + \left(\hat{C}^m_{iq_1hk} N^{(1,0)}_{hpq_2,k}\right)\Big] =$$

$$= \frac{1}{2}\langle \hat{C}^m_{iq_2hq_1} + \left(\hat{C}^m_{iq_2hk} N^{(1,0)}_{hpq_1,k}\right) + \hat{C}^m_{iq_1hq_2} + \left(\hat{C}^m_{iq_1hk} N^{(1,0)}_{hpq_2,k}\right)\rangle, \tag{2.47}$$

with interface conditions

$$\left[\left[N^{(2,0)}_{ipq_1q_2}\right]\right]\Big|_{\boldsymbol{\xi}\in\Sigma_1} = 0, \tag{2.48}$$

$$\left[\left[\left(\hat{C}^m_{ijhk} N^{(2,0)}_{hpq_1q_2,k} + \frac{1}{2}\left(\hat{C}^m_{ijhq_2} N^{(1,0)}_{hpq_1} + \hat{C}^m_{ijhq_1} N^{(1,0)}_{hpq_2}\right)\right)n_j\right]\right]\Big|_{\boldsymbol{\xi}\in\Sigma_1} = 0.$$

The solution of the cell problem (2.47) and (2.48) is the perturbation function $N^{(2,0)}_{ipq_1q_2}$. The cell problem at the order ε^w with $w \in \mathbb{Z}$ and $w \geq 1$ is

$$\left(\hat{C}^m_{ijhk} N^{(w+2,0)}_{hpq_1\dots q_{w+2},k}\right)_{,j} + \frac{1}{w+2}\sum_{\mathcal{P}^*(q)}\Big[(\hat{C}^m_{ijhq_{w+2}} N^{(w+1,0)}_{hpq_1\dots q_{w+1}})_{,j} +$$

$$+ \hat{C}^m_{iq_{w+2}hj} N^{(w+1,0)}_{hpq_1\dots q_{w+1},j} + \hat{C}^m_{iq_{w+2}hq_{w+1}} N^{(w,0)}_{hpq_1\dots q_w} \Big] =$$

$$= \frac{1}{w+2} \sum_{\mathcal{P}^*(q)} \langle \hat{C}^m_{iq_{w+2}hj} N^{(w+1,0)}_{hpq_1\dots q_{w+1},j} + \hat{C}^m_{iq_{w+2}hq_{w+1}} N^{(w,0)}_{hpq_1\dots q_w} \rangle, \tag{2.49}$$

and the corresponding interface conditions are

$$\Big[\Big[N^{(w+2,0)}_{ipq_1\dots q_{w+2}} \Big]\Big]\Big|_{\boldsymbol{\xi}\in\Sigma_1} = 0 \tag{2.50}$$

$$\Big[\Big[\Big(\hat{C}^m_{ijhk} N^{(w+2,0)}_{hpq_1\dots q_{w+2},k} + \frac{1}{w+2} \sum_{P^*(q)} \hat{C}^m_{ijhq_{w+2}} N^{(w+1,0)}_{hpq_1\dots q_{w+1}} \Big) n_j \Big]\Big]\Big|_{\boldsymbol{\xi}\in\Sigma_1} = 0,$$

where symbol $\mathcal{P}^*(q)$ denotes all the possible permutations of the multi-index $q = q_1, q_2, ..., q_l$ that does not exhibit fixed indices, see A. The resolution of cell problem (2.49) allows determining the form of the perturbation function $N^{(w+2,0)}_{ipq_1\dots q_{w+2}}$.

Cell problems related to s^2

The substitution of solution (2.31) into Eq. (2.29) generates the cell problem at the order ε^0

$$\Big(\hat{C}^m_{ijhk} N^{(2,2)}_{hp,k} \Big)_{,j} - \rho^m \delta_{ip} = -\delta_{ip} \Big\langle \rho^m \Big\rangle, \tag{2.51}$$

with interface conditions:

$$\Big[\Big[N^{(2,2)}_{ip} \Big]\Big]\Big|_{\boldsymbol{\xi}\in\Sigma_1} = 0, \quad \Big[\Big[\hat{C}^m_{ijhk} N^{(2,2)}_{hp,k} \Big]\Big]\Big|_{\boldsymbol{\xi}\in\Sigma_1} = 0, \tag{2.52}$$

as well as the cell problem (2.47), which is related to the case s^0. From the resolution of problem (2.51) and (2.52), the perturbation function $N^{(2,2)}_{ip}$ is derived.

The perturbation function $N^{(3,2)}_{ipq_1}$ is the solution of the cell problem obtained at the order ε^1

$$\Big(\hat{C}^m_{ijhk} N^{(3,2)}_{hpq_1,k} \Big)_{,j} + \Big[(\hat{C}^m_{ijhq_1} N^{(2,2)}_{hp})_{,j} + \hat{C}^m_{iq_1hj} N^{(2,2)}_{hp,j} - \rho^m N^{(1,0)}_{ipq_1} \Big] =$$

$$= \Big\langle \hat{C}^m_{iq_1hj} N^{(2,2)}_{hp,j} - \rho^m N^{(1,0)}_{ipq_1} \Big\rangle, \tag{2.53}$$

with interface conditions

$$\Big[\Big[N^{(3,2)}_{ipq_1}\Big]\Big]\Big|_{\boldsymbol{\xi}\in\Sigma_1} = 0, \quad \Big[\Big[\hat{C}^m_{ijhk} N^{(3,2)}_{hpq_1,k} + \hat{C}^m_{ijhq_1} N^{(2,2)}_{hp}) n_j\Big]\Big]\Big|_{\boldsymbol{\xi}\in\Sigma_1} = 0. \tag{2.54}$$

Meanwhile, at the order ε^2, the perturbation function $N^{(4,2)}_{ipq_1q_2}$ is the solution of the cell problem

$$\Big(\hat{C}^m_{ijhk} N^{(4,2)}_{hpq_1q_2,k}\Big)_{,j} + \frac{1}{2}\Big[(\hat{C}^m_{ijhq_2} N^{(3,2)}_{hpq_1})_{,j} + \hat{C}^m_{iq_2hq_1} N^{(2,2)}_{hp} + \hat{C}^m_{iq_2hk} N^{(3,2)}_{hpq_1,k} +$$

$$- \rho^m N^{(2,0)}_{hpq_1q_2} + (\hat{C}^m_{ijhq_1} N^{(3,2)}_{hpq_2})_{,j} + \hat{C}^m_{iq_1hq_2} N^{(2,2)}_{hp} + \hat{C}^m_{iq_1hk} N^{(3,2)}_{hpq_2,k} +$$

$$- \rho^m N^{(2,0)}_{hpq_2q_1}\Big] = \frac{1}{2}\langle \hat{C}^m_{iq_2hq_1} N^{(2,2)}_{hp} + \hat{C}^m_{iq_2hk} N^{(3,2)}_{hpq_1,k} - \rho^m N^{(2,0)}_{hpq_1q_2} +$$

$$+ \hat{C}^m_{iq_1hq_2} N^{(2,2)}_{hp} + \hat{C}^m_{iq_1hk} N^{(3,2)}_{hpq_2,k} - \rho^m N^{(2,0)}_{hpq_2q_1}\rangle, \tag{2.55}$$

whose interface conditions read

$$\Big[\Big[N^{(4,2)}_{ipq_1q_2}\Big]\Big]\Big|_{\boldsymbol{\xi}\in\Sigma_1} = 0, \tag{2.56}$$

$$\Big[\Big[\Big(\hat{C}^m_{ijhk} N^{(4,2)}_{hpq_1q_2,k} + \frac{1}{2}\Big(\hat{C}^m_{ijhq_2} N^{(3,2)}_{hpq_1} + \hat{C}^m_{ijhq_1} N^{(3,2)}_{hpq_2}\Big)\Big) n_j\Big]\Big]\Big|_{\boldsymbol{\xi}\in\Sigma_1} = 0.$$

Finally, at the order ε^{w+2}, with $w \in \mathbb{Z}$ and $w \geq 1$, the perturbation function $N^{(w+4,2)}_{ipq_1\dots q_{w+2}}$ is derived from the cell problem

$$\Big(\hat{C}^m_{ijhk} N^{(w+4,2)}_{hpq_1\dots q_{w+2},k}\Big)_{,j} + \frac{1}{w+2}\sum_{P^*(q)}\Big[\Big(\hat{C}^m_{ijhq_{w+2}} N^{(w+3,2)}_{hpq_1\dots q_{w+1}}\Big)_{,j} +$$

$$+ \hat{C}^m_{iq_{w+2}hq_{w+1}} N^{(w+2,2)}_{hpq_1\dots q_w} + \hat{C}^m_{iq_{w+2}hj} N^{(w+3,2)}_{hpq_1\dots q_{w+1},j} - \rho^m N^{(w+2)}_{ipq_1\dots q_{w+2}}\Big] =$$

$$= \frac{1}{w+2}\sum_{P^*(q)}\langle \hat{C}^m_{iq_{w+2}hq_{w+1}} N^{(w+2,2)}_{hpq_1\dots q_w} + \hat{C}^m_{iq_{w+2}hj} N^{(w+3,2)}_{hpq_1\dots q_{w+1},j} +$$

$$- \rho^m N^{(w+2,0)}_{ipq_1\dots q_{w+2}}\rangle, \tag{2.57}$$

equipped with the interface conditions

$$\Big[\Big[N^{(w+4,2)}_{ipq_1\dots q_{w+2}}\Big]\Big]\Big|_{\boldsymbol{\xi}\in\Sigma_1} = 0, \tag{2.58}$$

$$\Big[\Big[\Big(\hat{C}^m_{ijhq_{w+2}} N^{(w+4,2)}_{hpq_1\dots q_{w+2},k} + \frac{1}{w+2}\sum_{P^*(q)}\Big(\hat{C}^m_{ijhq_{w+2}} N^{(w+3,2)}_{hpq_1\dots q_{w+1}}\Big)\Big)n_j\Big]\Big]\Big|_{\boldsymbol{\xi}\in\Sigma_1} = 0.$$

Cell problems related to s^{2n}

The cell problems related to power s^{2n} are here devised and their corresponding perturbation functions are established. At the order $\varepsilon^{(2n-2)}$, with $n \in \mathbb{Z}$ and $n \geq 2$, the cell problem is

$$\Big(\hat{C}^m_{ijhk} N^{(2n,2n)}_{hp,k}\Big)_{,j} - \rho^m N^{(2n-2,2n-2)}_{ip} = -\langle \rho^m N^{(2n-2,2n-2)}_{ip}\rangle, \tag{2.59}$$

with interface conditions

$$\Big[\Big[N^{(2n,2n)}_{ip}\Big]\Big]\Big|_{\boldsymbol{\xi}\in\Sigma_1} = 0, \quad \Big[\Big[\hat{C}^m_{ijhk} N^{(2n,2n)}_{hp,k}\Big]\Big]\Big|_{\boldsymbol{\xi}\in\Sigma_1} = 0, \tag{2.60}$$

and its solution is the perturbation function $N^{(2n,2n)}_{ip}$.
Whereas at the order $\varepsilon^{(2n-1)}$, the perturbation function $N^{(2n+1,2n)}_{ipq_1}$ is the solution of the cell problem

$$\Big(\hat{C}^m_{ijhk} N^{(2n+1,2n)}_{hpq_1,k}\Big)_{,j} + \Big[\Big(\hat{C}^m_{ijhq_1} N^{(2n,2n)}_{hp}\Big)_{,j} + \hat{C}^m_{iq_1hk} N^{(2n,2n)}_{hp,k} +$$

$$- \rho^m N^{(2n-1,2n-2)}_{ipq_1}\Big] = \Big\langle \hat{C}^m_{iq_1hk} N^{(2n,2n)}_{hp,k} - \rho^m N^{(2n-1,2n-2)}_{ipq_1}\Big\rangle, \tag{2.61}$$

with interface conditions:

$$\Big[\Big[N^{(2n+1,2n)}_{ipq_1}\Big]\Big]\Big|_{\boldsymbol{\xi}\in\Sigma_1} = 0,$$

$$\Big[\Big[(\hat{C}^m_{ijhk} N^{(2n+1,2n)}_{hpq_1,k} + \hat{C}^m_{ijhq_1} N^{(2n,2n)}_{hp})n_j\Big]\Big]\Big|_{\boldsymbol{\xi}\in\Sigma_1} = 0. \tag{2.62}$$

The cell problem evaluated for $\varepsilon^{(2n)}$ is

$$\Big(\hat{C}^m_{ijhk}N^{(2n+2,2n)}_{hpq_1q_2,k}\Big)_{,j}+\frac{1}{2}\Big[\Big(\hat{C}^m_{ijhq_2}N^{(2n+1,2n)}_{hpq_1}\Big)_{,j}+\hat{C}^m_{iq_2hq_1}N^{(2n,2n)}_{hp}+$$

$$+\hat{C}^m_{iq_2hj}N^{(2n+1,2n)}_{hpq_1,j}-\rho^m N^{(2n,2n-2)}_{ipq_1q_2}+\Big(\hat{C}^m_{ijhq_1}N^{(2n+1,2n)}_{hpq_2}\Big)_{,j}+$$

$$+\hat{C}^m_{iq_1hq_2}N^{(2n,2n)}_{hp}+\hat{C}^m_{iq_1hj}N^{(2n+1,2n)}_{hpq_2,j}-\rho^m N^{(2n,2n-2)}_{ipq_2q_1}\Big]=$$

$$\Big\langle\frac{1}{2}\hat{C}^m_{iq_2hq_1}N^{(2n,2n)}_{hp}+\hat{C}^m_{iq_2hj}N^{(2n+1,2n)}_{hpq_1,j}-\rho^m N^{(2n,2n-2)}_{ipq_1q_2}+$$

$$+\hat{C}^m_{iq_1hq_2}N^{(2n,2n)}_{hp}+\hat{C}^m_{iq_1hj}N^{(2n+1,2n)}_{hpq_2,j}-\rho^m N^{(2n,2n-2)}_{ipq_2q_1}\Big\rangle, \tag{2.63}$$

with interface conditions

$$\Big[\Big[N^{(2n+2,2n)}_{ipq_1q_2}\Big]\Big]\Big|_{\boldsymbol{\xi}\in\Sigma_1}=0, \tag{2.64}$$

$$\Big[\Big[\Big(\hat{C}^m_{ijhk}N^{(2n+2,2n)}_{hpq_1q_2,k}+\frac{1}{2}\Big(\hat{C}^m_{ijhq_2}N^{(2n+1,2n)}_{hpq_1}+\hat{C}^m_{ijhq_1}N^{(2n+1,2n)}_{hpq_2}\Big)\Big)n_j\Big]\Big]\Big|_{\boldsymbol{\xi}\in\Sigma_1}=0,$$

and its solution is the perturbation function $N^{(2n+2,2n)}_{ipq_1q_2}$. Finally, the perturbation function $N^{(w+2n+2,2n)}_{ipq_1\dots q_{w+2}}$ is the solution of the cell problem for ε^{w+2n}

$$\Big(\hat{C}^m_{ijhk}N^{(w+2n+2,2n)}_{hpq_1\dots q_{w+2},k}\Big)_{,j}+\frac{1}{w+2}\sum_{P^*(q)}\Big[\Big(\hat{C}^m_{ijhq_{w+2}}N^{(w+2n+1,2n)}_{hpq_1\dots q_{w+1}}\Big)_{,j}+$$

$$+\hat{C}^m_{iq_{w+2}hq_{w+1}}N^{(w+2n,2n)}_{hpq_1\dots q_w}+\hat{C}^m_{iq_{w+2}hj}N^{(w+2n+1,2n)}_{hpq_1\dots q_{w+1},j}-\rho^m N^{(w+2n,2n-2)}_{ipq_1\dots q_{w+2}}\Big]=$$

$$=\frac{1}{w+2}\sum_{P(q)}\langle\hat{C}^m_{iq_{w+2}hq_{w+1}}N^{(w+2n,2n)}_{hpq_1\dots q_w}+\hat{C}^m_{iq_{w+2}hj}N^{(w+2n+1,2n)}_{hpq_1\dots q_{w+1},j}+$$

$$- \rho^m N^{(w+2n,2n-2)}_{ipq_1\dots q_{w+2}}\rangle, \tag{2.65}$$

whose interface conditions are

$$\Big[\Big[N^{(w+2n+2,2n)}_{ipq_1\dots q_{w+2}}\Big]\Big]\Big|_{\boldsymbol{\xi}\in\Sigma_1} = 0, \tag{2.66}$$

$$\Big[\Big[\Big(\hat{C}^m_{ijhk} N^{(w+2n+2,2n)}_{hpq_1\dots q_{w+2},k} + \frac{1}{w+2}\sum_{P^*(q)}\Big(\hat{C}^m_{ijhq_{w+2}} N^{(w+2n+1,2n)}_{hpq_1\dots q_{w+1}}\Big)\Big)n_j\Big]\Big]\Big|_{\boldsymbol{\xi}\in\Sigma_1} = 0.$$

In Smyshlyaev and Cherednichenko (2000) and Bacigalupo (2014), it is emphasized that the uniqueness of the perturbation functions $N^{(i,2r)}_{hpq_1\dots q_{i-2r}}$, derived from the cell problems (2.45)-(2.66), is guaranteed by imposing the normalization condition $\langle N^{(i,2r)}_{hpq_1\dots q_{i-2r}}\rangle = 0$.

2.5 Down-scaling relation and up-scaling relation.

The down-scaling relation referred to the transformed micro-displacement is expressed as an asymptotic expansion of powers of the microscopic length ε relying on the transformed macro-displacement $\hat{U}^M_h(\boldsymbol{x}, s)$, its gradients and the $\mathcal{Q}$-periodic perturbation functions. Such functions are delivered by solving the cell problems that are listed in the Section 2.4. Therefore, the replacement of the solutions of the recursive differential problems (2.22), (2.26), (2.31), (2.35) and (2.39) into the asymptotic expansion (2.15) enables establishing the transformed micro-displacement $\hat{u}_h(\boldsymbol{x}, \boldsymbol{\xi}, s)$ as

$$\hat{u}_h\Big(\boldsymbol{x}, \frac{\boldsymbol{x}}{\varepsilon}, s\Big) = \Big(\sum_{l,j=0}^{+\infty}\varepsilon^{j+l}\sum_{|q|=l} N^{(2j+l,2j)}_{hpq}(\boldsymbol{\xi})\frac{\partial^l \hat{U}^M_p}{\partial x_q}s^{2j}\Big)\Big|_{\boldsymbol{\xi}=\frac{\boldsymbol{x}}{\varepsilon}} = \tag{2.67}$$

$$= \Big(\hat{U}^M_h(\boldsymbol{x}, s) + \varepsilon N^{(1,0)}_{hpq_1}(\boldsymbol{\xi})\frac{\partial \hat{U}^M_p}{\partial x_{q_1}} + \varepsilon^2\Big(N^{(2,0)}_{hpq_1q_2}(\boldsymbol{\xi})\frac{\partial^2 \hat{U}^M_p}{\partial x_{q1}\partial x_{q2}} +$$

$$+ N^{(2,2)}_{hp}(\boldsymbol{\xi})s^2\hat{U}^M_p\Big) + \varepsilon^3\Big(N^{(3,0)}_{hpq_1q_2q_3}(\boldsymbol{\xi})\frac{\partial^3 \hat{U}^M_p}{\partial x_{q1}\partial x_{q2}\partial x_{q3}} + N^{(3,2)}_{hpq_1}(\boldsymbol{\xi})s^2\frac{\partial \hat{U}^M_p}{\partial x_{q1}}\Big) +$$

$$\varepsilon^4\Big(N^{(4,0)}_{hpq_1q_2q_3q_4}(\boldsymbol{\xi})\frac{\partial^4\hat{U}^M_p}{\partial x_{q1}\partial x_{q2}\partial x_{q3}\partial x_{q4}}+N^{(4,2)}_{hpq_1q_2}(\boldsymbol{\xi})s^2\frac{\partial^2\hat{U}^M_p}{\partial x_{q1}\partial x_{q2}}+$$

$$+N^{(4,4)}_{hp}(\boldsymbol{\xi})s^4\hat{U}^M_p\Big)+O(\varepsilon^5)\Big)\Big|_{\boldsymbol{\xi}=\frac{\boldsymbol{x}}{\varepsilon}}.$$

In Eq. (2.67), $|q|$ describes the length of the multi-index and the derivative with respect to q is written as $\frac{\partial^l(\cdot)}{\partial x_q}=\frac{\partial^l(\cdot)}{\partial x_{q_1}\ldots x_{q_l}}$. Moreover, the perturbation function $N^{(0,0)}_{hp}$ stands for the Kronecker delta δ_{hp}. There is point in observing that the $\mathcal{Q}$-periodic perturbation functions $N^{(2j+l,2j)}_{hpq}$ are affected by the microstructural inhomogeneities of the material and this is emphasized by their dependency on the fast variable $\boldsymbol{\xi}=\frac{\boldsymbol{x}}{\varepsilon}$. On the other hand, the transformed macro displacement $\hat{U}^M_h(\boldsymbol{x},s)$ is $\mathcal{L}$-periodic and relies on the slow variable $\boldsymbol{x}$ and the time. The transformed macro-displacement field is supposed to be the mean value of the transformed micro-displacement field over the unit cell $\mathcal{Q}$

$$\hat{U}^M_h(\boldsymbol{x},t)=\Big\langle\hat{u}_h\Big(\boldsymbol{x},\frac{\boldsymbol{x}}{\varepsilon}+\boldsymbol{\zeta},s\Big)\Big\rangle. \tag{2.68}$$

Eq. (2.68) is said to be the up-scaling relation and it links the transformed macro-displacement field with the transformed micro-displacement field. In Eq. (2.68) the variable $\boldsymbol{\zeta}\in\mathcal{Q}$ identifies a family of translations of the heterogeneous domain with respect to the $\mathcal{L}-$periodic body forces $\boldsymbol{b}(\boldsymbol{x},t)$, see Bacigalupo (2014). Therefore, the transformed body forces in the Laplace space $\hat{\boldsymbol{b}}(\boldsymbol{x},t)$ are $\mathcal{L}-$periodic.

2.6 Average field equations of infinite order and macroscopic problems

Replacing the down-scaling relation (2.67) into the micro-field Eq. (2.12) and assembling the terms with equal powers of ε, the average field equations of infinite order read, at the second order ε^2,

$$n^{(2,0)}_{ipq_1q_2}\frac{\partial^2\hat{U}^M_p}{\partial x_{q_1}\partial x_{q_2}}-n^{(2,2)}_{ip}s^2\hat{U}^M_p+\varepsilon\Big(n^{(3,0)}_{ipq_1q_2q_3}\frac{\partial^3\hat{U}^M_p}{\partial x_{q_1}\partial x_{q_2}\partial x_{q_3}}+n^{(3,2)}_{ipq_1}s^2\frac{\partial\hat{U}^M_p}{\partial x_{q_1}}\Big)+$$

$$+\varepsilon^2\Big(n^{(4,0)}_{ipq_1q_2q_3q_4}\frac{\partial^4\hat{U}^M_p}{\partial x_{q_1}\partial x_{q_2}\partial x_{q_3}\partial x_{q_4}}+n^{(4,2)}_{ipq_1q_2}s^2\frac{\partial^2\hat{U}^M_p}{\partial x_{q_1}\partial x_{q_2}}-n^{(4,4)}_{ip}s^4\hat{U}^M_p\Big)+..$$

$$...+\hat{b}_i(\boldsymbol{x},s)=0, \tag{2.69}$$

where the coefficients of the gradients of the transformed macro-displacement are the known terms of the corresponding cell problems. Thus, it results

$$n^{(2,0)}_{ipq_1q_2}=\frac{1}{2}\langle\hat{C}^m_{iq_2hq_1}+\hat{C}^m_{iq_2hk}N^{(1,0)}_{hpq_1,k}+\hat{C}^m_{iq_1hq_2}+\hat{C}^m_{iq_1hk}N^{(1,0)}_{hpq_2,k}\rangle, \tag{2.70}$$

$$n^{(2,2)}_{ip}=\delta_{ip}\langle\rho^m\rangle, \tag{2.71}$$

$$n^{(w+2,0)}_{ipq_1\dots q_{w+2}}=\frac{1}{w+2}\sum_{P^*(q)}\langle\hat{C}^m_{iq_{w+2}hj}N^{(w+1,0)}_{hpq_1\dots q_{w+1},j}+\hat{C}^m_{iq_{w+2}hq_{w+1}}N^{(w,0)}_{hpq_1\dots q_w}\rangle, \tag{2.72}$$

$$n^{(3,2)}_{ipq_1}=\langle\rho^m N^{(1,0)}_{ipq_1}-\hat{C}^m_{iq_1hj}N^{(2,2)}_{hp,j}\rangle, \tag{2.73}$$

$$n^{(4,2)}_{ipq_1q_2}=\frac{1}{2}\langle\rho^m N^{(2,0)}_{ipq_1q_2}-\hat{C}^m_{iq_2hq_1}N^{(2,2)}_{hp}-\hat{C}^m_{iq_2hk}N^{(3,2)}_{hpq_1,k}+\rho^m N^{(2,0)}_{ipq_2q_1}+$$

$$-\hat{C}^m_{iq_1hq_2}N^{(2,2)}_{hp}-\hat{C}^m_{iq_1hk}N^{(3,2)}_{hpq_2,k}\rangle, \tag{2.74}$$

where $w\in\mathbb{Z}$ and $w\geq 1$. Eq.(2.69) is expanded at the infinite order as

$$n^{(2,0)}_{ipq_1q_2}\frac{\partial^2\hat{U}^M_p}{\partial x_{q_1}\partial x_{q_2}}-n^{(2,2)}_{ip}s^2\hat{U}^M_p+\sum_{n=0}^{+\infty}\varepsilon^{n+1}\sum_{|q|=n+3}n^{(n+3,0)}_{ipq}\frac{\partial^{n+3}\hat{U}^M_p}{\partial x_q}+$$

$$+\sum_{n=0}^{+\infty}\varepsilon^{n+1}\sum_{|q|=n+1}n^{(n+3,2)}_{ipq}s^2\frac{\partial^{n+1}\hat{U}^M_p}{\partial x_q}-\sum_{\tilde{n}=0}^{+\infty}\varepsilon^{2\tilde{n}+2}n^{(2\tilde{n}+4,2\tilde{n}+4)}_{ip}s^{2\tilde{n}+4}\hat{U}^M_p+$$

$$-\sum_{\tilde{n},n=0}^{+\infty}\varepsilon^{2\tilde{n}+n+3}\sum_{|q|=n+1}n^{(2\tilde{n}+n+5,2\tilde{n}+4)}_{ipq}s^{2\tilde{n}+4}\frac{\partial^{n+1}\hat{U}^M_p}{\partial x_q}+\hat{b}_i(\boldsymbol{x},s)=0, \tag{2.75}$$

where

$$n_{ipq_1\dots q_{w+2}}^{(w+4,2)} = \frac{1}{w+2}\sum_{P^*(q)}\langle \rho^m N_{ipq_1\dots q_{w+2}}^{(w+2,0)} +$$

$$- \hat{C}_{iq_{w+2}hq_{w+1}}^m N_{hpq_1\dots q_w}^{(w+2,2)} - \hat{C}_{iq_{w+2}hj}^m N_{hpq_1\dots q_{w+1},j}^{(w+3,2)}\rangle, \tag{2.76}$$

$$n_{ip}^{(2\tilde{n}+4,2\tilde{n}+4)} = \langle \rho^m N_{ip}^{(2\tilde{n}+2,2\tilde{n}+2)}\rangle, \tag{2.77}$$

$$n_{ipq_1}^{(2\tilde{n}+5,2\tilde{n}+4)} = \langle \rho^m N_{ipq_1}^{(2\tilde{n}+3,2\tilde{n}+2)} - \hat{C}_{iq_1hk}^m N_{hp,k}^{(2\tilde{n}+4,2\tilde{n}+4)}\rangle, \tag{2.78}$$

$$n_{ipq_1q_2}^{(2\tilde{n}+6,2\tilde{n}+4)} = \frac{1}{2}\langle \rho^m N_{ipq_1q_2}^{(2\tilde{n}+4,2\tilde{n}+4)} - \hat{C}_{iq_2hq_1}^m N_{hp}^{(2\tilde{n}+4,2\tilde{n}+4)} +$$

$$- \hat{C}_{iq_2hj}^m N_{hpq_1,j}^{(2\tilde{n}+5,2\tilde{n}+4)} + \rho^m N_{ipq_2q_1}^{(2\tilde{n}+4,2\tilde{n}+2)} - \hat{C}_{iq_1hq_2}^m N_{hp}^{(2\tilde{n}+4,2\tilde{n}+2)} +$$

$$- \hat{C}_{iq_1hj}^m N_{hpq_2,j}^{(2\tilde{n}+5,2\tilde{n}+4)}\rangle,$$

$$n_{ipq_1\dots q_{w+2}}^{(2\tilde{n}+w+6,2\tilde{n}+w+4)} = \frac{1}{w+2}\sum_{P^*(q)}\langle \rho^m N_{ipq_1\dots q_{w+2}}^{(2\tilde{n}+w+4,2\tilde{n}+2)} +$$

$$- \hat{C}_{iq_{w+2}hq_{w+1}}^m N_{hpq_1\dots q_w}^{(2\tilde{n}+w+4,2\tilde{n}+4)} - \hat{C}_{iq_{w+2}hj}^m N_{hpq_1\dots q_{w+1},j}^{(2\tilde{n}+w+5,2\tilde{n}+4)}\rangle, \tag{2.79}$$

with $w \in \mathbb{Z}$, $w \geq 1$, $\tilde{n} \in \mathbb{Z}$ and $\tilde{n} \geq 0$. The average field equations of infinite order (2.75) are formally solved by performing an asymptotic expansion of the transformed macro-displacement $\hat{U}_p^M(\boldsymbol{x})$ in power of ε, namely

$$\hat{U}_p^M(\boldsymbol{x}) = \sum_{j=0}^{+\infty}\varepsilon^j U_p^j(\boldsymbol{x}). \tag{2.80}$$

The substitution of Eq. (2.80) into Eq. (2.75) leads to

$$n_{ipq_1q_2}^{(2,0)}\left(\varepsilon^0\frac{\partial^2\hat{U}_p^{(0)}}{\partial x_{q_1}\partial x_{q_2}} + \varepsilon\frac{\partial^2\hat{U}_p^{(1)}}{\partial x_{q_1}\partial x_{q_2}} + \dots\right) - n_{ip}^{(2,2)}s^2(\hat{U}_p^{(0)} + \varepsilon\hat{U}_p^{(1)} + \dots) +$$

$$+\varepsilon n^{(3,0)}_{ipq_1\dots q_3}\Big(\frac{\partial^3\hat{U}^{(0)}_p}{\partial x_{q_1}\dots\partial x_{q_3}}+\varepsilon\frac{\partial^3\hat{U}^{(1)}_p}{\partial x_{q_1}\dots\partial x_{q_3}}+\dots\Big)+$$

$$+\varepsilon^2 n^{(4,0)}_{ipq_1\dots q_4}\Big(\frac{\partial^4\hat{U}^{(0)}_p}{\partial x_{q_1}\dots\partial x_{q_4}}+\varepsilon\frac{\partial^4\hat{U}^{(1)}_p}{\partial x_{q_1}\dots\partial x_{q_4}}+\dots\Big)+$$

$$+\dots-\varepsilon n^{(3,2)}_{ipq_1}s^2\Big(\frac{\partial\hat{U}^{(0)}_p}{\partial x_{q_1}}+\varepsilon\frac{\partial\hat{U}^{(1)}_p}{\partial x_{q_1}}+\dots\Big)+$$

$$-\varepsilon^2 n^{(4,2)}_{ipq_1q_2}s^2\Big(\frac{\partial^2\hat{U}^{(0)}_p}{\partial x_{q_1}\partial x_{q_2}}+\varepsilon\frac{\partial^2\hat{U}^{(1)}_p}{\partial x_{q_1}\partial x_{q_2}}+\dots\Big)+$$

$$+\dots-\varepsilon^2 n^{(4,4)}_{ip}s^4\Big(\hat{U}^{(0)}_p+\varepsilon\hat{U}^{(1)}+\dots\Big)-\varepsilon^4 n^{(6,6)}_{ip}s^6\Big(\hat{U}^{(0)}_p+\varepsilon\hat{U}^{(1)}+\dots\Big)+\dots+$$

$$+\varepsilon^3 n^{(5,4)}_{ipq_1}s^4\Big(\frac{\partial\hat{U}^{(0)}_p}{\partial x_{q_1}}+\varepsilon\frac{\partial\hat{U}^{(1)}_p}{\partial x_{q_1}}+\dots\Big)+$$

$$-\varepsilon^4 n^{(6,4)}_{ipq_1q_2}s^4\Big(\frac{\partial^2\hat{U}^{(0)}_p}{\partial x_{q_1}\partial x_{q_2}}+\varepsilon\frac{\partial^2\hat{U}^{(1)}_p}{\partial x_{q_1}\partial x_{q_2}}+\dots\Big)+\dots+$$

$$+\varepsilon^5 n^{(7,6)}_{ipq_1}s^6\Big(\frac{\partial^8\hat{U}^{(0)}_p}{\partial x_{q_1}}+\varepsilon\frac{\partial\hat{U}^{(1)}_p}{\partial x_{q_1}}+\dots\Big)+$$

$$-\varepsilon^6 n^{(8,6)}_{ipq_1q_2}s^6\Big(\frac{\partial^2\hat{U}^{(0)}_p}{\partial x_{q_1}\partial x_{q_2}}+\varepsilon\frac{\partial^2\hat{U}^{(1)}_p}{\partial x_{q_1}\partial x_{q_2}}+\dots\Big)+\dots+\hat{b}_i(\boldsymbol{x},s)=0, \qquad (2.81)$$

which provides the following macroscopic recursive problems for the different orders of ε. Namely, at the order ε^0 it results

$$n^{(2,0)}_{ipq_1q_2}\frac{\partial^2\hat{U}^{(0)}_p}{\partial x_{q_1}\partial x_{q_2}}-n^{(2,2)}_{ip}s^2\hat{U}^{(0)}_p+b_i(\boldsymbol{x})=0, \qquad (2.82)$$

at the order ε the problem is

$$n^{(2,0)}_{ipq_1q_2}\frac{\partial^2\hat{U}^{(1)}_p}{\partial x_{q_1}\partial x_{q_2}} - n^{(2,2)}_{ip}s^2\hat{U}^{(1)}_p + n^{(3,0)}_{ipq_1\dots q_3}\frac{\partial^3\hat{U}^{(0)}_p}{\partial x_{q_1}\dots\partial x_{q_3}} - n^{(3,2)}_{ipq_1}s^2\frac{\partial\hat{U}^{(0)}_p}{\partial x_{q_1}} = 0, \tag{2.83}$$

instead at the order ε^2 it reads

$$n^{(2,0)}_{ipq_1q_2}\frac{\partial^2\hat{U}^{(2)}_p}{\partial x_{q_1}\partial x_{q_2}} - n^{(2,2)}_{ip}s^2\hat{U}^{(2)}_p + n^{(3,0)}_{ipq_1\dots q_3}\frac{\partial^3\hat{U}^{(1)}_p}{\partial x_{q_1}\dots\partial x_{q_3}} +$$

$$+ n^{(4,0)}_{ipq_1\dots q_4}\frac{\partial^4\hat{U}^{(0)}_p}{\partial x_{q_1}\dots\partial x_{q_4}} - n^{(3,2)}_{ipq_1}s^2\frac{\partial\hat{U}^{(0)}_p}{\partial x_{q_1}} - n^{(4,2)}_{ipq_1q_2}s^2\frac{\partial^2\hat{U}^{(0)}_p}{\partial x_{q_1}\partial x_{q_2}} - n^{(4,4)}_{ip}s^4\hat{U}^0_p = 0. \tag{2.84}$$

A generic recursive problem, at odd order $\varepsilon^{2\tilde{w}-1}$, with $\tilde{w}\in\mathbb{Z}$ and $\tilde{w}\geq 2$ is

$$n^{(2\tilde{w}-1,0)}_{ipq_1q_2}\frac{\partial^2\hat{U}^{(2\tilde{w}-1)}_p}{\partial x_{q_1}\partial x_{q_2}} - n^{(2\tilde{w}-1,2\tilde{w}-1)}_{ip}s^2\hat{U}^{(2\tilde{w}-1)}_p +$$

$$+\sum_{r=3}^{2\tilde{w}+1}\sum_{|q|=r} n^{(r,0)}_{ipq}\frac{\partial^r\hat{U}^{(2\tilde{w}+1-r)}_p}{\partial x_q} +$$

$$-s^2\sum_{r=3}^{2\tilde{w}+1}\sum_{|q|=r-2} n^{(r,2)}_{ipq}\frac{\partial^{r-2}\hat{U}^{(2\tilde{w}+1-r)}_p}{\partial x_q} +$$

$$-(1-\delta_{2\tilde{w}})\sum_{n=0}^{\tilde{w}-3+\delta_{2\tilde{w}}} s^{2n+4}\left(n^{(2n+4,2n+4)}_{ip}\hat{U}^{(2\tilde{w}-3-2n)}_p\right) +$$

$$+\sum_{r=3}^{2\tilde{w}-1-2n}\sum_{|q|=r-2} n^{(r+2+2n,2n+4)}_{ipq}\frac{\partial^{r-2}\hat{U}^{(2\tilde{w}-1-r-2n)}_p}{\partial x_q} +$$

$$- n_{ip}^{(2\tilde{w},2\tilde{w})} s^{2\tilde{w}} \hat{U}_p^{(1)} - n_{ipq_1}^{(2\tilde{w},2\tilde{w})} s^{2\tilde{w}} \frac{\hat{U}_p^{(0)}}{\partial x_{q_1}} = 0, \tag{2.85}$$

whereas a generic recursive problem at even order $\varepsilon^{2\tilde{w}}$ is

$$n_{ipq_1q_2}^{(2\tilde{w},0)} \frac{\partial^2 \hat{U}_p^{(2\tilde{w})}}{\partial x_{q_1} \partial x_{q_2}} - n_{ip}^{(2\tilde{w},2\tilde{w})} s^2 \hat{U}_p^{(2\tilde{w})} + \sum_{r=3}^{2\tilde{w}+2} \sum_{|q|=r} n_{ipg}^{(r,0)} \frac{\partial^r \hat{U}_p^{(2\tilde{w}+1-r)}}{\partial x_q} +$$

$$- s^2 \sum_{r=3}^{2\tilde{w}+2} \sum_{|q|=r-2} n_{ipq}^{(r,2)} \frac{\partial^{r-2} \hat{U}_p^{(2\tilde{w}+2-r)}}{\partial x_q} +$$

$$+ \sum_{r=3}^{2\tilde{w}-2n} \sum_{|q|=r-2} n_{ipq}^{(r+2+2n,2n+4)} \frac{\partial^{r-2} \hat{U}_p^{(2\tilde{w}-r-2n)}}{\partial x_q} +$$

$$- n_{ip}^{(2\tilde{w}+2,2\tilde{w}+2)} s^{2\tilde{w}+2} \hat{U}_p^{(0)} = 0, \tag{2.86}$$

where $n \in \mathbb{Z}$ and $n \geq 2$. There is no point in managing the averaged equation of infinite order (2.75). Furthermore, the ellepticity of the differential problem could be not guaranteed if Eq. (2.75) is truncated at a certain order. To overcome such a disadvantage, an asymptotic-variational approach is pursued.

2.7 Asymptotic expansion of the energy and second order homogenization

A finite order governing equation is herein provided by exploiting a variational-asymptotic procedure, see Smyshlyaev and Cherednichenko (2000) and Bacigalupo (2014). Let Λ be the energy-like functional, Fabrizio and Morro (1992), written in terms of the energy-like density λ_m at the micro-scale and referred to the periodic domain L,

$$\Lambda = \int_L \lambda_m\Big(\boldsymbol{x}, \frac{\boldsymbol{x}}{\varepsilon}\Big) d\boldsymbol{x} = \int_L \Big(\frac{1}{2}\rho^m \dot{\boldsymbol{u}} * \dot{\boldsymbol{u}} + \frac{1}{2}\nabla \boldsymbol{u} * (\mathbb{G}^m * \nabla \dot{\boldsymbol{u}}) - \boldsymbol{u} * \boldsymbol{b}\Big) d\boldsymbol{x}. \tag{2.87}$$

Let $\mathcal{L}(\Lambda)$ be the energy-like functional in the Laplace domain, which is expressed in terms of the energy-like density $\hat{\lambda}_m$ in the Laplace domain

$$\hat{\Lambda} = \mathcal{L}(\Lambda) = \int_L \hat{\lambda}_m\Big(\boldsymbol{x}, \frac{\boldsymbol{x}}{\varepsilon}\Big) d\boldsymbol{x} = \int_L \Big(\frac{1}{2}\rho^m s^2 \hat{\boldsymbol{u}} \cdot \hat{\boldsymbol{u}} + \frac{1}{2}\nabla\hat{\boldsymbol{u}} : \hat{\mathbb{G}}^m \nabla\hat{\boldsymbol{u}} - \hat{\boldsymbol{u}} \cdot \hat{\boldsymbol{b}}\Big) d\boldsymbol{x}, \tag{2.88}$$

where the symbol : denotes the second order inner product.
The tranformed energy-like functional $\hat{\Lambda}$ and its corresponding energy-like density $\hat{\lambda}_m$ are influenced by the translation variable $\boldsymbol{\zeta} \in \mathcal{Q}$. Such a variable is introduced because the actual "phase" of the microstructure is undetectable and a family of translated microstructures is taken into account. Therefore, the transformed micro-relaxation tensor $\hat{\mathbb{G}}^m$ depends on the translation variable $\boldsymbol{\zeta}$ and it may be written as $\hat{\mathbb{G}}^{m,\zeta}\Big(\boldsymbol{x}, \frac{\boldsymbol{x}}{\varepsilon}\Big) = \hat{\mathbb{G}}^m\Big(\boldsymbol{x}, \frac{\boldsymbol{x}}{\varepsilon} + \boldsymbol{\zeta}\Big)$ and the perturbation functions $N^{(1,0)}_{hpq_1}, N^{(2,0)}_{hpq_1q_2}$, ..., which are solutions of the cell problems previously determined, reckon on variable $\boldsymbol{\zeta}$.
The energy-like density $\hat{\lambda}_m$ in the Laplace domain complies with the property $\hat{\lambda}^{\zeta}_m\Big(\boldsymbol{x}, \frac{\boldsymbol{x}}{\varepsilon}\Big) = \hat{\lambda}_m\Big(\boldsymbol{x}, \frac{\boldsymbol{x}}{\varepsilon} + \boldsymbol{\zeta}\Big)$ and so the Laplace transform of the energy-like functional Λ, depending on the parameter ζ, is

$$\hat{\Lambda}^{\zeta} = \hat{\Lambda}(\boldsymbol{\zeta}) = \int_L \hat{\lambda}^{\zeta}_m\Big(\boldsymbol{x}, \frac{\boldsymbol{x}}{\varepsilon}\Big) d\boldsymbol{x} = \int_L \hat{\lambda}_m\Big(\boldsymbol{x}, \frac{\boldsymbol{x}}{\varepsilon} + \boldsymbol{\zeta}\Big) d\boldsymbol{x}. \tag{2.89}$$

Let $\hat{\Lambda}_m$ be the average transformed energy-like functional at the microscale

$$\hat{\Lambda}_m \doteq \langle\hat{\Lambda}^{\zeta}\rangle = \frac{1}{|\mathcal{Q}|}\int_{\mathcal{Q}} \hat{\Lambda}^{\zeta} d\boldsymbol{\zeta} = \frac{1}{|\mathcal{Q}|}\int_{\mathcal{Q}} \hat{\Lambda}(\boldsymbol{\zeta}) d\boldsymbol{\zeta} = \int_L \Big\langle \hat{\lambda}_m\Big(\boldsymbol{x}, \frac{\boldsymbol{x}}{\varepsilon} + \boldsymbol{\zeta}\Big)\Big\rangle d\boldsymbol{x}, \tag{2.90}$$

where the Fubini theorem is applied.
The average transformed energy-like functional $\langle\hat{\Lambda}^{\zeta}\rangle$ at the microscale does not rely on the translation variable ζ because the energy-like functional $\hat{\Lambda}^{\zeta}$ is averaged with respect to the translated realizations of the microstructure and so the transformed energy-like density at the microscale satisfies

$$\Big\langle \hat{\lambda}_m\Big(\boldsymbol{x}, \frac{\boldsymbol{x}}{\varepsilon} + \boldsymbol{\zeta}\Big)\Big\rangle = \frac{1}{|\mathcal{Q}|}\int_{\mathcal{Q}} \hat{\lambda}_m\Big(\boldsymbol{x}, \frac{\boldsymbol{x}}{\varepsilon} + \boldsymbol{\zeta}\Big) d\boldsymbol{\zeta} =$$

$$= \frac{1}{|\mathcal{Q}|}\int_{\mathcal{Q}} \hat{\lambda}_m\Big(\boldsymbol{x},\boldsymbol{\xi}\Big)d\boldsymbol{\xi} = \langle\hat{\lambda}_m(\boldsymbol{x},\boldsymbol{\xi})\rangle. \tag{2.91}$$

Two methods are herein proposed to determine the governing field equation at the macroscale and the overall constitutive and inertial tensors.

2.7.1 *Approximation of the energy-like functional through truncation of its asymptotic expansion*

Let us consider the down scaling relation related to the transformed micro-displacement $\hat{\boldsymbol{u}}(\boldsymbol{x},\boldsymbol{\xi},s)$, i.e.

$$\hat{u}_h(\boldsymbol{x},\boldsymbol{\xi},s) = \hat{U}_h(\boldsymbol{x},s) + \varepsilon N^{(1,0)}_{hpq_1}(\boldsymbol{\xi})\frac{\partial\hat{U}^M_p}{\partial x_{q_1}} + \tag{2.92}$$

$$+\varepsilon^2\Big(N^{(2,0)}_{hpq_1q_2}(\boldsymbol{\xi})\frac{\partial^2\hat{U}^M_p}{\partial x_{q_1}\partial x_{q_2}} + N^{(2,2)}_{hp}(\boldsymbol{\xi})s^2\hat{U}^M_p\Big) +$$

$$+\varepsilon^3\Big(N^{(3,0)}_{hpq_1q_2q_3}(\boldsymbol{\xi})\frac{\partial^3\hat{U}^M_p}{\partial x_{q1}\partial x_{q2}\partial x_{q3}} + N^{(3,2)}_{hpq_1}(\boldsymbol{\xi})s^2\frac{\partial\hat{U}^M_p}{\partial x_{q1}}\Big) + O(\varepsilon^4).$$

Let us replace the down scaling relation (2.92) into the tranformed energy-like functional (2.89) and let us suppose that $\hat{\Lambda}_m$ is truncated at the second order. After applying the divergence theorem, the transformed energy-like functional at the second order is

$$\hat{\Lambda}^{II}_m = \int_L \langle\hat{\lambda}^{II}_m(\boldsymbol{x},\boldsymbol{\xi})\rangle d\boldsymbol{x} = \frac{1}{2}s^2\langle\rho^m\rangle\int_L \hat{U}^M_h\hat{U}^M_h d\boldsymbol{x} + \tag{2.93}$$

$$+\varepsilon s^2\langle\rho^m N^{(1,0)}_{rpq_1}\rangle\int_L \frac{\partial\hat{U}^M_p}{\partial x_{q_1}}\hat{U}^M_r d\boldsymbol{x} +$$

$$+\varepsilon s^3\langle\hat{G}^m_{hkij}B^{(1,0)}_{hkpq_1}B^{(2,2)}_{ijr}\rangle\int_L \frac{\partial\hat{U}^M_p}{\partial x_{q_1}}\hat{U}^M_r d\boldsymbol{x} +$$

$$+\varepsilon s\langle\hat{G}^m_{hkij}B^{(1,0)}_{hkpq_1}B^{(2,0)}_{ijrw_1w_2}\rangle\int_L \frac{\partial\hat{U}^M_p}{\partial x_{q_1}}\frac{\partial^2\hat{U}^M_r}{\partial x_{w_1}\partial x_{w_2}} d\boldsymbol{x} +$$

$$+\varepsilon^2 s^2\Big\langle\frac{1}{2}\rho^m N^{(1,0)}_{hpq_1}N^{(1,0)}_{hrq_2}-\rho^m N^{(2,0)}_{rpq_1q_2}\Big\rangle\int_L\frac{\partial\hat{U}^M_p}{\partial x_{q_1}}\frac{\partial\hat{U}^M_r}{\partial x_{q_2}}d\boldsymbol{x}+$$

$$+\varepsilon^2 s^3\langle\hat{G}^m_{hkij}B^{(1,0)}_{hkpq_1}B^{(3,2)}_{ijrq_2}-\hat{G}^m_{hkij}B^{(2,0)}_{hkpq_1q_2}B^{(2,2)}_{ijr}\rangle\int_L\frac{\partial\hat{U}^M_p}{\partial x_{q_1}}\frac{\partial\hat{U}^M_r}{\partial x_{q_2}}d\boldsymbol{x}+$$

$$+\varepsilon^2 s^4\langle\rho^m N^{(2,2)}_{rp}\rangle\int_L\hat{U}^M_p\hat{U}^M_r d\boldsymbol{x}+$$

$$+\varepsilon^2 s^5\frac{1}{2}\langle\hat{G}^m_{hkij}B^{(2,2)}_{hkp}B^{(2,2)}_{ijr}\rangle\int_L\hat{U}^M_p\hat{U}^M_r d\boldsymbol{x}+$$

$$+\frac{1}{2}s\langle\hat{G}^m_{hkij}B^{(1,0)}_{hkpq_1}B^{(1,0)}_{ijrw_1}\rangle\int_L\frac{\partial\hat{U}^M_p}{\partial x_{q_1}}\frac{\partial\hat{U}^M_r}{\partial x_{w_1}}d\boldsymbol{x}+$$

$$+\varepsilon^2 s\Big\langle\frac{1}{2}\hat{G}^m_{hkij}B^{(2,0)}_{hkpq_1q_2}B^{(2,0)}_{ijrw_1w_2}\Big\rangle\int_L\frac{\partial^2\hat{U}^M_p}{\partial x_{q_1}\partial x_{q_2}}\frac{\partial^2\hat{U}^M_r}{\partial x_{w_1}\partial x_{w_2}}d\boldsymbol{x}+$$

$$+\Big\langle\hat{G}^m_{hkij}B^{(1,0)}_{ijrw_1}B^{(3,0)}_{hkpq_1q_2w_2}\Big\rangle\int_L\frac{\partial^2\hat{U}^M_p}{\partial x_{q_1}\partial x_{q_2}}\frac{\partial^2\hat{U}^M_r}{\partial x_{w_1}\partial x_{w_2}}d\boldsymbol{x}-\frac{1}{s}\int_L\hat{U}^M_h b_h d\boldsymbol{x}.$$

It is important to note that second-order gradients of the transformed macro-displacement are takent into account as well as the first-order gradient of the displacement (i.e., strain), by generalizing the standard continuum mechanics.

The localization tensors, appearing in Eq. (2.93), assume the form

$$B^{(1,0)}_{hkpq_1}=\delta_{hp}\delta_{kq_1}+N^{(1,0)}_{hpq_1,k},\tag{2.94}$$

$$B^{(2,0)}_{hkpq_1q_2}=\frac{1}{2}\Big(\delta_{kq_2}N^{(1,0)}_{hpq_1}+\delta_{kq_1}N^{(1,0)}_{hpq_2}\Big)+N^{(2,0)}_{hpq_1q_2,k},\tag{2.95}$$

$$B^{(2,2)}_{hkp}=N^{(2,2)}_{hp,k},\tag{2.96}$$

$$B^{(3,0)}_{hkpq_1q_2q_3} = \frac{1}{3}\Big(\delta_{kq_3}N^{(2,0)}_{hpq_1q_2} + \delta_{kq_1}N^{(2,0)}_{hpq_2q_3} + \delta_{kq_2}N^{(2,0)}_{hpq_3q_1}\Big) + N^{(3,0)}_{hpq_1q_2q_3,k}, \tag{2.97}$$

$$B^{(3,2)}_{hkpq_1} = \delta_{kq_1}N^{(2,2)}_{hp} + N^{(3,2)}_{hpq_1,k}. \tag{2.98}$$

The localization tensors are periodic functions with respect to the fast coordinate $\boldsymbol{\xi}$ since the perturbation functions and their gradients are $\mathcal{Q}$-periodic functions. Both $B^{(2,0)}_{hkpq_1q_2}$ and $B^{(3,0)}_{hkpq_1q_2q_3}$ are symmetrized in A with respect to the indices q_1, q_2 and q_1, q_2, q_3, respectively.
The governing equation of a non-local homogeneous continuum is delivered by determining the stability condition of the transformed energy-like functional $\hat{\Lambda}^{II}_m$, which is found to be the first variation of the average transformed energy-like functional $\delta\hat{\Lambda}^{II}_m$.

Such a variation $\delta\hat{\Lambda}_m$ is computed by applying the Gâteaux derivative, Fabrizio and Morro (1992)

$$\delta\hat{\Lambda}_m(\hat{U}^M_t, \delta\hat{U}^M_t) = \frac{d}{d\eta}\hat{\Lambda}_m(\hat{U}^M_t + \eta\delta\hat{U}^M_t)\Big|_{\eta=0}. \tag{2.99}$$

According to (2.99), let $\hat{\Lambda}_m(\hat{U}^M_t + \eta\delta\hat{U}^M_t)$ be written in terms of the direction $\delta\hat{U}^M_t$ as

$$\hat{\Lambda}_m(\hat{U}^M_t + \eta\delta\hat{U}^M_t) = \frac{1}{2}s^2\langle\rho^m\rangle\int_L(\hat{U}^M_t + \eta\delta\hat{U}^M_t)(\hat{U}^M_t + \eta\delta\hat{U}^M_t)d\boldsymbol{x}+$$

$$+ s^2\varepsilon\langle N^{(1,0)}_{rpq_1}\rangle\int_L\Big(\frac{\partial\hat{U}^M_p}{\partial x_{q_1}} + \eta\frac{\partial\delta\hat{U}^M_p}{\partial x_{q_1}}\Big)(\hat{U}^M_r + \eta\delta\hat{U}^M_r)d\boldsymbol{x}+$$

$$+ \varepsilon s^3\langle\hat{G}^m_{hkij}B^{(1,0)}_{hkpq_1}B^{(2,2)}_{ijr}\rangle\int_L\Big(\frac{\partial\hat{U}^M_p}{\partial x_{q_1}} + \eta\frac{\partial\delta\hat{U}^M_p}{\partial x_{q_1}}\Big)(\hat{U}^M_r + \eta\delta\hat{U}^M_r)d\boldsymbol{x}+$$

$$+\varepsilon s\langle\hat{G}^m_{hkij}B^{(1,0)}_{hkpq_1}B^{(2,0)}_{ijrw_1w_2}\rangle\int_L\Big(\frac{\partial\hat{U}^M_p}{\partial x_{q_1}} + \eta\frac{\partial\delta\hat{U}^M_p}{\partial x_{q_1}}\Big)\Big(\frac{\partial^2\hat{U}^M_r}{\partial x_{w_1}\partial x_{w_2}} + \eta\frac{\partial^2\delta\hat{U}^M_r}{\partial x_{w_1}\partial x_{w_2}}\Big)d\boldsymbol{x}+$$

$$+\varepsilon^2 s^2 \Big\langle \frac{1}{2}\rho^m N^{(1,0)}_{hpq_1} N^{(1,0)}_{hrq_2} \Big\rangle \int_L \Big(\frac{\partial \hat{U}^M_p}{\partial x_{q_1}} + \eta \frac{\partial \delta \hat{U}^M_p}{\partial x_{q_1}}\Big)\Big(\frac{\partial \hat{U}^M_r}{\partial x_{q_2}} + \eta \frac{\partial \delta \hat{U}^M_r}{\partial x_{q_2}}\Big) d\boldsymbol{x} +$$

$$- \varepsilon^2 s^2 \Big\langle \rho^m N^{(2,0)}_{rpq_1q_2} \Big\rangle \int_L \Big(\frac{\partial \hat{U}^M_p}{\partial x_{q_1}} + \eta \frac{\partial \delta \hat{U}^M_p}{\partial x_{q_1}}\Big)\Big(\frac{\partial \hat{U}^M_r}{\partial x_{q_2}} + \eta \frac{\partial \delta \hat{U}^M_r}{\partial x_{q_2}}\Big) d\boldsymbol{x} +$$

$$+ \varepsilon^2 s^3 \langle \hat{G}^m_{hkij} B^{(1,0)}_{hkpq_1} B^{(3,2)}_{ijrq_2} \rangle \int_L \Big(\frac{\partial \hat{U}^M_p}{\partial x_{q_1}} + \eta \frac{\partial \delta \hat{U}^M_p}{\partial x_{q_1}}\Big)\Big(\frac{\partial \hat{U}^M_r}{\partial x_{q_2}} + \eta \frac{\partial \delta \hat{U}^M_r}{\partial x_{q_2}}\Big) d\boldsymbol{x} +$$

$$- \varepsilon^2 s^3 \langle \hat{G}^m_{hkij} B^{(2,0)}_{hkpq_1q_2} B^{(2,2)}_{ijr} \rangle \int_L \Big(\frac{\partial \hat{U}^M_p}{\partial x_{q_1}} + \eta \frac{\partial \delta \hat{U}^M_p}{\partial x_{q_1}}\Big)\Big(\frac{\partial \hat{U}^M_r}{\partial x_{q_2}} + \eta \frac{\partial \delta \hat{U}^M_r}{\partial x_{q_2}}\Big) d\boldsymbol{x} +$$

$$+ \varepsilon^2 s^4 \langle \rho^m N^{(2,2)}_{rp} \rangle \int_L (\hat{U}^M_p + \eta \delta \hat{U}^M_p)(\hat{U}^M_r + \eta \delta \hat{U}^M_r) d\boldsymbol{x} +$$

$$+ \varepsilon^2 s^5 \frac{1}{2} \langle \hat{G}^m_{hkij} B^{(2,2)}_{hkp} B^{(2,2)}_{ijr} \rangle \int_L (\hat{U}^M_p + \eta \delta \hat{U}^M_p)(\hat{U}^M_r + \eta \delta \hat{U}^M_r) d\boldsymbol{x} +$$

$$+ \frac{1}{2} s \langle \hat{G}^m_{hkij} B^{(1,0)}_{hkpq_1} B^{(1,0)}_{ijrw_1} \rangle \int_L \Big(\frac{\partial \hat{U}^M_p}{\partial x_{q_1}} + \eta \frac{\partial \delta \hat{U}^M_p}{\partial x_{q_1}}\Big)\Big(\frac{\partial \hat{U}^M_r}{\partial x_{w_1}} + \eta \frac{\partial \delta \hat{U}^M_r}{\partial x_{w_1}}\Big) d\boldsymbol{x} +$$

$$+ \varepsilon^2 s \Big\langle \frac{1}{2} \hat{G}^m_{hkij} B^{(2,0)}_{hkpq_1q_2} B^{(2,0)}_{ijrw_1w_2} - \hat{G}^m_{hkij} B^{(1,0)}_{ijrw_1} B^{(3,0)}_{hkpq_1q_2w_2} \Big\rangle \times$$

$$\times \int_L \Big(\frac{\partial^2 \hat{U}^M_p}{\partial x_{q_1} \partial x_{q_2}} + \eta \frac{\partial^2 \delta \hat{U}^M_r}{\partial x_{q_1} \partial x_{q_2}}\Big)\Big(\frac{\partial^2 \hat{U}^M_r}{\partial x_{w_1} \partial x_{w_2}} + \eta \frac{\partial^2 \delta \hat{U}^M_r}{\partial x_{w_1} \partial x_{w_2}}\Big) d\boldsymbol{x} +$$

$$- \int_L (\hat{U}^M_t + \eta \delta \hat{U}^m_t) \hat{b}_t d\boldsymbol{x}. \tag{2.100}$$

In accordance with the Gâteaux derivative (2.99), after performing the derivative of $\hat{\Lambda}_m(\hat{U}^M_t + \eta \delta \hat{U}^M_t)$ with respect to η, the condition $\eta = 0$ is imposed to (2.100) yielding to

$$\delta \hat{\Lambda}_m(\hat{U}^M_t, \delta \hat{U}^M_t) = \frac{1}{2} s^2 \langle \rho^m \rangle \int_L (\delta \hat{U}^M_t \hat{U}^M_t + \delta \hat{U}^M_t \hat{U}^M_t) d\boldsymbol{x} + \tag{2.101}$$

$$+ s^2\varepsilon\langle N^{(1,0)}_{rpq_1}\rangle \int_L \Big(\frac{\partial \hat{U}^M_p}{\partial x_{q_1}}\hat{U}^M_r + \frac{\partial \delta\hat{U}^M_p}{\partial x_{q_1}}\hat{U}^M_r\Big)d\boldsymbol{x}+$$

$$+ \varepsilon s^3\langle \hat{G}^m_{hkij}B^{(1,0)}_{hkpq_1}B^{(2,2)}_{ijr}\rangle \int_L \frac{\partial \delta\hat{U}^M_p}{\partial x_{q_1}}\hat{U}^M_r + \frac{\partial \hat{U}^M_p}{\partial x_{q_1}}\delta\hat{U}^M_r d\boldsymbol{x}+$$

$$+ \varepsilon s\langle \hat{G}^m_{hkij}B^{(1,0)}_{hkpq_1}B^{(2,0)}_{ijrw_1w_2}\rangle \int_L \frac{\partial \hat{U}^M_p}{\partial x_{q_1}}\frac{\partial^2 \delta\hat{U}^M_r}{\partial x_{w_1}\partial x_{w_2}} + \frac{\partial \delta\hat{U}^M_p}{\partial x_{q_1}}\frac{\partial^2 \hat{U}^M_r}{\partial x_{w_1}\partial x_{w_2}}d\boldsymbol{x}+$$

$$- \varepsilon^2 s^2\Big\langle \frac{1}{2}\rho^m N^{(1,0)}_{hpq_1}N^{(1,0)}_{hrq_2}\Big\rangle \int_L \frac{\partial \hat{U}^M_p}{\partial x_{q_1}}\frac{\partial \delta\hat{U}^M_r}{\partial x_{q_2}} + \frac{\partial \delta\hat{U}^M_p}{\partial x_{q_1}}\frac{\partial \hat{U}^M_r}{\partial x_{q_2}}d\boldsymbol{x}+$$

$$- \varepsilon^2 s^2\Big\langle \rho^m N^{(2,0)}_{rpq_1q_2}\Big\rangle \int_L \frac{\partial \hat{U}^M_p}{\partial x_{q_1}}\frac{\partial \delta\hat{U}^M_r}{\partial x_{q_2}} + \frac{\partial \delta\hat{U}^M_p}{\partial x_{q_1}}\frac{\partial \hat{U}^M_r}{\partial x_{q_2}}d\boldsymbol{x}+$$

$$+ \varepsilon^2 s^3\langle \hat{G}^m_{hkij}B^{(1,0)}_{hkpq_1}B^{(3,2)}_{ijrq_2}\rangle \int_L \Big(\frac{\partial \hat{U}^M_p}{\partial x_{q_1}}\frac{\partial \delta\hat{U}^M_r}{\partial x_{q_2}} + \frac{\partial \delta\hat{U}^M_p}{\partial x_{q_1}}\frac{\partial \hat{U}^M_r}{\partial x_{q_2}}\Big)d\boldsymbol{x}+$$

$$- \varepsilon^2 s^3\langle \hat{G}^m_{hkij}B^{(2,0)}_{hkpq_1q_2}B^{(2,2)}_{ijr}\rangle \int_L \Big(\frac{\partial \hat{U}^M_p}{\partial x_{q_1}}\frac{\partial \delta\hat{U}^M_r}{\partial x_{q_2}} + \frac{\partial \delta\hat{U}^M_p}{\partial x_{q_1}}\frac{\partial \hat{U}^M_r}{\partial x_{q_2}}\Big)d\boldsymbol{x}+$$

$$+ \varepsilon^2 s^4\langle \rho^m(N^{(2,2)}_{rp} + N^{(2,2)}_{pr})\rangle \int_L \hat{U}^M_p\delta\hat{U}^M_r d\boldsymbol{x}+$$

$$+ \varepsilon^2 s^5\frac{1}{2}\langle \hat{G}^m_{hkij}B^{(2,2)}_{hkp}B^{(2,2)}_{ijr} + \hat{G}^m_{hkij}B^{(2,2)}_{hkr}B^{(2,2)}_{ijp}\rangle \int_L \hat{U}^M_p\delta\hat{U}^M_r d\boldsymbol{x}+$$

$$- \frac{1}{2}s\langle \hat{G}^m_{hkij}B^{(1,0)}_{hkpq_1}B^{(1,0)}_{ijrw_1}\rangle \int_L \frac{\partial \hat{U}^M_p}{\partial x_{q_1}}\frac{\partial \delta\hat{U}^M_r}{\partial x_{w_1}} + \frac{\partial \delta\hat{U}^M_p}{\partial x_{q_1}}\frac{\partial \hat{U}^M_r}{\partial x_{w_1}}d\boldsymbol{x}+$$

$$- \frac{1}{2}s\langle \hat{G}^m_{hkij}B^{(1,0)}_{hkrw_1}B^{(1,0)}_{ijpq_1}\rangle \int_L \frac{\partial \hat{U}^M_p}{\partial x_{q_1}}\frac{\partial \delta\hat{U}^M_r}{\partial x_{w_1}} + \frac{\partial \delta\hat{U}^M_p}{\partial x_{q_1}}\frac{\partial \hat{U}^M_r}{\partial x_{w_1}}d\boldsymbol{x}+$$

$$+\varepsilon^2 s\Big\langle\frac{1}{2}\hat{G}^m_{hkij}B^{(2,0)}_{hkpq_1q_2}B^{(2,0)}_{ijrw_1w_2}-\hat{G}^m_{hkij}B^{(1,0)}_{ijrw_1}B^{(3,0)}_{hkpq_1q_2w_2}\Big\rangle\times$$

$$\int_L\Big(\frac{\partial^2\hat{U}^M_p}{\partial x_{q_1}\partial x_{q_2}}\frac{\partial^2\delta\hat{U}^M_r}{\partial x_{w_1}\partial x_{w_2}}+\frac{\partial^2\delta\hat{U}^M_r}{\partial x_{q_1}\partial x_{q_2}}\frac{\partial^2\hat{U}^M_r}{\partial x_{w_1}\partial x_{w_2}}\Big)d\boldsymbol{x}+$$

$$-\int_L\delta\hat{U}^m_t\hat{b}_t d\boldsymbol{x}.$$

The integration by parts applied to (2.101) issues line integrals along the boundary ∂L that vanish because of the $\mathcal{L}$-periodicity of the transformed macro-displacement $\hat{U}^M_p$ and the antiperiodicity of the outward normal vectors, resulting

$$\delta\hat{\Lambda}_m(\hat{U}^M_t,\delta\hat{U}^M_t)=s^2\langle\rho^m\rangle\int_L\hat{U}^M_t\delta\hat{U}^M_t d\boldsymbol{x}+ \tag{2.102}$$

$$+\varepsilon s^2\langle\rho^m(N^{(1,0)}_{rpq_1}-N^{(1,0)}_{prq_1})\rangle\int_L\frac{\partial\hat{U}^M_p}{\partial x_{q_1}}\delta\hat{U}^M_r d\boldsymbol{x}+$$

$$+\varepsilon s^3\langle\hat{G}^m_{hkij}B^{(1,0)}_{hkpq_1}B^{(2,2)}_{ijr}-\hat{G}^m_{hkij}B^{(1,0)}_{hkrq_1}B^{(2,2)}_{ijp}\rangle\int_L\frac{\partial\hat{U}^M_p}{\partial x_{q_1}}\delta\hat{U}^M_r d\boldsymbol{x}+$$

$$+\varepsilon s\langle\hat{G}^m_{hkij}B^{(1,0)}_{hkpq_1}B^{(2,0)}_{ijrw_1w_2}\rangle\int_L\frac{\partial^3\hat{U}^M_p}{\partial x_{w_1}\partial x_{w_2}\partial x_{q_1}}\delta\hat{U}^M_r d\boldsymbol{x}+$$

$$-\varepsilon s\langle\hat{G}^m_{hkij}B^{(1,0)}_{hkrw_1}B^{(2,0)}_{ijpq_1w_2}\rangle\int_L\frac{\partial^3\hat{U}^M_p}{\partial x_{w_1}\partial x_{w_2}\partial x_{q_1}}\delta\hat{U}^M_r d\boldsymbol{x}+$$

$$-\varepsilon^2 s^2\langle\frac{1}{2}\rho^m N^{(1,0)}_{hpq_1}N^{(1,0)}_{hrq_2}+\frac{1}{2}\rho^m N^{(1,0)}_{hrq_2}N^{(1,0)}_{hpq_1}\rangle\int_L\frac{\partial^2\hat{U}^M_p}{\partial x_{q_1}\partial x_{q_2}}\delta\hat{U}^M_r d\boldsymbol{x}+$$

$$-\varepsilon^2 s^2\langle\rho^m(N^{(2,0)}_{rpq_1q_2}+N^{(2,0)}_{prq_2q_1})\rangle\int_L\frac{\partial^2\hat{U}^M_p}{\partial x_{q_1}\partial x_{q_2}}\delta\hat{U}^M_r d\boldsymbol{x}+$$

$$- \varepsilon^2 s^3 \langle \hat{G}^m_{hkij} B^{(1,0)}_{hkpq_1} B^{(3,2)}_{ijrq_2} - \hat{G}^m_{hkij} B^{(2,0)}_{hkpq_1q_2} B^{(2,2)}_{ijp} \rangle \int_L \frac{\partial^2 \hat{U}^M_p}{\partial x_{q_1} \partial x_{q_2}} \delta \hat{U}^M_r d\boldsymbol{x} +$$

$$+ \varepsilon^2 s^3 \langle \hat{G}^m_{hkij} B^{(1,0)}_{hkrq_2} B^{(3,2)}_{ijpq_1} - \hat{G}^m_{hkij} B^{(2,0)}_{hkrq_2q_1} B^{(2,2)}_{ijp} \rangle \int_L \frac{\partial^2 \hat{U}^M_p}{\partial x_{q_1} \partial x_{q_2}} \delta \hat{U}^M_r d\boldsymbol{x} +$$

$$+ \varepsilon^2 s^4 \langle \rho^m (N^{(2,2)}_{rp} + N^{(2,2)}_{pr}) \rangle \int_L \hat{U}^M_p \delta \hat{U}^M_r d\boldsymbol{x} +$$

$$+ \varepsilon^2 s^5 \frac{1}{2} \langle \hat{G}^m_{hkij} B^{(2,2)}_{hkp} B^{(2,2)}_{ijr} + \hat{G}^m_{hkij} B^{(2,2)}_{hkr} B^{(2,2)}_{ijp} \rangle \int_L \hat{U}^M_p \delta \hat{U}^M_r d\boldsymbol{x} +$$

$$- \frac{1}{2} s \langle \hat{G}^m_{hkij} B^{(1,0)}_{hkpq_1} B^{(1,0)}_{ijrw_1} + \hat{G}^m_{hkij} B^{(1,0)}_{hkrw_1} B^{(1,0)}_{ijpq_1} \rangle \int_L \frac{\partial^2 \hat{U}^M_p}{\partial x_{w_1} \partial x_{q_1}} \delta \hat{U}^M_r d\boldsymbol{x} +$$

$$+ \varepsilon^2 s \langle \frac{1}{2} \hat{G}^m_{hkij} B^{(2,0)}_{hkpq_1q_2} B^{(2,0)}_{ijrw_1w_2} \rangle \int_L \frac{\partial^4 \hat{U}^M_p}{\partial x_{q_1} \partial x_{q_2} \partial x_{w_1} \partial x_{w_2}} \delta \hat{U}^M_r d\boldsymbol{x} +$$

$$- \varepsilon^2 s \langle \hat{G}^m_{hkij} B^{(1,0)}_{ijrw_1} B^{(3,0)}_{hkpq_1q_2w_2} \rangle \int_L \frac{\partial^4 \hat{U}^M_p}{\partial x_{q_1} \partial x_{q_2} \partial x_{w_1} \partial x_{w_2}} \delta \hat{U}^M_r d\boldsymbol{x} +$$

$$+ \varepsilon^2 s \langle \frac{1}{2} \hat{G}^m_{hkij} B^{(2,0)}_{hkrw_1w_2} B^{(2,0)}_{ijpq_1q_2} \rangle \int_L \frac{\partial^4 \hat{U}^M_p}{\partial x_{q_1} \partial x_{q_2} \partial x_{w_1} \partial x_{w_2}} \delta \hat{U}^M_r d\boldsymbol{x} +$$

$$- \varepsilon^2 s \langle \hat{G}^m_{hkij} B^{(1,0)}_{ijpq_1} B^{(3,0)}_{hkrw_1w_2q_2} \rangle \int_L \frac{\partial^4 \hat{U}^M_p}{\partial x_{q_1} \partial x_{q_2} \partial x_{w_1} \partial x_{w_2}} \delta \hat{U}^M_r d\boldsymbol{x} +$$

$$- \int_L \delta \hat{U}^M_t \hat{b}_t d\boldsymbol{x}.$$

The major simmetry property fulfilled by the viscoelastic tensor $\hat{G}^m_{hkij}$, i.e. $\hat{G}^m_{hkij} = \hat{G}^m_{ijhk}$, is employed to Eq. (2.102), leading to

$$\delta \hat{\Lambda}^{II}_m (\hat{U}^M_t, \delta \hat{U}^M_t) = s^2 \langle \rho^m \rangle \int_L \hat{U}^M_t \delta \hat{U}^M_t d\boldsymbol{x} + \tag{2.103}$$

$$+\varepsilon s^2\langle\rho^m(N^{(1,0)}_{rpq_1}-N^{(1,0)}_{prq_1})\rangle\int_L\frac{\partial\hat{U}^M_p}{\partial x_{q_1}}\delta\hat{U}^M_r d\boldsymbol{x}+$$

$$+\varepsilon s^3\langle\hat{G}^m_{hkij}B^{(1,0)}_{hkpq_1}B^{(2,2)}_{ijr}-\hat{G}^m_{hkij}B^{(1,0)}_{hkrq_1}B^{(2,2)}_{ijp}\rangle\int_L\frac{\partial\hat{U}^M_p}{\partial x_{q_1}}\delta\hat{U}^M_r d\boldsymbol{x}+$$

$$+\varepsilon s\langle\hat{G}^m_{hkij}B^{(1,0)}_{hkpq_1}B^{(2,0)}_{ijrw_1w_2}\rangle\int_L\frac{\partial^3\hat{U}^M_p}{\partial x_{w_1}\partial x_{w_2}\partial x_{q_1}}\delta\hat{U}^M_r d\boldsymbol{x}+$$

$$-\varepsilon s\langle\hat{G}^m_{hkij}B^{(1,0)}_{hkrw_1}B^{(2,0)}_{ijpq_1w_2}\rangle\int_L\frac{\partial^3\hat{U}^M_p}{\partial x_{w_1}\partial x_{w_2}\partial x_{q_1}}\delta\hat{U}^M_r d\boldsymbol{x}+$$

$$-\varepsilon^2 s^2\langle\rho^m N^{(1,0)}_{hpq_1}N^{(1,0)}_{hrq_2}-\rho^m(N^{(2,0)}_{rpq_1q_2}+N^{(2,0)}_{prq_2q_1})\rangle\int_L\frac{\partial^2\hat{U}^M_p}{\partial x_{q_1}\partial x_{q_2}}\delta\hat{U}^M_r d\boldsymbol{x}+$$

$$-\varepsilon^2 s^3\langle\hat{G}^m_{hkij}B^{(1,0)}_{hkpq_1}B^{(3,2)}_{ijrq_2}-\hat{G}^m_{hkij}B^{(2,0)}_{hkpq_1q_2}B^{(2,2)}_{ijp}\rangle\int_L\frac{\partial^2\hat{U}^M_p}{\partial x_{q_1}\partial x_{q_2}}\delta\hat{U}^M_r d\boldsymbol{x}+$$

$$+\varepsilon^2 s^3\langle\hat{G}^m_{hkij}B^{(1,0)}_{hkrq_2}B^{(3,2)}_{ijpq_1}-\hat{G}^m_{hkij}B^{(2,0)}_{hkrq_2q_1}B^{(2,2)}_{ijp}\rangle\int_L\frac{\partial^2\hat{U}^M_p}{\partial x_{q_1}\partial x_{q_2}}\delta\hat{U}^M_r d\boldsymbol{x}+$$

$$+\varepsilon^2 s^4\langle\rho^m(N^{(2,2)}_{rp}+N^{(2,2)}_{pr})\rangle\int_L\hat{U}^M_p\delta\hat{U}^M_r d\boldsymbol{x}+$$

$$+\varepsilon^2 s^5\langle\hat{G}^m_{hkij}B^{(2,2)}_{hkp}B^{(2,2)}_{ijr}\rangle\int_L\hat{U}^M_p\delta\hat{U}^M_r d\boldsymbol{x}+$$

$$-s\langle\hat{G}^m_{hkij}B^{(1,0)}_{hkpq_1}B^{(1,0)}_{ijrw_1}\rangle\int_L\frac{\partial^2\hat{U}^M_p}{\partial x_{w_1}\partial x_{q_1}}\delta\hat{U}^M_r d\boldsymbol{x}+$$

$$+\varepsilon^2 s\langle\hat{G}^m_{hkij}B^{(2,0)}_{hkpq_1q_2}B^{(2,0)}_{ijrw_1w_2}\rangle\int_L\frac{\partial^4\hat{U}^M_p}{\partial x_{w_2}\partial x_{w_1}\partial x_{q_1}\partial x_{q_2}}\delta\hat{U}^M_r d\boldsymbol{x}+$$

$$- \varepsilon^2 s \langle \hat{G}^m_{hkij} B^{(1,0)}_{hkrq_1} B^{(3,0)}_{ijpq_1q_2w_2} \rangle \int_L \frac{\partial^4 \hat{U}^M_p}{\partial x_{w_2} \partial x_{w_1} \partial x_{q_1} \partial x_{q_2}} \delta \hat{U}^M_r d\boldsymbol{x} +$$

$$- \varepsilon^2 s \langle \hat{G}^m_{hkij} B^{(1,0)}_{hkpq_1} B^{(3,0)}_{ijrw_1w_2q_2} \rangle \int_L \frac{\partial^4 \hat{U}^M_p}{\partial x_{w_2} \partial x_{w_1} \partial x_{q_1} \partial x_{q_2}} \delta \hat{U}^M_r d\boldsymbol{x} +$$

$$- \int_L \delta \hat{U}^M_t \hat{b}_t d\boldsymbol{x},$$

where the $\mathcal{Q}-$periodicity of the functions $\hat{G}^m_{hkij}$, $N^{(1,0)}_{ipq_1}$, $N^{(2,0)}_{ipq_1q_2}$ and the localization tensors $B^{(1,0)}_{hkpq_1}$, $B^{(2,0)}_{hkpq_1q_2}$,..., $B^{(3,2)}_{hkpq_1}$ is taken into account.

The first variation $\delta \hat{\Lambda}^{II}_m$ must vanish for all admissible $\delta \hat{U}^M_t$ and so the Euler-Lagrangian differential equation associated with the variational problem (2.103) in the Laplace domain is

$$s^2 \rho \hat{U}^M_t + s^2 \rho (\hat{I}_{tpq_1} - \hat{\tilde{I}}_{tq_1p}) \frac{\partial \hat{U}^M_p}{\partial x_{q_1}} - s^2 \rho \hat{I}_{tq_2pq_1} \frac{\partial^2 \hat{U}^M_p}{\partial x_{q_1} \partial x_{q_2}} + s^4 \rho \hat{I}^\sharp_{tp} \hat{U}^M_p =$$

$$- s^3 (\hat{J}_{tpq_1} - \hat{\tilde{J}}_{tq_1p}) \frac{\partial \hat{U}^M_p}{\partial x_{q_1}} + s^3 \hat{J}^1_{tq_2pq_1} \frac{\partial^2 \hat{U}^M_p}{\partial x_{q_1} \partial x_{q_2}} +$$

$$- s^5 \hat{J}^\sharp_{tp} \hat{U}^M_p + s \hat{G}_{tr_1pq_1} \frac{\partial^2 \hat{U}^M_p}{\partial x_{q_1} \partial x_{r_1}} + s (\hat{Y}_{tr_1pq_1r_2} - \hat{\tilde{Y}}_{tr_1r_2pq_1}) \frac{\partial^3 \hat{U}^M_p}{\partial x_{r_1} \partial x_{r_2} \partial x_{q_1}} +$$

$$- s \hat{S}^1_{tr_1r_2pq_1q_2} \frac{\partial^4 \hat{U}^M_p}{\partial x_{q_1} \partial x_{q_2} \partial x_{r_1} \partial x_{r_2}} + \hat{b}_t, \tag{2.104}$$

which is formulated in terms of the transformed macro-displacement and its gradients up to the fourth order. The components of the constitutive tensors in the Laplace domain related to the homogenized continuum are defined as

$$\hat{G}_{tr_1pq_1} = \langle \hat{G}^m_{hkij} B^{(1,0)}_{hkpq_1} B^{(1,0)}_{ijtr_1} \rangle, \tag{2.105}$$

$$\hat{Y}_{tr_1pq_1r_2} = \varepsilon\langle \hat{G}^m_{hkij} B^{(1,0)}_{hktr_1} B^{(2,0)}_{ijpq_1r_1} \rangle, \tag{2.106}$$

$$\hat{\tilde{Y}}_{tr_1r_2pq_1} = \hat{Y}_{pq_1tr_1r_2} = \varepsilon\langle \hat{G}^m_{hkij} B^{(1,0)}_{hkpq_1} B^{(2,0)}_{ijtr_1r_2} \rangle, \tag{2.107}$$

$$\hat{S}^1_{tr_1r_2pq_1q_2} = \varepsilon^2\langle \hat{G}^m_{hkij} B^{(2,0)}_{hkpq_1q_2} B^{(2,0)}_{hktr_1r_2} + \tag{2.108}$$

$$- \hat{G}^m_{hkij} B^{(1,0)}_{ijtr_1} B^{(3,0)}_{hkpq_1q_2r_2} - \hat{G}^m_{hkij} B^{(1,0)}_{ijpq_1} B^{(3,0)}_{hktr_1r_2q_2} \rangle,$$

$$\hat{J}_{tpq_1} = \varepsilon\langle \hat{G}^m_{hkij} B^{(1,0)}_{hkpq_1} B^{(2,2)}_{ijt} \rangle, \tag{2.109}$$

$$\hat{\tilde{J}}_{tq_1p} = \hat{J}_{ptq_1} = \varepsilon\langle \hat{G}^m_{hkij} B^{(1,0)}_{hktq_1} B^{(2,2)}_{ijp} \rangle, \tag{2.110}$$

$$\hat{J}^\sharp_{tp} = \hat{J}_{tp} + \hat{\tilde{J}}_{pt} = \frac{\varepsilon^2}{2}\langle \hat{G}^m_{hkij} B^{(2,2)}_{hkp} B^{(2,2)}_{ijt} \rangle + \frac{\varepsilon^2}{2}\langle \hat{G}^m_{hkij} B^{(2,2)}_{hkt} B^{(2,2)}_{ijp} \rangle =$$

$$= \varepsilon^2\langle \hat{G}^m_{hkij} B^{(2,2)}_{hkp} B^{(2,2)}_{ijt} \rangle, \tag{2.111}$$

$$\hat{J}^1_{tq_2pq_1} = \hat{J}^1_{pq_1tq_2} = -\varepsilon^2\langle -\hat{G}^m_{hkij} B^{(1,0)}_{hkpq_1} B^{(3,2)}_{ijtq_2} + \hat{G}^m_{hkij} B^{(2,0)}_{hkpq_1q_2} B^{(2,2)}_{ijp} +$$

$$- \hat{G}^m_{hkij} B^{(1,0)}_{hktq_2} B^{(3,2)}_{ijpq_1} + \hat{G}^m_{hkij} B^{(2,0)}_{hktq_2q_1} B^{(2,2)}_{ijt} \rangle, \tag{2.112}$$

where the components $\hat{G}^m_{tr_1pq_1}$, $\hat{Y}_{tr_1pq_1r_2}$ and $\hat{S}^1_{tr_1r_2pq_1q_2}$ of the constitutive tensors in the Laplace domain are computed due to the micro-fluctuation functions $N^{(1,0)}_{ikl}$, $N^{(2,0)}_{iklp}$ and $N^{(3,0)}_{iklpq}$. Such tensors are in accordance with the ones determined in Bagigalupo and Gambarotta (2014b).

The transformed inertial tensor components are given as

$$\rho = \langle \rho^m \rangle, \tag{2.113}$$

$$\hat{I}_{tpq_1} = \varepsilon\langle \rho^m N^{(1,0)}_{tpq_1} \rangle \frac{1}{\rho}, \tag{2.114}$$

$$\hat{\tilde{I}}_{tq_1p} = \hat{I}_{ptq_1} = \varepsilon\langle\rho^m N^{(1,0)}_{ptq_1}\rangle\frac{1}{\rho}, \tag{2.115}$$

$$\hat{I}^{\sharp}_{pt} = \hat{I}_{tp} + \hat{\tilde{I}}_{pt} = \varepsilon^2\langle\rho^m(N^{(2,2)}_{tp} + N^{(2,2)}_{pt})\rangle\frac{1}{\rho}, \tag{2.116}$$

$$\hat{I}_{tp} = \frac{\varepsilon^2}{\rho}\langle\rho^m N^{(2,2)}_{tp}\rangle, \tag{2.117}$$

$$\hat{\tilde{I}}_{pt} = \frac{\varepsilon^2}{\rho}\langle\rho^m N^{(2,2)}_{pt}\rangle, \tag{2.118}$$

$$\hat{I}_{tq_2pq_1} = \varepsilon^2\langle\rho^m N^{(1,0)}_{hpq_1}N^{(1,0)}_{htq_2} - \rho^m(N^{(2,0)}_{tpq_1q_2} + N^{(2,0)}_{tpq_2q_1})\rangle\frac{1}{\rho}. \tag{2.119}$$

The Euler-Lagrange Eq. (2.104), which has been derived through the truncation of the average transformed energy-like functional and the asymptotic development of the transformed micro-dispacement, is characterized by positive definite constitutive tensors. Thus, it is clear that the existence and the uniqueness of the solution of the dynamic problem is guaranteed by the validity of the Legendre-Hadamard condition.

2.7.2 *Approximation of the energy-like functional through truncation of the down-scaling relation*

An alternative approach is here presented to evaluate the overall constitutive and inertial tensors. To this purpose, the gradient referred to the down-scaling relation (2.92) is approximated at the first order as

$$\Big(\frac{D\hat{u}_h}{Dx_k}\Big)^I = \frac{\partial\hat{U}_h}{\partial x_k} + N^{(1,0)}_{hpq_1,k}\frac{\partial\hat{U}^M_p}{\partial x_{q_1}} + \varepsilon\Big(N^{(1,0)}_{hpq_1}\frac{\partial^2\hat{U}^M_p}{\partial x_{q_1}\partial x_{q_2}} + \tag{2.120}$$

$$+ N^{(2,0)}_{hpq_1q_2,k}(\boldsymbol{\xi})\frac{\partial^2\hat{U}^M_p}{\partial x_{q_1}\partial x_{q_2}} + N^{(2,2)}_{hp,k}(\boldsymbol{\xi})s^2\hat{U}^M_p\Big).$$

Moreover, the transformed micro-displacement at the second order is formulated as

$$\hat{u}_h^{II}(\boldsymbol{x},\boldsymbol{\xi},s) = \hat{U}_h(\boldsymbol{x},s) + \varepsilon N^{(1,0)}_{hpq_1}(\boldsymbol{\xi})\frac{\partial \hat{U}_p^M}{\partial x_{q_1}} + \tag{2.121}$$

$$+ \varepsilon^2\Big(N^{(2,0)}_{hpq_1q_2}(\boldsymbol{\xi})\frac{\partial^2 \hat{U}_p^M}{\partial x_{q_1}\partial x_{q_2}} + N^{(2,2)}_{hp}(\boldsymbol{\xi})s^2\hat{U}_p^M\Big),$$

where the perturbation functions are helpful to determine a consistent approximation of the gradient at the first order. Then, the gradient approximation (Eq. (2.120)) and the displacement approximation (Eq. (2.121)) are replaced into the transformed energy-like functional (2.90), which is approximated at the second order as

$$\hat{\Lambda}_m^{II} = \int_L \langle \hat{\lambda}_m^{II}(\boldsymbol{x},\boldsymbol{\xi})\rangle d\boldsymbol{x} = \frac{1}{2}s^2\langle\rho^m\rangle\int_L \hat{U}_h^M\hat{U}_h^M d\boldsymbol{x} + \tag{2.122}$$

$$+ \varepsilon s^2\langle\rho^m N^{(1,0)}_{rpq_1}\rangle\int_L \frac{\partial \hat{U}_p^M}{\partial x_{q_1}}\hat{U}_r^M d\boldsymbol{x} +$$

$$+ \varepsilon s^3\langle\hat{G}^m_{hkij}B^{(1,0)}_{hkpq_1}B^{(2,2)}_{ijr}\rangle\int_L \frac{\partial \hat{U}_p^M}{\partial x_{q_1}}\hat{U}_r^M d\boldsymbol{x} +$$

$$+ \varepsilon s\langle\hat{G}^m_{hkij}B^{(1,0)}_{hkpq_1}B^{(2,0)}_{ijrw_1w_2}\rangle\int_L \frac{\partial \hat{U}_p^M}{\partial x_{q_1}}\frac{\partial^2 \hat{U}_r^M}{\partial x_{w_1}\partial x_{w_2}} d\boldsymbol{x} +$$

$$+ \varepsilon^2 s^2\Big\langle\frac{1}{2}\rho^m N^{(1,0)}_{hpq_1}N^{(1,0)}_{hrq_2} - \rho^m N^{(2,0)}_{rpq_1q_2}\Big\rangle\int_L \frac{\partial \hat{U}_p^M}{\partial x_{q_1}}\frac{\partial \hat{U}_r^M}{\partial x_{q_2}} d\boldsymbol{x} +$$

$$+ \varepsilon^2 s^3\langle-\hat{G}^m_{hkij}B^{(2,0)}_{hkpq_1q_2}B^{(2,2)}_{ijr}\rangle\int_L \frac{\partial \hat{U}_p^M}{\partial x_{q_1}}\frac{\partial \hat{U}_r^M}{\partial x_{q_2}} d\boldsymbol{x} +$$

$$+ \varepsilon^2 s^4\langle\rho^m N^{(2,2)}_{rp}\rangle\int_L \hat{U}_p^M\hat{U}_r^M d\boldsymbol{x} +$$

$$+\varepsilon^2 s^5 \frac{1}{2}\langle \hat{G}^m_{hkij} B^{(2,2)}_{hkp} B^{(2,2)}_{ijr}\rangle \int_L \hat{U}^M_p \hat{U}^M_r d\boldsymbol{x}+$$

$$+\frac{1}{2} s\langle \hat{G}^m_{hkij} B^{(1,0)}_{hkpq_1} B^{(1,0)}_{ijrw_1}\rangle \int_L \frac{\partial \hat{U}^M_p}{\partial x_{q_1}} \frac{\partial \hat{U}^M_r}{\partial x_{w_1}} d\boldsymbol{x}+$$

$$+\varepsilon^2 s\Big\langle \frac{1}{2} \hat{G}^m_{hkij} B^{(2,0)}_{hkpq_1q_2} B^{(2,0)}_{ijrw_1w_2}\Big\rangle \int_L \frac{\partial^2 \hat{U}^M_p}{\partial x_{q_1}\partial x_{q_2}} \frac{\partial^2 \hat{U}^M_r}{\partial x_{w_1}\partial x_{w_2}} d\boldsymbol{x} - \int_L \hat{U}^M_h \hat{b}_h d\boldsymbol{x}.$$

In accordance with the procedure proposed in the previous section, the Euler-Lagrangian equation deriving from the first variation of the transformed energy-like functional (2.122) in the Laplace domain is

$$s^2\rho\hat{U}^M_t + s^2\rho(\hat{I}_{tpq_1} - \hat{\tilde{I}}_{tq_1p})\frac{\partial \hat{U}^M_p}{\partial x_{q_1}} - s^2\rho\hat{I}_{tq_2pq_1}\frac{\partial^2 \hat{U}^M_p}{\partial x_{q_1}\partial x_{q_2}} + s^4\rho\hat{I}^\sharp_{tp}\hat{U}^M_p =$$

$$= -s^3(\hat{J}_{tpq_1} - \hat{\tilde{J}}_{tq_1p})\frac{\partial \hat{U}^M_p}{\partial x_{q_1}} - s^3\hat{J}^2_{tq_2pq_1}\frac{\partial^2 \hat{U}^M_p}{\partial x_{q_1}\partial x_{q_2}}+$$

$$- s^5\hat{J}^\sharp_{tp}\hat{U}^M_p + s\hat{G}_{tr_1pq_1}\frac{\partial^2 \hat{U}^M_p}{\partial x_{q_1}\partial x_{r_1}} + s(\hat{Y}_{tr_1pq_1r_2} - \hat{\tilde{Y}}_{tr_1r_2pq_1})\frac{\partial^3 \hat{U}^M_p}{\partial x_{r_1}\partial x_{r_2}\partial x_{q_1}}+$$

$$- s\hat{S}^2_{tr_1r_2pq_1q_2}\frac{\partial^4 \hat{U}^M_p}{\partial x_{q_1}\partial x_{q_2}\partial x_{r_1}\partial x_{r_2}} + \hat{b}_t, \tag{2.123}$$

where the overall inertial tensors are (2.113), (2.114), (2.116), (2.119) and the overall constitutive tensors are (2.105), (2.106), (2.109), (2.111) respectively, and

$$\hat{S}^2_{tr_1r_2pq_1q_2} = \varepsilon^2\langle \hat{G}^m_{hkij} B^{(2,0)}_{hkpq_1q_2} B^{(2,0)}_{hktr_1r_2}\rangle, \tag{2.124}$$

$$\hat{J}^2_{tq_2pq_1} = \hat{J}^2_{pq_1tq_2} = -\varepsilon^2\langle \hat{G}^m_{hkij} B^{(2,0)}_{hkpq_1q_2} B^{(2,2)}_{ijp} + \hat{G}^m_{hkij} B^{(2,0)}_{hktq_2q_1} B^{(2,2)}_{ijt}\rangle. \tag{2.125}$$

By applying the inverse Laplace transform $\mathcal{L}^{-1}$ to Eq. (2.104) and Eq. (2.123), the field equation at the macro-scale related to Eq. (2.4) is recast in the time domain as

$$\rho\ddot{U}_t^M + \rho(I_{tpq_1} - \tilde{I}_{tq_1p}) * \frac{\partial\ddot{U}_p^M}{\partial x_{q_1}} - \rho I_{tq_2pq_1} * \frac{\partial^2\ddot{U}_p^M}{\partial x_{q_1}\partial x_{q_2}} + \rho I_{tp}^\sharp * \dddot{U}_p^M =$$

$$= -(\dot{J}_{tpq_1} - \dot{\tilde{J}}_{tq_1p}) * \frac{\partial\ddot{U}_p^M}{\partial x_{q_1}} - \dot{J}^i_{tq_2pq_1} * \frac{\partial^2\ddot{U}_p^M}{\partial x_{q_1}\partial x_{q_2}} +$$

$$- \dot{J}_{tp}^\sharp * \dddot{U}_p^M + G_{tr_1pq_1} * \frac{\partial^2\dot{U}_p^M}{\partial x_{q_1}\partial x_{r_1}} + (Y_{tr_1pq_1r_2} - \tilde{Y}_{tr_1r_2pq_1}) * \frac{\partial^3\dot{U}_p^M}{\partial x_{r_1}\partial x_{r_2}\partial x_{q_1}} +$$

$$- S^i_{tr_1r_2pq_1q_2} * \frac{\partial^4\dot{U}_p^M}{\partial x_{q_1}\partial x_{q_2}\partial x_{r_1}\partial x_{r_2}} + b_t, \tag{2.126}$$

where the superscript $i = 1$ denotes that the tensors $J^1_{tq_2pq_1}$ and $S^1_{tr_1r_2pq_1q_2}$ derive from the procedure described in Subsection 2.7.1, where the energy-like functional is approximated by means of its asymptotic expansion. The superscript $i = 2$ points out that the tensors $J^2_{tq_2pq_1}$ and $S^2_{tr_1r_2pq_1q_2}$ elicit from the approach presented in Subsection 2.7.2.
Moreover, the symbol $*$ stands for the convolution and the time derivative can be moved from the constitutive tensor to the variable.
The constitutive tensor components in the time domain are

$$G^m_{tr_1pq_1} = \mathcal{L}^{-1}(\hat{G}^m_{tr_1pq_1}), \tag{2.127}$$

$$(Y_{tr_1pq_1r_2} - \tilde{Y}_{tr_1r_2pq_1}) = \mathcal{L}^{-1}(\hat{Y}_{tr_1pq_1r_2} - \hat{\tilde{Y}}_{tr_1r_2pq_1}), \tag{2.128}$$

$$S^i_{tr_1r_2pq_1q_2} = \mathcal{L}^{-1}(\hat{S}^i_{tr_1r_2pq_1q_2}), \tag{2.129}$$

$$\dot{J}_{tpq_1} - \dot{\tilde{J}}_{tq_1p} = \mathcal{L}^{-1}(s(\hat{J}_{tpq_1} - \hat{\tilde{J}}_{tq_1p})), \tag{2.130}$$

$$\dot{J}^{i}_{tq_2pq_1} = \mathcal{L}^{-1}(s\hat{J}^{i}_{tq_2pq_1}), \tag{2.131}$$

$$\dot{J}^{\sharp}_{tp} = \mathcal{L}^{-1}(s\hat{J}^{\sharp}_{tp}), \tag{2.132}$$

with $i = \{1, 2\}$, whereas in the time domain the inertial tensor components and the acceleration result to be

$$(I_{tpq_1} - \tilde{I}_{tq_1p}) = \mathcal{L}^{-1}(\hat{I}_{tpq_1} - \hat{\tilde{I}}_{tq_1p}), \tag{2.133}$$

$$I_{tq_2pq_1} = \mathcal{L}^{-1}(\hat{I}_{tq_2pq_1}), \tag{2.134}$$

$$I^{\sharp}_{tp} = \mathcal{L}^{-1}(\hat{I}^{\sharp}_{tp}), \tag{2.135}$$

$$\ddot{U}^{M}_{t} = \mathcal{L}^{-1}(s^2\hat{U}^{M}_{t}). \tag{2.136}$$

In case of a locally homogeneous material, i.e. if the miscrostructure disappears, the perturbation functions $N^{(1,0)}_{ikl}$, $N^{(2,0)}_{iklp}$,...., $N^{(3,0)}_{iklpq}$ are zero and the components of the localization tensors vanish except for $B^{(1,0)}_{hkpq_1}$, which becomes $B^{(1,0)}_{hkpq_1} = \frac{1}{2}\Big(\delta_{hp}\delta_{kq_1} + \delta_{hq_1}\delta_{kp}\Big)$ and so the equation of motion of a classical homogeneous continuum is retrieved.

The problem of the numerical inverse Laplace transform has been extensively investigated in the literature, and different methods of solution have been proposed. A review of the methods can be found in Davies and Martin (1979). Moreover, Donolato (2002) proposed a method for inverting the Laplace-Carson transform by considering its property of conserving the physical dimensions of the original function. Therefore, the transform can be converted into a Mellin deconvolution problem, which is approximately solved by a differential method. In the work of Selivanov and Chernoivan (2007), a method for the numerical inversion of the Laplace transform using Padè approximation is proposed, which takes into account the viscoelastic characteristics of material.

Form an analytical point of view, see Paley (1934), the inverse Laplace transform of a function $\hat{f}(s)$ is defined as

$$\mathcal{L}^{-1}(\hat{f}(s)) = f(t) = \frac{1}{2\pi i}\int_{x-i\infty}^{x+i\infty} e^{ts}\hat{f}(s)ds, \tag{2.137}$$

which is evaluated as

$$f(t) = \frac{1}{2\pi i}\int_{x-i\infty}^{x+i\infty} e^{ts}\hat{f}(s)ds = \sum_{poles \quad of \quad \hat{f}(s)} R(\hat{f}(s)e^{ts}), \tag{2.138}$$

where R denotes the residual of $\hat{f}(s)e^{ts}$. In case of polar singularities, $\hat{f}(s)$ is written as a rational function, namely $\hat{f}(s) = \frac{P(s)}{Q(s)}$. Such a funaction has n poles, which can be divided into h groups. Each of them consists of r_k, ($k = 1..h$), coincident poles, namely p_1,...,p_h are poles characterized by the moltiplicities r_1,...,r_h, greater or equal to 1. Under those assumptions, $\hat{f}(s)$ is rewritten as

$$\hat{f}(s) = \frac{P(s)}{(s+p_1)^{r_1}(s+p_1)^{r_2}...(s+p_1)^{r_k}} = \sum_{k=1}^{h}\sum_{l=1}^{r_k}\frac{R_{kl}}{(s+p_1)^{r_k-l+1}}, \tag{2.139}$$

where the residuals R_{kl} related to $\hat{f}(s)$ are found as

$$R_{kl} = \frac{1}{(l-1)!}\Big[\frac{d^{l-1}}{ds^{l-1}}\Big((s+p_k)^{r_k}\frac{P(s)}{Q(s)}\Big)\Big]_{s=p_k}, l = 1...r_k, k = 1...h. \tag{2.140}$$

Finally, the inverse Laplace transform $f(t)$ has the form

$$f(t) = \sum_{k=1}^{h}\sum_{l=1}^{r_k}\frac{R_{kl}}{(r_k-l)}t^{r_k-l}e^{-p_k t}. \tag{2.141}$$

2.7.3 *Dispersive wave propagation*

The Laplace and the Fourier transforms are applied to Eq. (2.126) with respect to time t and to the slow variable $\boldsymbol{x}$ to obtain the field equation at the macro-scale within the frequency and the wave vector domain.
In particular, the two-sided Fourier transform of an arbitrary function $f(x)$ is defined as Paley (1934):

$$\mathcal{F}(f(\boldsymbol{x})) = \check{f}(k) = \int_{-\infty}^{+\infty} f(\boldsymbol{x})e^{\iota \boldsymbol{k}\cdot\boldsymbol{x}}d\boldsymbol{x} = \int_{-\infty}^{+\infty} f(\boldsymbol{x})e^{\iota k_s x_s}d\boldsymbol{x}, \quad \boldsymbol{k} \in \mathbb{R}^2, \tag{2.142}$$

where $\boldsymbol{k}$ is a bidimensional vector and so the field equation at the macroscale in the transformed space is rephrased as

$$s^2\rho\check{\hat{U}}_t^M + s^2\rho\iota(\hat{I}_{tpq_1} + \hat{\tilde{I}}_{tq_1p})\check{\hat{U}}_p^M k_{q_1} + s^2\rho\hat{I}_{tq_2pq_1}\check{\hat{U}}_p^M k_{q_1}k_{q_2} + s^4\rho\hat{I}_{tp}^\sharp\check{\hat{U}}_p^M =$$

$$- s^3\iota(\hat{J}_{tpq_1} - \hat{\tilde{J}}_{tq_1p})\check{\hat{U}}_p^M k_{q_1} - s^3\hat{J}_{tq_2pq_1}\check{\hat{U}}_p^M k_{q_1}k_{q_2} +$$

$$- s^5\hat{J}_{tp}^\sharp\check{\hat{U}}_p^M - s\hat{G}_{tr_1pq_1}\check{\hat{U}}_p^M k_{q_1}k_{r_2} - s\iota(\hat{Y}_{tr_1pq_1r_2} - \hat{\tilde{Y}}_{tr_1r_2pq_1})\check{\hat{U}}_p^M k_{r_1}k_{r_2}k_{q_1} +$$

$$- s\hat{S}^i_{tr_1r_2pq_1q_2}\check{\hat{U}}_p^M k_{q_1}k_{q_2}k_{r_1}k_{r_2} + \check{\tilde{b}}_t, \quad i = \{1,2\}. \tag{2.143}$$

The vector $\boldsymbol{k}$ is written respect to the wave director vector $\boldsymbol{n}$ as $\boldsymbol{k} = k\boldsymbol{n}$ ($k = ||\boldsymbol{k}||$ and $||\boldsymbol{n}|| = 1$), therefore the Eq. (2.143) becomes

$$s^2\rho\check{\hat{U}}_t^M + s^2\rho\iota(\hat{I}_{tpq_1} + \hat{\tilde{I}}_{tq_1p})\check{\hat{U}}_p^M kn_{q_1} + s^2\rho\hat{I}_{tq_2pq_1}\check{\hat{U}}_p^M k^2 n_{q_1}n_{q_2} + s^4\rho\hat{I}_{tp}^\sharp\check{\hat{U}}_p^M =$$

$$= -s^3\iota(\hat{J}_{tpq_1} - \hat{\tilde{J}}_{tq_1p})\check{\hat{U}}_p^M kn_{q_1} - s^3\hat{J}^i_{tq_2pq_1}\check{\hat{U}}_p^M k^2 n_{q_1}n_{q_2} - s^5\hat{J}_{tp}^\sharp\check{\hat{U}}_p^M +$$

$$- s\hat{G}_{tr_1pq_1}\check{\hat{U}}_p^M k^2 n_{q_1}n_{r_2} - s\iota(\hat{Y}_{tr_1pq_1r_2} - \hat{\tilde{Y}}_{tr_1r_2pq_1})\check{\hat{U}}_p^M k^3 n_{r_1}n_{r_2}n_{q_1} +$$

$$- s\hat{S}^i_{tr_1r_2pq_1q_2}\check{\hat{U}}_p^M k^4 n_{q_1}n_{q_2}n_{r_1}n_{r_2} + \check{\tilde{b}}_t, \quad i = \{1,2\}. \tag{2.144}$$

In case of an orthotropic material, the motion equation in the Laplace domain (2.123) along the direction $\boldsymbol{e}_\beta$ ($\beta = 1,2$) is rephased as

$$s^2\rho\hat{U}_\alpha^M - s^2\rho\hat{I}_{\alpha\beta\alpha\beta}\frac{\partial^2\hat{U}_\alpha}{\partial x_\beta^2} + s^4\rho\hat{I}_{\alpha\alpha}\hat{U}_\alpha^M = \tag{2.145}$$

$$= s^3\hat{J}^i_{\alpha\beta\alpha\beta}\frac{\partial^2\hat{U}_\alpha^M}{\partial x_\beta^2} - s^5\hat{J}_{\alpha\alpha}\hat{U}_\alpha^M + s\hat{G}_{\alpha\beta\alpha\beta}\frac{\partial^2\hat{U}_\alpha^M}{\partial x_\beta^2} - s\hat{S}^i_{\alpha\beta\beta\alpha\beta\beta}\frac{\partial^4\hat{U}_\alpha^M}{\partial x_\beta^4},$$

with $i = \{1,2\}$ and $\alpha = 1,2$.
The Fourier transform (2.142) is applied to Eq. (2.145) with respect to

the slow variable $\boldsymbol{x}$ to retrieve the Christoffel equation depending on the complex angular frequency s and the wave vector k_β,

$$(s^2\rho + s^2\rho\hat{I}_{\alpha\beta\alpha\beta}k_\beta^2 + s^4\rho\hat{I}_{\alpha\alpha} + s^3\hat{J}^i_{\alpha\beta\alpha\beta}k_\beta^2 + s^5\hat{J}_{\alpha\alpha} + s\hat{G}_{\alpha\beta\alpha\beta}k_\beta^2 +$$

$$+ s\hat{S}^i_{\alpha\beta\beta\alpha\beta\beta}k_\beta^4)\check{\hat{U}}^M_\alpha(k_\beta, s) = 0, \quad i = \{1, 2\}, \tag{2.146}$$

where $\check{\hat{U}}(k_\beta, s)$ stands for the Fourier transform of the transformed macro-displacement $\hat{U}(x, s)$. The Christoffel equation (2.146) defines the wave propagation in the viscoelastic medium that is embedded in the Laplace-Fourier space. The dispersion function stemmed from Eq. (2.146) is

$$s^2\rho + s^2\rho\hat{I}_{\alpha\beta\alpha\beta}k_\beta^2 + s^4\rho\hat{I}_{\alpha\alpha} + s^3\hat{J}^i_{\alpha\beta\alpha\beta}k_\beta^2 + s^5\hat{J}_{\alpha\alpha} +$$

$$+ s\hat{G}_{\alpha\beta\alpha\beta}k_\beta^2 + s\hat{S}^i_{\alpha\beta\beta\alpha\beta\beta}k_\beta^4 = 0, \quad i = \{1, 2\}. \tag{2.147}$$

The dispersion function describes the waves that propagate through the viscoelastic homogenized continuum with complex frequency s and wave vector k_β. It is worth noting that the complex group velocity might contain information about the energy transport as well as the energy dissipated in the medium, (Gerasik and Stastna (2010)), by interpreting the physical meaning of the imaginary part in the circumstance of a loss rate and the real part related to the axial wavenumber, see Sharma (2008) and Wolff et al. (2018).

Novelties and outline This Chapter dealt with the description of the field equations in the time domain and in the Laplace domain at the microscale. The recursive differential problems and their solutions are shown, in particular the higher order recursive differential problems are detailed and the cell problems and the related perturbation functions are introduced. The average field equations of infinite order is properly described. Moreover, by means of a variational approach, the overall constitutive tensors and the overall inertial tensor related to the homogenized continuum are derived in the Laplace domain for the class of periodic viscoelastic materials, after introducing the energy-like functional in

the Laplace domain. Later, the Euler-Lagrangian differential equation at the macro-scale is determined and expressed in terms of the transformed macro-displacement and its gradients up to the fourth order. Finally, the problem of wave propagation and the related dispersion curves is analysed.

Chapter 3

Assessment of the accuracy of the homogenized model and application to a bi-phase layered material

3.1 Homogenization of a bi-phase layered material

The model proposed in Chapter 2 is herein applied to a domain made of two layered materials, which have thickness s_1 and s_2, and subject to $\mathcal{L}$-periodic body forces $\boldsymbol{b}(\boldsymbol{x}, t)$. The domain displays orthotropic phases and the orthotropic axis is supposed to be parallel to the direction $\boldsymbol{e}_1$, see Fig. 13. In case of isotropic phases, for the plane-stress state we have $\tilde{E} = E$ and $\tilde{\nu} = \nu$, whereas for the plane-strain state $\tilde{E} = \frac{E}{1-\nu^2}$ and $\tilde{\nu} = \frac{\nu}{1-\nu}$, where E is the Young's modulus and ν is the Poisson's ratio. For sake of simplicity but without loss of generality, the components of the viscoelastic tensor are

$$G^i_{1111} = G^i_{2222} = G^{i,\infty}_{1111}(e^{-\frac{t}{\tau_r}} + \gamma), \quad G^i_{1122} = G^{i,\infty}_{1122}(e^{-\frac{t}{\tau_r}} + \gamma),$$

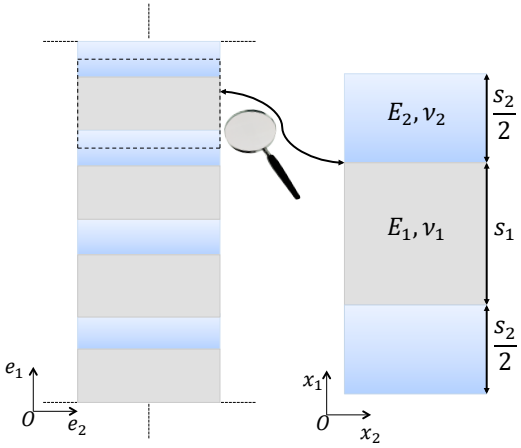

Figure 13: heterogeneous $2D$ domain with its layered periodic cell.

$$G^i_{1212} = G^{i,\infty}_{1212}(e^{-\frac{t}{\tau_r}} + \gamma), \quad i \in \{1,2\}, \quad \gamma \in \mathbb{R}, \tag{3.1}$$

where $G^{i,\infty}_{1111} = \frac{\tilde{E}}{1-\tilde{\nu}^2}$, $G^{i,\infty}_{1122} = \frac{\tilde{E}\tilde{\nu}}{1-\tilde{\nu}^2}$ and $G^{i,\infty}_{1212} = \frac{\tilde{E}}{2(1+\tilde{\nu})}$ are the equilibrium elastic modulus, Fabrizio and Morro (1992), with $G^{i,\infty}_{1111} = G^{i,\infty}_{2222}$. It can be noticed that the viscoelastic tensor can be deemed as a term of the Prony series (Ferry (1989)) and so the proposed homogenization technique can be applied to any kind of sufficiently regular kernel, since the overall constitutive and inertial tensor components have a general structure. In addition, τ_r stands for the relaxation time and the superscript i represents either phase 1 or the phase 2. The Laplace transform (2.8) applied to the components of the viscoelastic tensor (3.1) leads to

$$\hat{G}^i_{1111} = \hat{G}^i_{2222} = \frac{\tilde{E}}{1-\tilde{\nu}^2}\frac{\tau_r s(1+\gamma)+1}{s(s\tau_r+1)}, \quad \hat{G}^i_{1122} = \frac{\tilde{E}\tilde{\nu}}{1-\tilde{\nu}^2}\frac{\tau_r s(1+\gamma)+1}{s(s\tau_r+1)},$$

$$\hat{G}^i_{1212} = \frac{\tilde{E}}{2(1+\tilde{\nu})}\frac{\tau_r s(1+\gamma)+1}{s(s\tau_r+1)}, \quad i \in \{1,2\}, \quad \gamma \in \mathbb{R}. \tag{3.2}$$

Moreover, there is point in observing that in case of the transformed constitutive tensor $\hat{\mathbb{G}}^m$ characterizing a Maxwell viscosity model, the Eqs.

(3.2) depend on the mechanical properties, the relaxation time τ_r as well as the complex parameter s. Finally the relation $\hat{\mathbb{C}}^m\left(\frac{\boldsymbol{x}}{\varepsilon}, s\right) = s\hat{\mathbb{G}}^m\left(\frac{\boldsymbol{x}}{\varepsilon}, s\right)$ provides the viscoelastic tensor components as

$$\hat{C}^i_{1111} = \hat{C}^i_{2222} = \frac{\tilde{E}}{1-\tilde{\nu}^2}\frac{\tau_r s(1+\gamma)+1}{(s\tau_r+1)}, \quad \hat{C}^i_{1122} = \frac{\tilde{E}\tilde{\nu}}{1-\tilde{\nu}^2}\frac{\tau_r s(1+\gamma)+1}{(s\tau_r+1)},$$

$$\hat{C}^i_{1212} = \frac{\tilde{E}}{2(1+\tilde{\nu})}\frac{\tau_r s(1+\gamma)+1}{(s\tau_r+1)}, \quad i \in \{1,2\}, \quad \gamma \in \mathbb{R}. \tag{3.3}$$

The transformed components of the viscoelastic tensor (3.3) are employed to determine the perturbation functions of first, second and third order (see the following paragraphs for explicit details).
To simplify the matter, the following dimensionless quantities are introduced

$$r_\rho = \frac{\rho_1}{\rho_2}, \quad r_E = \frac{\tilde{E}_1}{\tilde{E}_2}, \quad \tau^i_\varsigma = \frac{\tau^i_r}{s_2}\sqrt{\frac{\tilde{E}_2}{\rho_2}}, \quad \eta = \frac{s_1}{s_2}, \quad i = 1,2.$$

where r_ρ stands for the ratio between the densities, r_E is the ratio between the Young's moduli related to phase 1 and phase 2, τ^i_ς is the relaxation time associated to phase 1 and phase 2, respectively, and η is the ratio between the thicknesses of the layers s_1 and s_2.

Perturbation functions of first order $N^{(1,0)}_{hpq}$

The micro-fluctuation functions $N^{(1,0)_i}_{hpq}$ are analytically obtained by solving the first cell problems (2.45) and considering Fig. 13. The superscript $i = \{1,2\}$ stands for the phase 1 and the phase 2 and they are formulated as

$$N^{(1,0)_1}_{211} = -\frac{\left(\hat{C}^1_{1122} - \hat{C}^2_{1122}\right)\xi_2}{\hat{C}^2_{2222}\,\eta + \hat{C}^1_{2222}}, \tag{3.4}$$

$$N^{(1,0)_2}_{211} = \frac{\eta\left(\hat{C}^1_{1122} - \hat{C}^2_{1122}\right)\xi_2}{\hat{C}^2_{2222}\,\eta + \hat{C}^1_{2222}},$$

$$N_{222}^{(1,0)_1} = -\frac{\left(\hat{C}_{2222}^1 - \hat{C}_{2222}^2\right)\xi_2}{\hat{C}_{2222}^2\,\eta + \hat{C}_{2222}^1} \tag{3.5}$$

$$N_{222}^{(1,0)_2} = \frac{\eta\,\left(\hat{C}_{2222}^1 - \hat{C}_{2222}^2\right)\xi_2}{\hat{C}_{2222}^2\,\eta + \hat{C}_{2222}^1},$$

$$N_{112}^{(1,0)_1} = N_{121}^{(1,0)_1} = -\frac{\left(\hat{C}_{1212}^1 - \hat{C}_{1212}^2\right)\xi_2}{\hat{C}_{1212}^2\,\eta + \hat{C}_{1212}^1}, \tag{3.6}$$

$$N_{112}^{(1,0)_2} = N_{121}^{(1,0)_2} = \frac{\eta\,\left(\hat{C}_{1212}^1 - \hat{C}_{1212}^2\right)\xi_2}{\hat{C}_{1212}^2\,\eta + \hat{C}_{1212}^1}.$$

Such functions depend on the fast variable $\boldsymbol{\xi}$, since the microstructure enjoys the simmetry property. In the following it is assumed that the coordinate ξ_2 is centered in both layers.

Perturbation functions of second order $N_{hpqr}^{(2,0)}$

The perturbation functions $N_{hpqr}^{(2,0)_i}$, $i = \{1, 2\}$, deriving from the cell problem (2.47) are:

$$N_{1111}^{(2,0)_1} = A_{1111}^2\xi_2^2 + A_{1111}^0, \tag{3.7}$$

$$N_{1111}^{(2,0)_2} = B_{1111}^2\xi_2^2 + B_{1111}^0,$$

$$N_{2211}^{(2,0)_1} = A_{2211}^2\xi_2^2 + A_{2211}^0, \tag{3.8}$$

$$N_{2211}^{(2,0)_2} = B_{2211}^2\xi_2^2 + B_{2211}^0,$$

$$N_{2222}^{(2,0)_1} = A_{2222}^2\xi_2^2 + A_{2222}^0, \tag{3.9}$$

$$N_{2222}^{(2,0)_2} = B_{2222}^{2}\xi_2^2 + B_{2222}^{0},$$

$$N_{1122}^{(2,0)_1} = A_{1122}^{2}\xi_2^2 + A_{1122}^{0}, \tag{3.10}$$

$$N_{1122}^{(2,0)_2} = B_{1122}^{2}\xi_2^2 + B_{1122}^{0},$$

where the constants A_{1111}^2, A_{1111}^0, B_{1111}^2, B_{1111}^0, A_{2211}^2, A_{2211}^0, B_{2211}^2, B_{2211}^0, A_{2222}^2, A_{2222}^0, B_{2222}^2, B_{2222}^0, A_{1122}^2, A_{1122}^0, B_{1122}^2 and B_{1122}^0 are determined as follows

$$A_{1111}^{2} = -\frac{1}{2}\,\frac{A_{1111}^{2,0} + \eta A_{1111}^{2,1}}{(\eta+1)\left(\hat{C}_{2222}^{2}\,\eta + \hat{C}_{2222}^{1}\right)\hat{C}_{1212}^{1}}, \tag{3.11}$$

$$A_{1111}^{0} = \frac{1}{24}\,\frac{\eta\left(A_{1111}^{0,3}\,\eta^3 + A_{1111}^{0,2}\,\eta^2 + A_{1111}^{0,1}\,\eta + A_{1111}^{0,0}\right)}{(\eta+1)^4\left(\hat{C}_{2222}^{2}\,\eta + \hat{C}_{2222}^{1}\right)\hat{C}_{1212}^{2}\,\hat{C}_{1212}^{1}}, \tag{3.12}$$

$$B_{1111}^{2} = \frac{1}{2}\,\frac{\eta B_{1111}^{2,1} + \eta^2 B_{1111}^{2,2}}{(\eta+1)\left(\hat{C}_{2222}^{2}\,\eta + \hat{C}_{2222}^{1}\right)\hat{C}_{1212}^{2}}, \tag{3.13}$$

$$B_{1111}^{0} = \frac{1}{24}\,\frac{\eta\left(-2A_{1111}^{0,3}\,\eta^3 + B_{1111}^{0,2}\,\eta^2 + B_{1111}^{0,1}\,\eta - \frac{1}{2}A_{1111}^{0,0}\right)}{(\eta+1)^4\left(\hat{C}_{2222}^{2}\,\eta + \hat{C}_{2222}^{1}\right)\hat{C}_{1212}^{1}\,\hat{C}_{1212}^{2}}, \tag{3.14}$$

$$A_{2211}^{2} = \frac{1}{2}\,\frac{\hat{C}_{1122}^{1}\,\Delta_{1212}}{\left(\hat{C}_{1212}^{2}\,\eta + \hat{C}_{1212}^{1}\right)\hat{C}_{2222}^{1}}, \tag{3.15}$$

$$A_{2211}^{0} = -\,\frac{\Delta_{1212}\eta\left(C_{1122}^{1}\,\eta^2\hat{C}_{2222}^{2} + 3\,C_{1122}^{1}\,\eta\,\hat{C}_{2222}^{2} + 2\,C_{1122}^{2}\,\hat{C}_{2222}^{1}\right)}{24\,(\eta+1)^3\left(\hat{C}_{1212}^{2}\,\eta + \hat{C}_{1212}^{1}\right)\hat{C}_{2222}^{2}\,\hat{C}_{2222}^{1}}, \tag{3.16}$$

$$B^2_{2211} = -\frac{\eta C^2_{1122}\hat{C}^1_{2222}}{\hat{C}^2_{2222}C^1_{1122}}A^2_{2211}, \tag{3.17}$$

$$B^0_{2211} = \frac{\left(2\,C^1_{1122}\,\eta^2\hat{C}^2_{2222} + 3\,\eta\,C^2_{1122}\,\hat{C}^1_{2222} + C^2_{1122}\,\hat{C}^1_{2222}\right)\Delta_{1212}\eta}{24\,(\eta+1)^3\left(\hat{C}^2_{1212}\,\eta + \hat{C}^1_{1212}\right)\hat{C}^2_{2222}\,\hat{C}^1_{2222}}, \tag{3.18}$$

$$A^2_{2222} = \frac{\Delta_{2222}}{2\,\hat{C}^2_{2222}\,\eta + 2\,\hat{C}^1_{2222}}, \tag{3.19}$$

$$A^0_{2222} = -\frac{\Delta_{2222}\eta\ (\eta+2)}{24\left(\hat{C}^2_{2222}\,\eta + \hat{C}^1_{2222}\right)(\eta+1)^2}, \tag{3.20}$$

$$B^2_{2222} = -\eta A^2_{2222}, \tag{3.21}$$

$$B^0_{2222} = -\frac{2\eta+1}{\eta+2}A^0_{2222}, \tag{3.22}$$

$$A^2_{1122} = \frac{\Delta_{1212}}{2\,\hat{C}^2_{1212}\,\eta + 2\,\hat{C}^1_{1212}}, \tag{3.23}$$

$$A^0_{1122} = -\frac{\Delta_{1212}\eta\ (\eta+2)}{24\left(\hat{C}^2_{1212}\,\eta + \hat{C}^1_{1212}\right)(\eta+1)^2}, \tag{3.24}$$

$$B^2_{1122} = -\eta A^2_{1122}, \tag{3.25}$$

$$B^0_{1122} = -\frac{2\eta+1}{\eta+2}A^0_{1122}, \tag{3.26}$$

with $\Delta_{1212} = \left(\hat{C}^1_{1212} - \hat{C}^2_{1212}\right)$ and $\Delta_{2222} = \left(\hat{C}^1_{2222} - \hat{C}^2_{2222}\right)$.
The constants that characterize the perturbation functions of the second

order Eq. (3.11), Eq. (3.12), Eq. (3.13), Eq. (3.14), which are $A^{2,0}_{1111}$, $A^{2,1}_{1111}$, $A^{0,3}_{1111}$, $A^{0,2}_{1111}$,$A^{0,1}_{1111}$, $A^{0,0}_{1111}$, $B^{2,1}_{1111}$, $B^{2,2}_{1111}$, $B^{0,2}_{2222}$ and $B^{0,1}_{2222}$, assume the form

$$A^{2,1}_{1111} = \left(\hat{C}^2_{1122} + \hat{C}^1_{1212}\right)\hat{C}^1_{1122} - (\hat{C}^2_{1122})^2 + \tag{3.27}$$

$$- \hat{C}^2_{1122}\,\hat{C}^1_{1212} - \hat{C}^2_{2222}\Delta_{1111},$$

$$A^{2,0}_{1111} = {C^1_{1122}}^2 + \left(\hat{C}^1_{1212} - \hat{C}^2_{1122}\right)\hat{C}^1_{1122} + \tag{3.28}$$

$$- \hat{C}^2_{1122}\,\hat{C}^1_{1212} - \hat{C}^1_{2222}\,\Delta_{1111},$$

$$A^{0,3}_{1111} = \hat{C}^2_{1212}\,\left(\Delta_{1122}\hat{C}^1_{1212} - \hat{C}^1_{1122}\,\hat{C}^2_{1122} +\right) + \tag{3.29}$$

$$- \left(\hat{C}^2_{1122}\right)^2 + \hat{C}^2_{2222}\,\Delta_{1111},$$

$$A^{0,2}_{1111} = 4\,\Delta_{1122}\hat{C}^1_{1212} - {C^1_{1122}}^2 - 2\,\hat{C}^1_{1122}\,\hat{C}^2_{1122} + 3\,(\hat{C}^2_{1122})^2 +$$

$$+ (\hat{C}^1_{2222} + 3\hat{C}^2_{2222})\Delta_{1111}\hat{C}^2_{1212}, \tag{3.30}$$

$$A^{0,1}_{1111} = 5\left(\Delta_{1122}\hat{C}^1_{1212} - 3\,{C^1_{1122}}^2 + 3\,\hat{C}^1_{1122}\,\hat{C}^2_{1122}\right) + \tag{3.31}$$

$$+ \left(3\,\hat{C}^1_{2222}\,\Delta_{1111}\right)\hat{C}^2_{1212} +$$

$$+ 2\,\hat{C}^1_{1212}\,\left((\hat{C}^2_{1122})^2 - \hat{C}^1_{1122}\,\hat{C}^2_{1122} + \hat{C}^2_{2222}\,\Delta_{1111}\right),$$

$$A^{0,0}_{1111} = 2\,\hat{C}^1_{1212}\,\left(\Delta_{1122}\hat{C}^2_{1212}\right) + \tag{3.32}$$

$$- {C^1_{1122}}^2 + \hat{C}^1_{1122}\,\hat{C}^2_{1122} + \hat{C}^1_{2222}\,\Delta_{1111},$$

$$B^{2,2}_{1111} = \left(\hat{C}^2_{1122}\right)^2 + \Delta_{1111}\hat{C}^2_{1122} + \hat{C}^2_{1212}\,\hat{C}^1_{1122} + \hat{C}^2_{2222}\,\Delta_{1111}, \tag{3.33}$$

$$B^{2,1}_{1111} = -{C^1_{1122}}^2 + \left(\hat{C}^2_{1122} - \hat{C}^2_{1212}\right)\hat{C}^1_{1122} + \tag{3.34}$$

$$+\,\hat{C}^2_{1122}\,\hat{C}^2_{1212} + \hat{C}^1_{2222}\,\Delta_{1111},$$

$$B^{0,2}_{1111} = \left(5\Delta_{1122}\hat{C}^2_{1212} + 3\,\hat{C}^1_{1122}\,\hat{C}^2_{1122} - 3\,(\hat{C}^2_{1122})^2\right)\hat{C}^1_{1212} +$$

$$-\left(3\,\hat{C}^2_{2222}\,\Delta_{1111}\hat{C}^1_{1212}\right) +$$

$$-\,2\,\left(-{C^1_{1122}}^2 + \hat{C}^1_{1122}\,\hat{C}^2_{1122} + \hat{C}^1_{2222}\,\Delta_{1111}\right)\hat{C}^2_{1212}, \tag{3.35}$$

$$B^{0,1}_{1111} = 3\,({C^1_{1122}}^2 - (\,(\hat{C}^2_{1122}) + 2\,\hat{C}^2_{1212})\frac{2\hat{C}^1_{1122}}{3} - \frac{1}{3}\,(\hat{C}^2_{1122})^2\,) +$$

$$-\,\frac{4\hat{C}^2_{1212}\hat{C}^2_{1122}}{3} - 3\Delta_{1111}\left(\frac{\hat{C}^2_{2222}}{3} + \hat{C}^1_{2222}\right)\hat{C}^1_{1212}. \tag{3.36}$$

where the constants Δ_{1111} and Δ_{1122} assume the form $\Delta_{1111} = \left(\hat{C}^1_{1111} - \hat{C}^2_{1111}\right)$ and $\Delta_{1122} = \left(\hat{C}^1_{1122} - \hat{C}^2_{1122}\right)$.

Perturbation functions $N^{(2,2)}_{hp}$

The perturbation functions $N^{(2,2)_i}_{hp}$, $i = \{1, 2\}$, obtained by performing the cell problem (2.51) are:

$$N^{(2,2)_1}_{11} = A^2_{11}\xi^2_2 + A^0_{11}, \tag{3.37}$$

$$N^{(2,2)_2}_{11} = B^2_{11}\xi^2_2 + B^0_{11},$$

$$N_{22}^{(2,2)_1} = A_{22}^2 \xi_2^2 + A_{22}^0, \tag{3.38}$$

$$N_{22}^{(2,2)_2} = B_{22}^2 \xi_2^2 + B_{22}^0,$$

where the constants A_{11}^2, A_{11}^0, B_{11}^2, B_{11}^0, A_{22}^2, A_{22}^0, B_{22}^2 and B_{22}^0 assume the form

$$A_{11}^2 = \frac{1}{2} \frac{(\rho_1 - \rho_2)}{(\eta+1)\,\hat{C}_{1212}^1}, \tag{3.39}$$

$$A_{11}^0 = -\frac{1}{24} \frac{(\rho_1 - \rho_2)\;\eta\;\left(\hat{C}_{1212}^2\,\eta^2 + 3\,\hat{C}_{1212}^2\,\eta + 2\,\hat{C}_{1212}^1\right)}{\hat{C}_{1212}^2\;(\eta+1)^4\,\hat{C}_{1212}^1}, \tag{3.40}$$

$$B_{11}^2 = -\frac{1}{2} \frac{(\rho_1 - \rho_2)\,\eta}{(\eta+1)\,\hat{C}_{1212}^2}, \tag{3.41}$$

$$B_{11}^0 = \frac{1}{24} \frac{(\rho_1 - \rho_2)\;\eta\;\left(2\hat{C}_{1212}^2\,\eta^2 + 3\,\hat{C}_{1212}^1\,\eta + \hat{C}_{1212}^1\right)}{\hat{C}_{1212}^2\;(\eta+1)^4\,\hat{C}_{1212}^1}, \tag{3.42}$$

$$A_{22}^2 = \frac{1}{2} \frac{(\rho_1 - \rho_2)}{(\eta+1)\,\hat{C}_{2222}^1}, \tag{3.43}$$

$$A_{22}^0 = -\frac{1}{24} \frac{(\rho_1 - \rho_2)\;\eta\;\left(\hat{C}_{2222}^2\,\eta^2 + 3\,\hat{C}_{2222}^2\,\eta + 2\,\hat{C}_{2222}^1\right)}{\hat{C}_{2222}^2\;(\eta+1)^4\,\hat{C}_{2222}^1}, \tag{3.44}$$

$$B_{22}^2 = -\frac{1}{2} \frac{(\rho_1 - \rho_2)\,\eta}{(\eta+1)\,\hat{C}_{2222}^2}, \tag{3.45}$$

$$B_{22}^0 = \frac{1}{24} \frac{(\rho_1 - \rho_2)\;\eta\;\left(2\hat{C}_{2222}^2\,\eta^2 + 3\,\hat{C}_{2222}^1\,\eta + \hat{C}_{2222}^1\right)}{\hat{C}_{2222}^2\;(\eta+1)^4\,\hat{C}_{2222}^1}. \tag{3.46}$$

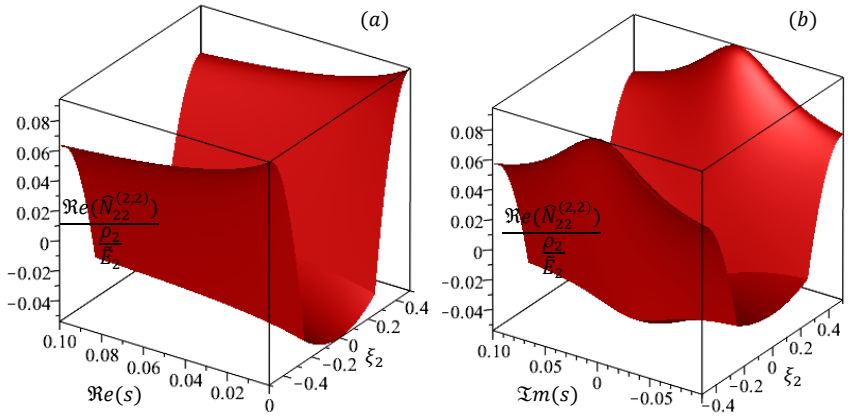

Figure 14: (a) dimensionless real part $\Re e(\hat{N}_{22}^{(2,2)})\tilde{E}_2/\rho_2$ vs. the real part of s, $\Re e(s)$, and the coordinate ξ_2. (b) Dimensionless real part $\Re e(\hat{N}_{22}^{(2,2)})\tilde{E}_2/\rho_2$ vs. the imaginary part of s, $\Im m(s)$, and ξ_2, obtained for $r_\rho = r_E = \tau_\varsigma^i = 10$, $i = 1, 2$, $\tilde{\nu}_1 = \tilde{\nu}_2 = 0.2$, $\eta = 1$ and $\gamma = 1$.

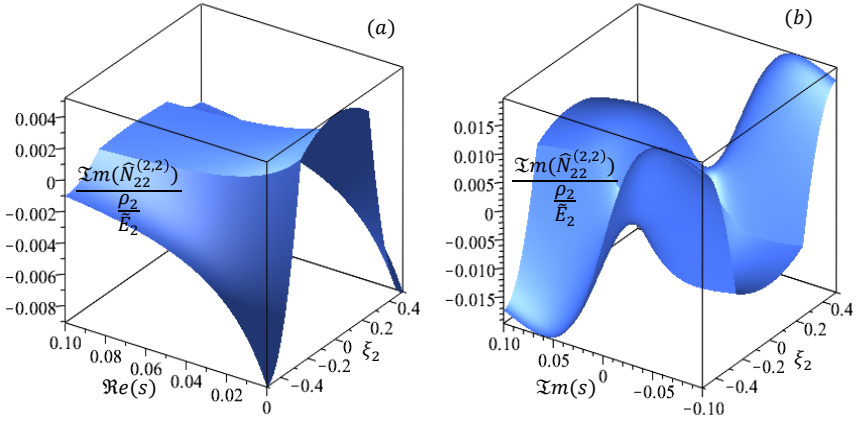

Figure 15: (a) dimensionless imaginary part $\Im m(\hat{N}_{22}^{(2,2)})\tilde{E}_2/\rho_2$ vs. the real part $\Re e(s)$ and ξ_2. (b) Dimensionless imaginary part $\Im m(\hat{N}_{22}^{(2,2)})\tilde{E}_2/\rho_2$ vs. $\Im m(s)$ and ξ_2, obtained for $r_\rho = r_E = \tau_\varsigma^i = 10$, $i = 1, 2$, $\tilde{\nu}_1 = \tilde{\nu}_2 = 0.2$, $\eta = 1$ and $\gamma = 1$.

In Figs. (14) and (15), the Poisson ratios are assumed to be equal for both phases $\tilde{\nu}_1 = \tilde{\nu}_2 = 0.2$, the dimensionless relaxation time is $\tau_\varsigma^i = 10$, $i = 1, 2$. the ratio between the Young's moduli is $r_E = 10$, the ratio between the densities is $r_\rho = 10$, the dimensionless relaxation time is $\tau_\varsigma^i = 10$, $i = 1, 2$, the ratio between the thicknesses is $\eta = 1$ and the parameter $\gamma = 1$. The perturbation function $N_{22}^{(2,2)}$ is analytically computed with respect to the phase 1 and the phase 2 by solving the cell problem (2.51) supplied with the interface conditions (2.52) in Sec. 2.4 and the structure of $N_{22}^{(2,2)}$ is reported in terms of the geometric and mechanical properties of the periodic domain in Eq. (3.38). Such function depends on the fast variable ξ_2, which is perpendicular to the transversal direction $\boldsymbol{e}_1$, as well as on the complex parameter s. The perturbation function is non-dimensionalized as $\frac{N_{22}^{(2,2)}\tilde{E}_2}{\rho_2}$ and its real part $\frac{\mathfrak{Re}(N_{22}^{(2,2)})\tilde{E}_2}{\rho_2}$ and its imaginary part $\frac{\mathfrak{Im}(N_{22}^{(2,2)})\tilde{E}_2}{\rho_2}$ are taken into account since s is a complex number. Fig. 14-(a) shows the real part of $\frac{N_{22}^{(2,2)}\tilde{E}_2}{\rho_2}$ along the periodic cell vs. the real part of s, $\mathfrak{Re}(s)$, and the vertical coordinate ξ_2. Fig. 14-(b) depicts the dependence of $\frac{\mathfrak{Re}(N_{22}^{(2,2)})\tilde{E}_2}{\rho_2}$ with respect to the imaginary part of s, $\mathfrak{Im}(s)$, and ξ_2. The imaginary part of $\frac{N_{22}^{(2,2)}\tilde{E}_2}{\rho_2}$ is shown in Fig. 15-(a) vs. $\mathfrak{Re}(s)$ and in Fig. 15-(b) vs. $\mathfrak{Im}(s)$, by varying the vertical coordinate ξ_2.

Perturbation functions $N_{hpqrs}^{(3,0)}$

The non-vanishing micro-fluctuation functions $N_{hpqrs}^{(3,0)_i}$, $i = \{1, 2\}$, obtained by performing the cell problem (2.49), with $w = 1$, are:

$$N_{21111}^{(3,0)_1} = A_{21111}^3 \xi_2^3 + A_{21111}^1 \xi_2, \tag{3.47}$$

$$N_{21111}^{(3,0)_2} = B_{21111}^3 \xi_2^3 + B_{21111}^1 \xi_2,$$

$$N_{11222}^{(3,0)_1} = A_{11222}^3 \xi_2^3 + A_{11222}^1 \xi_2, \tag{3.48}$$

$$N_{11222}^{(3,0)_2} = B_{11222}^{3}\xi_2^3 + B_{11222}^{1}\xi_2,$$

$$N_{12111}^{(3,0)_1} = A_{12111}^{3}\xi_2^3 + A_{12111}^{1}\xi_2, \tag{3.49}$$

$$N_{12111}^{(3,0)_2} = B_{12111}^{3}\xi_2^3 + B_{12111}^{1}\xi_2,$$

$$N_{22222}^{(3,0)_1} = A_{22222}^{3}\xi_2^3 + A_{22222}^{1}\xi_2, \tag{3.50}$$

$$N_{22222}^{(3,0)_2} = B_{22222}^{3}\xi_2^3 + B_{22222}^{1}\xi_2,$$

where the constants A_{21111}^{3}, A_{21111}^{1}, B_{21111}^{3}, B_{21111}^{1}, A_{11222}^{3}, A_{11222}^{1}, B_{11222}^{3}, B_{11222}^{1}, A_{12111}^{3}, A_{12111}^{1}, B_{12111}^{3}, B_{12111}^{1}, A_{22222}^{3}, A_{22222}^{1}, B_{22222}^{3} and B_{22222}^{1} read

$$A_{21111}^{3} = \frac{A_{21111}^{3,1}\eta + A_{21111}^{3,0}}{18\left(\hat{C}_{2222}^{2}\,\eta + \hat{C}_{2222}^{1}\right)(\eta+1)\,\hat{C}_{1212}^{1}\,\hat{C}_{2222}^{1}}, \tag{3.51}$$

$$A_{21111}^{1} = \frac{\eta(A_{21111}^{1,4}\eta^4 + A_{21111}^{1,3}\eta^3 + A_{21111}^{1,2}\eta^2 + A_{21111}^{1,1}\eta + A_{21111}^{1,0})}{72\left(\hat{C}_{2222}^{2}\,\eta + \hat{C}_{2222}^{1}\right)^2(\eta+1)^4\,\hat{C}_{1212}^{1}\,\hat{C}_{2222}^{1}\,\hat{C}_{1212}^{2}}, \tag{3.52}$$

$$B_{21111}^{3} = \frac{\eta(B_{21111}^{3,2}\eta + B_{21111}^{3,1})}{18\left(\hat{C}_{2222}^{2}\,\eta + \hat{C}_{2222}^{1}\right)(\eta+1)\,\hat{C}_{1212}^{2}\,\hat{C}_{2222}^{2}}, \tag{3.53}$$

$$B_{21111}^{1} = \frac{\eta(B_{21111}^{1,4}\eta^4 + B_{21111}^{1,3}\eta^3 + B_{21111}^{1,2}\eta^2 + B_{21111}^{1,1}\eta + B_{21111}^{1,0})}{72\left(\hat{C}_{2222}^{2}\,\eta + \hat{C}_{2222}^{1}\right)^2(\eta+1)^4\,\hat{C}_{1212}^{2}\,\hat{C}_{2222}^{2}\,\hat{C}_{1212}^{1}}, \tag{3.54}$$

$$A_{11222}^{3} = \frac{\Delta_{1212}\left(\hat{C}_{1212}^{2}\,\eta^3 + \left(\hat{C}_{1212}^{1} + 2\,\hat{C}_{1212}^{2}\right)\eta^2\right)}{18\left(\hat{C}_{1212}^{2}\,\eta + \hat{C}_{1212}^{1}\right)^2(\eta+1)^2} + \tag{3.55}$$

$$+\frac{\Delta_{1212}\Big(\Big(2\,\hat{C}^1_{1212}+\hat{C}^2_{1212}\Big)\,\eta+\hat{C}^1_{1212}\Big)}{18\left(\hat{C}^2_{1212}\,\eta+\hat{C}^1_{1212}\right)^2(\eta+1)^2},$$

$$A^1_{11222}=-\frac{\Delta_{1212}\left(-\frac{1}{4}\,\hat{C}^2_{1212}\,\eta^3+\left(\frac{3}{4}\,\hat{C}^1_{1212}-\frac{3}{2}\,\hat{C}^2_{1212}\right)\eta^2\right)}{18\left(\hat{C}^2_{1212}\,\eta+\hat{C}^1_{1212}\right)^2(\eta+1)^2}+ \tag{3.56}$$

$$+\frac{\left(-\frac{3}{2}\,\hat{C}^1_{1212}+\hat{C}^2_{1212}\right)\eta\Delta_{1212}}{18\left(\hat{C}^2_{1212}\,\eta+\hat{C}^1_{1212}\right)^2(\eta+1)^2},$$

$$B^3_{11222}=\frac{\eta\,\Delta_{1212}}{18\,\hat{C}^2_{1212}\,\eta+18\,\hat{C}^1_{1212}}, \tag{3.57}$$

$$B^1_{11222}=\frac{\eta\,\Delta_{1212}\left(\left(4\,\hat{C}^1_{1212}-6\,\hat{C}^2_{1212}\right)\eta^2\right)}{72\,(\eta+1)^2\left(\hat{C}^2_{1212}\,\eta+\hat{C}^1_{1212}\right)^2}+ \tag{3.58}$$

$$+\frac{\Delta_{1212}\Big(\Big(-6\,\hat{C}^1_{1212}+3\,\hat{C}^2_{1212}\Big)\,\eta-\hat{C}^1_{1212}\Big)}{72\,(\eta+1)^2\left(\hat{C}^2_{1212}\,\eta+\hat{C}^1_{1212}\right)^2}+$$

$$A^3_{12111}=\frac{\eta(A^{3,3}_{12111}\eta^3+A^{3,2}_{12111}\eta^2+A^{3,1}_{12111}\eta^1+A^{3,0}_{12111})}{18\,\left(\hat{C}^2_{1212}\,\eta+\hat{C}^1_{1212}\right)^2\hat{C}^1_{2222}\,\hat{C}^1_{1212}\,\hat{C}^2_{2222}\,(\eta+1)^3}, \tag{3.59}$$

$$A^1_{12111}=\frac{\eta(A^{1,3}_{12111}\eta^3+A^{1,2}_{12111}\eta^2+A^{1,1}_{12111}\eta^1+A^{1,0}_{12111})}{72\,\left(\hat{C}^2_{1212}\,\eta+\hat{C}^1_{1212}\right)^2\hat{C}^1_{2222}\,\hat{C}^1_{1212}\,\hat{C}^2_{2222}\,(\eta+1)^3}, \tag{3.60}$$

$$B^3_{12111}=-\frac{\eta\,\Delta_{1212}\left(C^2_{1111}\,\hat{C}^2_{2222}-{C^2_{1122}}^2-\hat{C}^2_{1122}\,\hat{C}^2_{1212}\right)}{18\left(\hat{C}^2_{1212}\,\eta+\hat{C}^1_{1212}\right)\hat{C}^2_{2222}\,\hat{C}^2_{1212}}, \tag{3.61}$$

$$B^1_{12111} = \frac{\eta(B^{1,3}_{12111}\eta^3 + B^{1,2}_{12111}\eta^2 + B^{1,1}_{12111}\eta^1 + B^{1,0}_{12111})}{72\left(\hat{C}^2_{1212}\,\eta + \hat{C}^1_{1212}\right)^2(\eta+1)^3\,\hat{C}^2_{2222}\,\hat{C}^2_{1212}\,\hat{C}^1_{2222}}, \tag{3.62}$$

where the constant Δ_{1212} has the form $\Delta_{1212} = \left(\hat{C}^1_{1212} - \hat{C}^2_{1212}\right)$.
The constants that appear in the perturbation functions Eq. (3.51)-Eq. (3.62) depend on the geometric and mechanical properties of the phases 1 and 2 and for sake of simplcity are not reported here.

$$A^3_{22222} = -\frac{\Delta_{2222}\left(\hat{C}^2_{2222}\,\eta^3 + \left(\hat{C}^1_{2222} + 2\,\hat{C}^2_{2222}\right)\eta^2\right)}{18\left(\hat{C}^2_{2222}\,\eta + \hat{C}^1_{2222}\right)^2(\eta+1)^2} + \tag{3.63}$$

$$-\frac{\Delta_{2222}\left(2\,\hat{C}^1_{2222} + \hat{C}^2_{2222}\right)\eta + \hat{C}^1_{2222}}{18\left(\hat{C}^2_{2222}\,\eta + \hat{C}^1_{2222}\right)^2(\eta+1)^2},$$

$$A^1_{22222} = -\frac{\Delta_{2222}\left(-\frac{1}{4}\,\hat{C}^2_{2222}\,\eta^3 + \left(\frac{3}{4}\,\hat{C}^1_{2222} - \frac{3}{2}\,\hat{C}^2_{2222}\right)\eta^2\right)}{18\left(\hat{C}^2_{2222}\,\eta + \hat{C}^1_{2222}\right)^2(\eta+1)^2} + \tag{3.64}$$

$$-\frac{\left(-\frac{3}{2}\,\hat{C}^1_{2222} + \hat{C}^2_{2222}\right)\eta\Delta_{2222}}{18\left(\hat{C}^2_{2222}\,\eta + \hat{C}^1_{2222}\right)^2(\eta+1)^2},$$

$$B^3_{22222} = \frac{\Delta_{2222}\left(\eta^3\hat{C}^2_{2222} + \left(\hat{C}^1_{2222} + 2\,\hat{C}^2_{2222}\right)\eta^2\right)\eta}{(\eta+1)^2\left(\hat{C}^2_{2222}\,\eta + \hat{C}^1_{2222}\right)^2} + \tag{3.65}$$

$$+\frac{\left(\left(2\,\hat{C}^1_{2222} + \hat{C}^2_{2222}\right)\eta + \hat{C}^1_{2222}\right)\Delta_{2222}\eta}{(\eta+1)^2\left(\hat{C}^2_{2222}\,\eta + \hat{C}^1_{2222}\right)^2},$$

$$B^1_{22222} = \frac{\Delta_{2222}\left(\left(\hat{C}^1_{2222} - \frac{3}{2}\hat{C}^2_{2222}\right)\eta^2 - \frac{1}{4}\hat{C}^1_{2222}\right)\eta}{18\left(\eta+1\right)^2\left(\hat{C}^2_{2222}\,\eta + \hat{C}^1_{2222}\right)^2} + \tag{3.66}$$

$$+ \frac{\left(-\frac{3}{2}\hat{C}^1_{2222} + \frac{3}{4}\hat{C}^2_{2222}\right)\eta\Delta_{2222}}{18\left(\eta+1\right)^2\left(\hat{C}^2_{2222}\,\eta + \hat{C}^1_{2222}\right)^2},$$

where the constants Δ_{2222} assumes the form $\Delta_{2222} = \left(\hat{C}^1_{2222} - \hat{C}^2_{2222}\right)$.

Perturbation functions $N^{(3,2)}_{hpq}$

The perturbation functions $N^{(3,2)_i}_{hpq}$, $i = \{1, 2\}$, obtained by performing the cell problem (2.53) are:

$$N^{(3,2)_1}_{211} = A^3_{211}\xi^3_2 + A^1_{211}\xi_2, \tag{3.67}$$

$$N^{(3,2)_2}_{211} = B^3_{211}\xi^3_2 + B^1_{211}\xi_2,$$

$$N^{(3,2)_1}_{121} = A^3_{121}\xi^3_2 + A^1_{121}\xi_2, \tag{3.68}$$

$$N^{(3,2)_2}_{121} = B^3_{121}\xi^3_2 + B^1_{121}\xi_2,$$

$$N^{(3,2)_1}_{112} = A^3_{112}\xi^3_2 + A^1_{112}\xi_2, \tag{3.69}$$

$$N^{(3,2)_2}_{112} = B^3_{112}\xi^3_2 + B^1_{112}\xi_2,$$

$$N^{(3,2)_1}_{222} = A^3_{222}\xi^3_2 + A^1_{222}\xi_2, \tag{3.70}$$

$$N^{(3,2)_2}_{222} = B^3_{222}\xi^3_2 + B^1_{222}\xi_2,$$

where the constants A^3_{211}, A^1_{211}, B^3_{211}, B^1_{211}, A^3_{121}, A^1_{121}, B^3_{121}, B^1_{121}, A^3_{112}, A^1_{112}, B^3_{112}, B^1_{112}, B^1_{122}, A^3_{222}, A^1_{222}, B^3_{222} and B^1_{222} are

$$A^3_{211} = \frac{1}{6}\,\frac{A^{3,1}_{211}\eta + A^{3,0}_{211}}{(\eta+1)\left(\hat{C}^2_{2222}\,\eta + \hat{C}^1_{2222}\right)\hat{C}^1_{1212}\,\hat{C}^1_{2222}}, \tag{3.71}$$

$$A^1_{211} = \frac{1}{24}\,\frac{\eta(A^{1,4}_{211}\eta^4 + A^{1,3}_{211}\eta^3 + A^{1,2}_{211}\eta^2 + A^{1,1}_{211}\eta + A^{1,0}_{211})}{(\eta+1)^4\left(\hat{C}^2_{2222}\,\eta + \hat{C}^1_{2222}\right)^2\hat{C}^1_{1212}\,\hat{C}^1_{2222}\,\hat{C}^2_{1212}}, \tag{3.72}$$

$$B^3_{211} = \frac{1}{6}\,\frac{\eta(B^{3,2}_{211}\eta + B^{3,1}_{211})}{(\eta+1)\left(\hat{C}^2_{2222}\,\eta + \hat{C}^1_{2222}\right)\hat{C}^2_{1212}\,\hat{C}^2_{2222}}, \tag{3.73}$$

$$B^1_{211} = \frac{1}{24}\,\frac{\eta(A^{1,4}_{211}\eta^4 + A^{1,3}_{211}\eta^3 + A^{1,2}_{211}\eta^2 + A^{1,1}_{211}\eta + A^{1,0}_{211})}{(\eta+1)^4\left(\hat{C}^2_{2222}\,\eta + \hat{C}^1_{2222}\right)^2\hat{C}^2_{1212}\,\hat{C}^2_{2222}\,\hat{C}^1_{1212}}, \tag{3.74}$$

$$A^3_{121} = \frac{\eta A^{3,1}_{121} + A^{3,0}_{121}}{6\,(\eta+1)\left(\hat{C}^2_{1212}\,\eta + \hat{C}^1_{1212}\right){C^1_{1212}}^2}, \tag{3.75}$$

$$A^1_{121} = \frac{\eta(A^{1,4}_{121}\eta^4 + A^{1,3}_{121}\eta^3 + A^{1,2}_{121}\eta^2 + A^{1,1}_{121}\eta + A^{1,0}_{121})}{24\,(\eta+1)^4\left(\hat{C}^2_{1212}\,\eta + C^1_{1212}\right)^2\hat{C}^2_{1212}\,{C^1_{1212}}^2}, \tag{3.76}$$

$$B^3_{121} = \frac{\eta(B^{3,2}_{121}\eta + B^{3,1}_{121})}{6\,(\eta+1)\,{C^2_{1212}}^2\left(\hat{C}^2_{1212}\,\eta + \hat{C}^1_{1212}\right)}, \tag{3.77}$$

$$B^1_{121} = \frac{\eta(B^{1,4}_{121}\eta^4 + B^{1,3}_{121}\eta^3 + B^{1,2}_{121}\eta^2 + B^{1,1}_{121}\eta + B^{1,0}_{121})}{24\,(\eta+1)^4\left(\hat{C}^2_{1212}\,\eta + \hat{C}^1_{1212}\right)^2{C^2_{1212}}^2\hat{C}^1_{1212}}, \tag{3.78}$$

$$A^3_{112} = \frac{1}{6}\,\frac{(-(\eta+3)\,\rho_1 + 2\,\rho_2)\,\hat{C}^1_{1212}}{\left(\hat{C}^2_{1212}\,\eta + \hat{C}^1_{1212}\right)(\eta+1)\,\hat{C}^1_{1212}}, \tag{3.79}$$

$$A^1_{112} = \frac{\eta(A^{1,4}_{112}\eta^4 + A^{1,3}_{112}\eta^3 + A^{1,2}_{112}\eta^2 + A^{1,1}_{112}\eta + A^{1,0}_{112})}{24\,\left(\hat{C}^2_{1212}\,\eta + \hat{C}^1_{1212}\right)^2 (\eta+1)^4\,\hat{C}^2_{1212}\,\hat{C}^1_{1212}}, \tag{3.80}$$

$$B^3_{112} = \frac{\left(\left(\left(\rho_1 - \frac{3\rho_2}{2}\right)\hat{C}^2_{1212} + \frac{\hat{C}^1_{1212}\rho_2}{2}\right)\eta - \frac{\rho_2\hat{C}^2_{1212}}{2} + \hat{C}^1_{1212}\,\left(\rho_1 - \frac{\rho_2}{2}\right)\right)\eta}{3\left(\hat{C}^2_{1212}\,\eta + \hat{C}^1_{1212}\right)(\eta+1)\,\hat{C}^2_{1212}}, \tag{3.81}$$

$$B^1_{112} = \frac{\eta(B^{1,4}_{112}\eta^4 + B^{1,3}_{112}\eta^3 + B^{1,2}_{112}\eta^2 + B^{1,1}_{112}\eta + B^{1,0}_{112})}{24\,(\eta+1)^4\left(\hat{C}^2_{1212}\,\eta + \hat{C}^1_{1212}\right)^2\hat{C}^2_{1212}\,\hat{C}^1_{1212}}, \tag{3.82}$$

$$A^3_{222} = \frac{1}{6}\,\frac{(-(\eta+3)\,\rho_1 + 2\,\rho_2)\,\hat{C}^1_{2222} + 2\,\hat{C}^2_{2222}\,\eta\;\rho_2}{\left(\hat{C}^2_{2222}\,\eta + \hat{C}^1_{2222}\right)(\eta+1)\,\hat{C}^1_{2222}}, \tag{3.83}$$

$$A^1_{222} = \frac{\eta(A^{1,4}_{222}\eta^4 + A^{1,3}_{222}\eta^3 + A^{1,2}_{222}\eta^2 + A^{1,1}_{222}\eta + A^{1,0}_{222})}{24\,(\eta+1)^4\left(\hat{C}^2_{2222}\,\eta + \hat{C}^1_{2222}\right)^2\hat{C}^1_{2222}\,\hat{C}^2_{2222}}, \tag{3.84}$$

$$B^3_{222} = \frac{\left(\left(\left(\frac{3\rho_2}{2} + \rho_1\right)\hat{C}^2_{2222} + \frac{\rho_2}{2}\;\hat{C}^1_{2222}\right)\eta\right)\eta}{3\left(\hat{C}^2_{2222}\,\eta + \hat{C}^1_{2222}\right)(\eta+1)\,\hat{C}^2_{2222}} + \tag{3.85}$$

$$- \frac{\left(\frac{\rho_2}{2}\;\hat{C}^2_{2222} + \left(\rho_1 - \frac{\rho_2}{2}\right)\hat{C}^1_{2222}\eta\right)}{3\left(\hat{C}^2_{2222}\,\eta + \hat{C}^1_{2222}\right)(\eta+1)\,\hat{C}^2_{2222}},$$

$$B^1_{222} = \frac{\eta(B^{1,4}_{222}\eta^4 + B^{1,3}_{222}\eta^3 + B^{1,2}_{222}\eta^2 + B^{1,1}_{222}\eta + B^{1,0}_{222})}{24\,(\eta+1)^4\left(\hat{C}^2_{2222}\,\eta + \hat{C}^1_{2222}\right)^2\hat{C}^1_{2222}\,\hat{C}^2_{2222}}. \tag{3.86}$$

The constants that appear in the perturbation functions Eq. (3.71)-Eq.(3.86) are not reported here, for sake of simplicity.

In Figs. (16) and (17), the Poisson ratios are assumed to be equal for both phases $\tilde{\nu}_1 = \tilde{\nu}_2 = 0.2$, the dimensionless relaxation time is $\tau_\varsigma^i = 10$, $i = 1, 2$. the ratio between the Young's moduli is $r_E = 10$, the ratio between the densities is $r_\rho = 10$, the dimensionless relaxation time is $\tau_\varsigma^i = 10$, $i = 1, 2$, the ratio between the thicknesses is $\eta = 1$ and the parameter $\gamma = 1$. The cell problem (2.53) equipped with the interface conditions (2.54) provides the perturbation function $N_{222}^{(3,2)}$ and its formulation is explicitely expressed in Eq. (3.70), where there is point in noticing they take into account the effect of the microstructural heterogeneities of the domain. The real part and the imaginary part of the dimensionless perturbation function $\frac{N_{222}^{(3,2)}\tilde{E}_2}{\rho_2}$ are considered, which are $\frac{\Re e(N_{222}^{(3,2)})\tilde{E}_2}{\rho_2}$ and $\frac{\Im m(N_{222}^{(3,2)})\tilde{E}_2}{\rho_2}$. Fig. 16-(a) and Fig. 16-(b) show how the real part of $\frac{N_{222}^{(3,2)}\tilde{E}_2}{\rho_2}$ depends on the real and the imaginary parts of s, by varying the vertical coordinate ξ_2. Fig. 17-(a) and Fig. 17-(b) show that the imaginary part

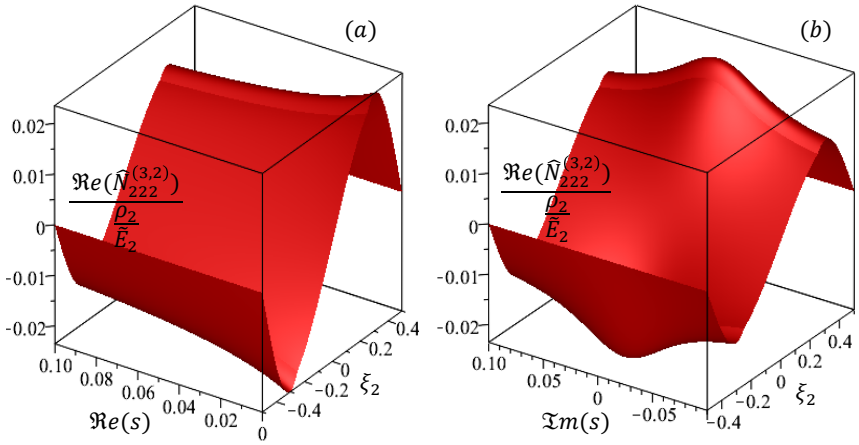

Figure 16: (a) dimensionless real part of the perturbation function $\hat{N}_{222}^{(3,2)}$, $\Re e(\hat{N}_{222}^{(3,2)})\tilde{E}_2/\rho_2$, vs. the real part of s, $\Re e(s)$, and the coordinate ξ_2. (b) Dimensionless real part $\Re e(\hat{N}_{222}^{(3,2)})\tilde{E}_2/\rho_2$ vs. the imaginary part of s, $\Im m(s)$, and ξ_2, obtained for $r_\rho = 10$, $r_E = 10$, $\tau_\varsigma = 10$, $\tilde{\nu}_1 = \tilde{\nu}_2 = 0.2$, $\tau_\varsigma^i = 10$, $i = 1, 2$ $\eta = 1$ and $\gamma = 1$.

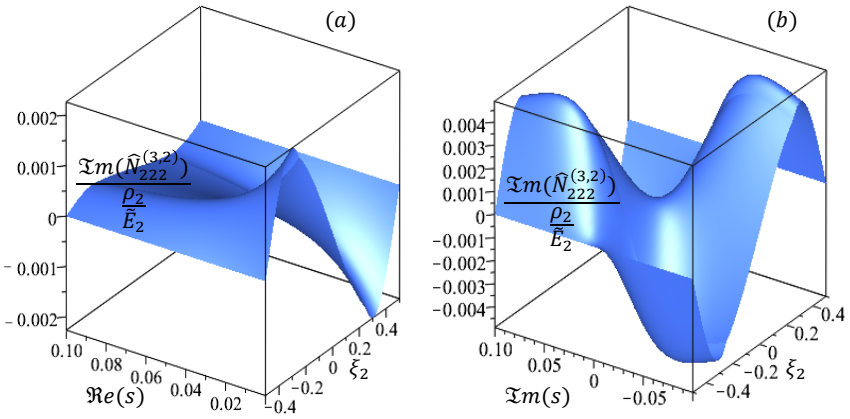

Figure 17: (a) dimensionless imaginary part $\Im m(\hat{N}_{222}^{(3,2)})\tilde{E}_2/\rho_2$ vs. the real part $\Re e(s)$ and ξ_2. (b) Dimensionless imaginary part $\Im m(\hat{N}_{222}^{(3,2)})\tilde{E}_2/\rho_2$ vs. $\Im m(s)$ and ξ_2, obtained for $r_\rho = r_E = \tau_\varsigma^i = 10$, $i = 1, 2$, $\tilde{\nu}_1 = \tilde{\nu}_2 = 0.2$, $\eta = 1$ and $\gamma = 1$.

of $\frac{N_{222}^{(3,2)}\tilde{E}_2}{\rho_2}$ depends on $\Re e(s)$ and $\Im m(s)$, by changing the vertical coordinate ξ_2.

In Fig. 14, 15 and Fig. 16, 17, it is emphasized that the dimensionless perturbation functions $\frac{\Re e(N_{22}^{(2,2)})\tilde{E}_2}{\rho_2}$, $\frac{\Im m(N_{22}^{(2,2)})\tilde{E}_2}{\rho_2}$ and $\frac{\Re e(N_{222}^{(3,2)})\tilde{E}_2}{\rho_2}$, $\frac{\Im m(N_{222}^{(3,2)})\tilde{E}_2}{\rho_2}$ are $\mathcal{Q}$-periodic, they have vanishing mean values over the unit cell $\mathcal{Q}$ and smooth along the boundaries of $\mathcal{Q}$, as expected.

Overall inertial terms and overall consitutive tensors

The perturbation functions of first, second and third order are helpful to determine the overall transformed inertial tensors, which appear in the dispersion relation (2.146). They are specialized according to the geometry of the layered domain in Fig. 13. By taking into account the approach presented in Subsection 2.7.1, the transformed inertial tensor componenets appearing in Eq. (2.146) assume the form:

$$\hat{I}_{2121} = \varepsilon^2\langle\rho^m(N_{121}^{(1,0)}N_{121}^{(1,0)}) - 2\rho^m N_{2211}^{(2,0)}\rangle\frac{1}{\rho}, \tag{3.87}$$

$$\hat{I}_{2222} = \varepsilon^2 \langle \rho^m (N_{222}^{(1,0)} N_{222}^{(1,0)}) - 2\rho^m N_{2222}^{(2,0)} \rangle \frac{1}{\rho}, \tag{3.88}$$

$$\hat{I}_{22} = \varepsilon^2 \langle \rho^m (N_{22}^{(2,2)} + N_{22}^{(2,2)}) \rangle \frac{1}{\rho}, \tag{3.89}$$

$$\hat{I}_{1212} = \varepsilon^2 \langle \rho^m (N_{112}^{(1,0)} N_{112}^{(1,0)}) - 2\rho^m N_{1122}^{(2,0)} \rangle \frac{1}{\rho}, \tag{3.90}$$

$$\hat{I}_{1111} = \varepsilon^2 \langle \rho^m (N_{211}^{(1,0)} N_{211}^{(1,0)}) - 2\rho^m N_{1111}^{(2,0)} \rangle \frac{1}{\rho}, \tag{3.91}$$

$$\hat{I}_{11} = \varepsilon^2 \langle \rho^m (N_{11}^{(2,2)} + N_{11}^{(2,2)}) \rangle \frac{1}{\rho}. \tag{3.92}$$

Referred to the Eq. (2.146), the constitutive tensor components in the Laplace space are

$$\hat{J}_{11} = \varepsilon^2 \langle \hat{G}_{1212} B_{121}^{(2,2)} B_{121}^{(2,2)} \rangle, \tag{3.93}$$

$$\hat{J}_{22} = \varepsilon^2 \langle \hat{G}_{2222} B_{222}^{(2,2)} B_{222}^{(2,2)} \rangle, \tag{3.94}$$

$$\hat{G}_{1111} = \langle \hat{G}_{1111} B_{1111}^{(1,0)} B_{1111}^{(1,0)} + \hat{G}_{2222} B_{2211}^{(1,0)} B_{2211}^{(1,0)} + \tag{3.95}$$

$$+ 2\hat{G}_{1122} B_{2211}^{(1,0)} B_{1111}^{(1,0)} \rangle,$$

$$\hat{G}_{2121} = \hat{G}_{1212} = \langle \hat{G}_{2222} B_{2221}^{(1,0)} B_{2221}^{(1,0)} \rangle, \tag{3.96}$$

$$\hat{G}_{2222} = \langle \hat{G}_{2222} B_{2222}^{(1,0)} B_{2222}^{(1,0)} \rangle, \tag{3.97}$$

$$\hat{J}_{2121}^{1} = -\varepsilon^2 \langle 2\hat{G}_{1122} B_{11211}^{(2,0)} B_{222}^{(2,2)} - 2\hat{G}_{1212} B_{1221}^{(1,0)} B_{1221}^{(3,2)} + \tag{3.98}$$

$$- 2\hat{G}_{1212} B_{2121}^{(1,0)} B_{1221}^{(3,2)} - 2\hat{G}_{1212} B_{2121}^{(1,0)} B_{2121}^{(3,2)} \rangle,$$

$$\hat{J}^1_{1212} = -\varepsilon^2\langle -2\hat{G}_{1212}B^{(1,0)}_{1212}B^{(3,2)}_{1212} + 2\hat{G}_{1212}B^{(2,0)}_{12122}B^{(2,2)}_{121}\rangle, \tag{3.99}$$

$$\hat{J}^1_{2222} = -\varepsilon^2\langle -2\hat{G}_{2222}B^{(1,0)}_{2222}B^{(3,2)}_{2222} + 2\hat{G}_{2222}B^{(2,0)}_{22222}B^{(2,2)}_{222}\rangle,$$

$$\hat{S}^1_{111111} = \varepsilon^2\langle -2\hat{G}_{1111}B^{(1,0)}_{1111}B^{(3,0)}_{111111} + \hat{G}_{1212}B^{(2,0)}_{12111}B^{(2,0)}_{12111} + \tag{3.100}$$

$$+ \hat{G}_{1212}B^{(2,0)}_{21111}B^{(2,0)}_{21111} + +2\hat{G}_{1212}B^{(2,0)}_{12111}B^{(2,0)}_{21111} - 2\hat{G}_{2222}B^{(1,0)}_{2211}B^{(3,0)}_{221111} +$$

$$- 2\hat{G}_{1122}B^{(1,0)}_{2211}B^{(3,0)}_{111111} - 2\hat{G}_{2211}B^{(1,0)}_{1111}B^{(3,0)}_{221111}\rangle,$$

$$\hat{S}^1_{211211} = \varepsilon^2\langle \hat{G}_{1111}B^{(2,0)}_{11211}B^{(2,0)}_{11211} + 2\hat{G}_{1122}B^{(2,0)}_{11211}B^{(2,0)}_{22211} + \tag{3.101}$$

$$+ \hat{G}_{2222}B^{(2,0)}_{22211}B^{(2,0)}_{22211} - 2\hat{G}_{1212}B^{(1,0)}_{1212}B^{(3,0)}_{12111} - 2\hat{G}_{1212}B^{(1,0)}_{1221}B^{(3,0)}_{122111} +$$

$$- 2\hat{G}_{1212}B^{(1,0)}_{2121}B^{(3,0)}_{122111} - 2\hat{G}_{1212}B^{(1,0)}_{1221}B^{(3,0)}_{212111} - 2\hat{G}_{1212}B^{(1,0)}_{2121}B^{(3,0)}_{212111}\rangle.$$

The inertial and constitutive tensor components described in Subsection 2.7.2 coincide with those ones from (3.87) to (3.97), whereas the inertial and constitutive tensor components from (3.98) to (3.101) are slightly different because the localization tensors $B^{(3,0)}_{hkpq_1q_2q_3}$ and $B^{(3,2)}_{hkpq_1}$ disappear in the formulation and so they assume the form:

$$\hat{J}^2_{1111} = -\varepsilon^2\langle 2\hat{G}_{1212}B^{(2,0)}_{12111}B^{(2,2)}_{121} + 2\hat{G}_{1212}B^{(2,0)}_{21111}B^{(2,2)}_{121}\rangle, \tag{3.102}$$

$$\hat{J}^2_{2121} = -\varepsilon^2\langle 2\hat{G}_{1122}B^{(2,0)}_{11211}B^{(2,2)}_{222} + 2\hat{G}_{2222}B^{(2,0)}_{22211}B^{(2,2)}_{222}\rangle, \tag{3.103}$$

$$\hat{J}^2_{1212} = -\varepsilon^2\langle 2\hat{G}_{1212}B^{(2,0)}_{12122}B^{(2,2)}_{121}\rangle, \tag{3.104}$$

$$\hat{J}^2_{2222} = -\varepsilon^2\langle 2\hat{G}_{2222}B^{(2,0)}_{22222}B^{(2,2)}_{222}\rangle, \tag{3.105}$$

$$\hat{S}^2_{111111} = \varepsilon^2\langle \hat{G}_{1212}B^{(2,0)}_{12111}B^{(2,0)}_{12111} + \hat{G}_{1212}B^{(2,0)}_{21111}B^{(2,0)}_{21111}\rangle + \tag{3.106}$$

$$+\varepsilon^2\langle 2\hat{G}_{1212}B^{(2,0)}_{12111}B^{(2,0)}_{21111}\rangle,$$

$$\hat{S}^2_{211211}=\varepsilon^2\langle\hat{G}_{1111}B^{(2,0)}_{11211}B^{(2,0)}_{11211}+2\hat{G}_{1122}B^{(2,0)}_{11211}B^{(2,0)}_{22211}\rangle+ \tag{3.107}$$

$$+\varepsilon^2\langle\hat{G}_{2222}B^{(2,0)}_{22211}B^{(2,0)}_{22211}\rangle.$$

The transformed inertial tensor components $\hat{J}_{11}$, $\hat{J}^2_{1111}$ and $\hat{I}_{11}$, referred to the wave propagation along the transversal direction $\boldsymbol{e}_1$, are taken into account. They are affected by the complex angular frequency s and their dimensionless components are written as $\frac{\hat{J}_{11}\sqrt{\frac{\tilde{E}_2}{\rho_2}}}{\varepsilon^2 s_2\rho_2}$, $\frac{\hat{J}^2_{1111}\sqrt{\frac{\tilde{E}_2}{\rho_2}}}{\varepsilon^2 s_2\rho_2}$ and $\frac{\hat{I}_{11}\tilde{E}_2}{\varepsilon^2\rho_2}$. The second order transformed inertial tensor component is computed by means of Eq. (3.93) and, due to the presence of the complex frequency s, $\frac{\hat{J}_{11}\sqrt{\frac{\tilde{E}_2}{\rho_2}}}{\varepsilon^2 s_2\rho_2}$ is decomposed into its real part $\frac{\Re e(\hat{J}_{11})\sqrt{\frac{\tilde{E}_2}{\rho_2}}}{\varepsilon^2 s_2\rho_2}$ and its imagi-

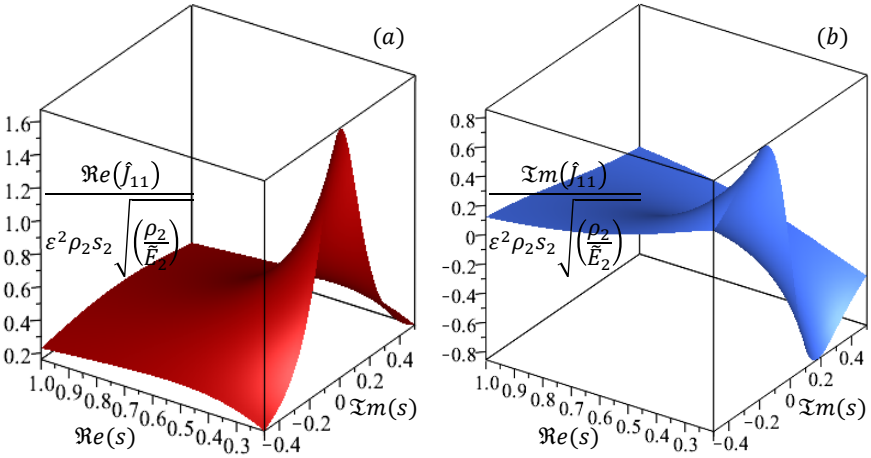

Figure 18: (a) dimensionless real part component $\Re e(\hat{J}_{11})\sqrt{\frac{\tilde{E}_2}{\rho_2}}/\varepsilon^2 s_2\rho_2$ vs. the real part of s, $\Re e(s)$, and the imaginary part of s, $\Im m(s)$. (b) Dimensionless imaginary part component $\Im m(\hat{J}^2_{11})\sqrt{\frac{\tilde{E}_2}{\rho_2}}/\varepsilon^2 s_2\rho_2$ vs. the real part of s, $\Re e(s)$, and the imaginary part of s, $\Im m(s)$, obtained for $r_\rho = r_E = \tau^i_\varsigma = 10$, $i = 1, 2$, $\tilde{\nu}_1 = \tilde{\nu}_2 = 0.2$, $\eta = 1$ and $\gamma = 1$.

nary part $\frac{\Im m(\hat{J}_{11})\sqrt{\frac{\tilde{E}_2}{\rho_2}}}{\varepsilon^2 s_2 \rho_2}$. Fig. 18-(a) shows the behaviour of $\frac{\Re e(\hat{J}_{11})\sqrt{\frac{\tilde{E}_2}{\rho_2}}}{\varepsilon^2 s_2 \rho_2}$ by varying the real part and the imaginary part of s. Specifically, it can be observed that the real part of $\frac{\hat{J}_{11}\sqrt{\frac{\tilde{E}_2}{\rho_2}}}{\varepsilon^2 s_2 \rho_2}$ is symmetric with respect to the $\Re e(s)$-axis and, by decreasing the values of the real part of s, the upward concavity of $\frac{\Re e(\hat{J}_{11})\sqrt{\frac{\tilde{E}_2}{\rho_2}}}{\varepsilon^2 s_2 \rho_2}$ increases. In Fig. 18-(b), the imaginary part $\frac{\Im m(\hat{J}_{11})\sqrt{\frac{\tilde{E}_2}{\rho_2}}}{\varepsilon^2 s_2 \rho_2}$ is plotted with respect to the real part of s, $\Re e(s)$, and the imaginary part of s, $\Im m(s)$. The function assumes either positive or negative values and it is symmetric with respect to zero.
The transformed second order inertial tensor component $\frac{\hat{I}_{11}\tilde{E}_2}{\varepsilon^2\rho_2}$ is computed by means of Eq. (2.117) and its real part $\frac{\Re e(\hat{I}_{11})\tilde{E}_2}{\varepsilon^2\rho_2}$ and its imaginary part $\frac{\Im m(\hat{I}_{11})\tilde{E}_2}{\varepsilon^2\rho_2}$ are considered. In Figs. 19-(a) and 19-(b), the de-

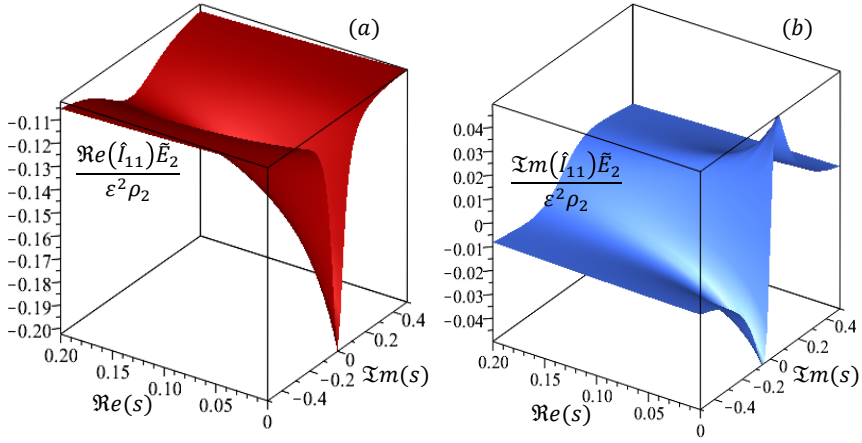

Figure 19: (a) dimensionless real part component $\Re e(\hat{I}_{11})\tilde{E}_2/\varepsilon^2 s_2$ vs. the real part of s, $\Re e(s)$, and the imaginary part of s, $\Im m(s)$. (b) Dimensionless component $\Im m(\hat{I}_{11})\tilde{E}_2/\varepsilon^2 s_2$ vs. the real part of s, $\Re e(s)$, and the imaginary part of s, $\Im m(s)$, obtained for $r_\rho = r_E = \tau_\varsigma^i = 10$, $i = 1, 2$, $\tilde{\nu}_1 = \tilde{\nu}_2 = 0.2$, $\eta = 1$ and $\gamma = 1$.

pendency of $\frac{\Re e(\hat{I}_{11})\tilde{E}_2}{\varepsilon^2\rho_2}$ and $\frac{\Im m(\hat{I}_{11})\tilde{E}_2}{\varepsilon^2\rho_2}$ on the real part and the imaginary part of s is shown. Fig. 19-(a) ensures that $\frac{\Re e(\hat{I}_{11})\tilde{E}_2}{\varepsilon^2\rho_2}$ assumes only negative values and it is symmetric with respect to $\Re e(s)$-axis. Moreover, by decreasing the real part of s, the downward concavity is more emphasized. Fig. 19-(b) depicts the symmetry of $\frac{\Im m(\hat{I}_{11})\tilde{E}_2}{\varepsilon^2\rho_2}$ with respect to zero. Finally, in Figs. 20-(a) and 20-(b), the real part of the dimensionless fourth order inertial tensor component $\frac{\Re e(\hat{J}^2_{1111})\sqrt{\frac{\tilde{E}_2}{\rho_2}}}{\varepsilon^2 s_2\rho_2}$ and its imaginary part $\frac{\Im m(\hat{J}^2_{1111})\sqrt{\frac{\tilde{E}_2}{\rho_2}}}{\varepsilon^2 s_2\rho_2}$ are plotted vs. the real and the imaginary parts of the complex frequency s. It is worth noticing that the inertial tensor component $\hat{J}^1_{1111}$ stemming from the approach 1 is vanishing.
Fig. 21-(a) shows that the magnitudes of the constitutive tensor components $\hat{S}^1_{111111}$ and $\hat{S}^2_{111111}$, determined for the compressional waves

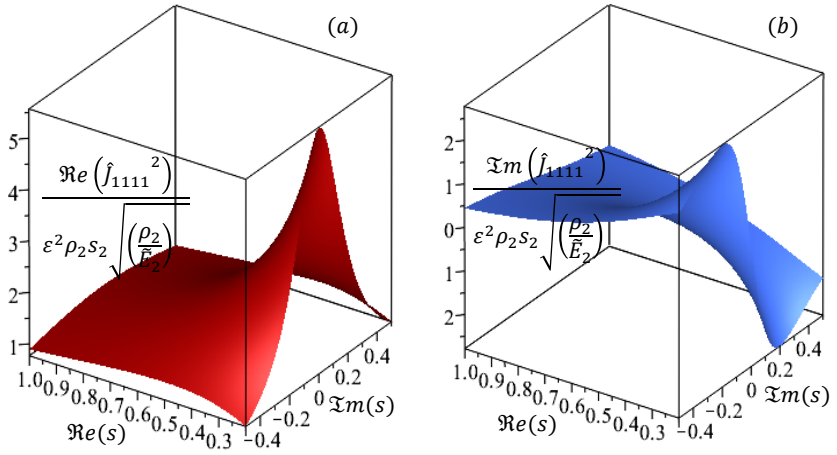

Figure 20: (a) dimensionless real part component $\Re e(\hat{J}^2_{1111})\sqrt{\frac{\tilde{E}_2}{\rho_2}}/\varepsilon^2 s_2\rho_2$ vs. the real part of s, $\Re e(s)$, and the imaginary part of s, $\Im m(s)$. (a) Dimensionless imaginary part component $\Im m(\hat{J}^2_{1111})\sqrt{\frac{\tilde{E}_2}{\rho_2}}/\varepsilon^2 s_2\rho_2$ vs. the real part of s, $\Re e(s)$, and the imaginary part of s, $\Im m(s)$. Both are retrieved for $r_\rho = r_E = \tau^i_\varsigma = 10$, $i = 1, 2$, $\check{\nu}_1 = \check{\nu}_2 = 0.2$, $\eta = 1$ and $\gamma = 1$.

along the direction $\boldsymbol{e}_1$, are compared in terms of the magnitude of $s = \sqrt{Re(s)^2 + Im(s)^2}$ and the non-dimensional Young's modulus r_E. As $\frac{1}{10} < r_E < 1$, the magnitude $|\hat{S}^1_{111111}|$ decreases more steadily than $|\hat{S}^2_{111111}|$ and both are equal to zero when the material is homogeneous, i.e. when $r_E = 1$. With increasing the non-dimensional Young's modulus r_E, a significant rise in $|\hat{S}^2_{111111}|$ is observed as compared to $|\hat{S}^1_{111111}|$. Finally, as $|s|$ goes up, $|\hat{S}^1_{111111}|$ decreases more slowly than $|\hat{S}^2_{111111}|$. In Fig. 21-(b), the magnitudes of $\hat{S}^1_{211211}$ and $\hat{S}^2_{211211}$ are plotted with respect to the magnitude of the complex angular frequency $|s|$ and the non-dimensional Young's modulus r_E. They are computed for the shear waves travelling along the layering direction $\boldsymbol{e}_1$. It can be observed that if $\frac{1}{10} < r_E < 1$, the magnitudes of $\hat{S}^1_{211211}$ and $\hat{S}^2_{211211}$ decrease down to zero when the material is homogeneous. A rise in r_E (with $r_E > 1$) makes $|\hat{S}^1_{211211}|$ and $|\hat{S}^2_{211211}|$ increasing rapidly. Moreover, growth in the

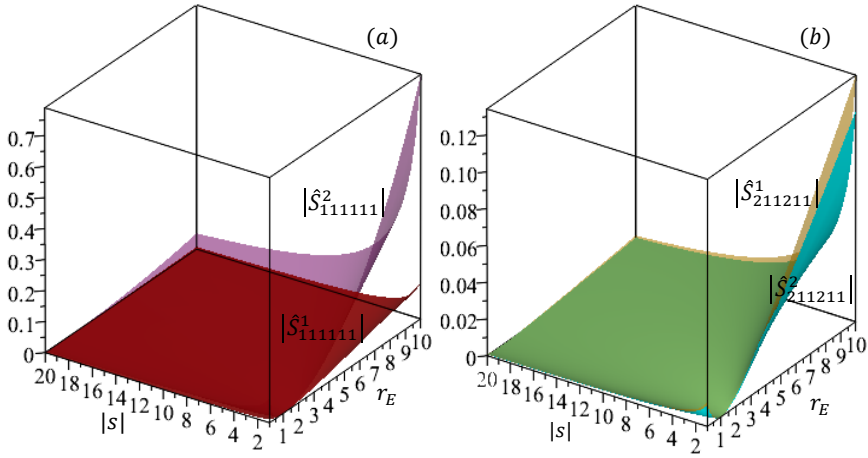

Figure 21: (a) magnitudes of the constitutive tensor $\hat{S}^1_{111111}$ and $|\hat{S}^1_{111111}|$ (red) are compared with $|\hat{S}^2_{111111}|$ (violet) by varying the dimensionless Young's modulus r_E and the magnitude of s. (b) Magnitudes $|\hat{S}^1_{211211}|$ (gold) and $|\hat{S}^2_{211211}|$ (green) are compared with respect to r_E and $|s|$. (a) and (b) are obtained for $r_\rho = 10$, $\tau^i_\varsigma = 10$, $i = 1, 2$, $\tilde{\nu}_1 = \tilde{\nu}_2 = 0.2$, $\eta = 1$ and the argument of s is zero and $\gamma = 1$.

magnitude of s leads $|\hat{S}^1_{211211}|$ and $|\hat{S}^2_{211211}|$ to decrease. The discrepancy between the magnitude of $\hat{S}^1_{111111}$ (red) and $\hat{S}^2_{111111}$ (violet) (Fig. (21)-(a)) and between the magnitude of $\hat{S}^1_{211211}$ (gold) and $\hat{S}^2_{211211}$ (green) (Fig. (21)-(b)) can be observed as r_E increases, whereas such a discrepancy decreases as the magnitude of s increases. Fig. 22-(a) depicts the behaviour of the magnitudes of the transformed viscoelastic components $\hat{G}_{1212}$ related to the shear wave travelling along $\boldsymbol{e}_2$. It is observed that the trend of $|\hat{G}_{1212}|$ steadely increases by a rise in the Young's modulus and by varying the magnitude of the complex frequency s. Fig. 22-(b) shows the magnitude of the transformed viscoelastic components $\hat{G}_{1111}$, concerning with the compressional wave along $\boldsymbol{e}_1$. The magnitude $|\hat{G}_{1111}|$ significantly grows up in the interval $\frac{1}{10} < r_E < 4$, by varying $|s|$, and then its trend becomes a plateau.

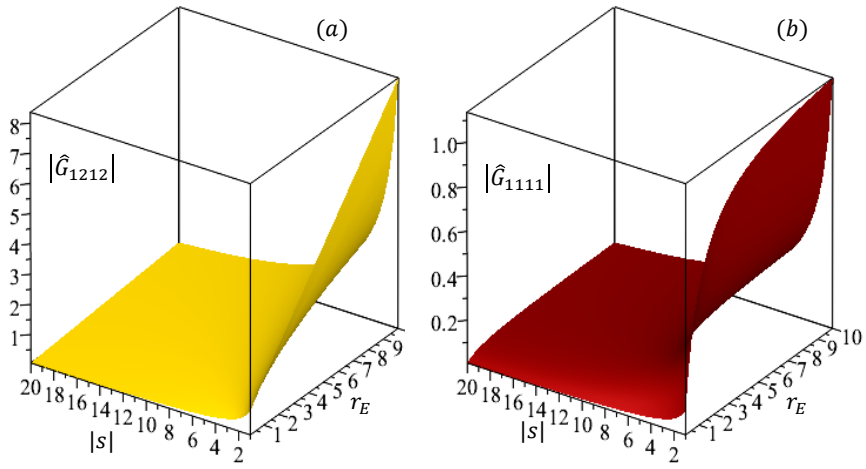

Figure 22: (a) magnitudes of the constitutive component $\hat{G}_{1212}$ and $|\hat{G}_{1212}|$ are depicted by varying the dimensionless Young's modulus r_E and the magnitude of s. (b) Magnitudes of the component $\hat{G}_{1111}$ and $|\hat{G}_{1111}|$ are represented by changing the dimensionless Young's modulus r_E and the magnitude of s. Both are obtained for $r_\rho = \tau^i_\varsigma = 10$, $i = 1, 2$, $\tilde{\nu}_1 = \tilde{\nu}_2 = 0.2$, $\eta = 1$, the argument of s is zero and $\gamma = 1$.

Let us consider a 2-D heterogeneous layered domain Fig. 13 subject to $\mathcal{L}$-periodic harmonic body forces $\hat{b}_\alpha = \Upsilon_\alpha e^{\iota \frac{2\pi k}{L_\beta} x_\beta}$, with $k = 1, 2, ..,$ applied in the direction of the orthogonal symmetry axis x_β, where $\alpha, \beta = 1, 2$, $\Upsilon_\alpha \in \mathbb{R}$ and $\iota^2 = -1$. A horizontal (or vertical) sample of length $L = L_1 (= L_2)$ is taken into account since the body forces and the heterogeneous domain are periodic. The solution of the heterogeneous model is provided by a numerical procedure accounting for the actual heterogeneous composition of the layered composite and it is compared with the solution stemming from the homogenized model. For sake of simplicity, only the static case is considered and the field equation (2.145) is rephrased as

$$s\hat{G}_{\alpha\beta\alpha\beta} \frac{\partial^2 \hat{U}^M_\alpha}{\partial x^2_\beta} - s\hat{S}^i_{\alpha\beta\beta\alpha\beta\beta} \frac{\partial^4 \hat{U}^M_\alpha}{\partial x^4_\beta} = -\hat{b}_\alpha, \tag{3.108}$$

with $i = \{1, 2\}$ and the indices α and β are not summed. The shear problem takes place for $\alpha \neq \beta$ whereas the compressional problem for $\alpha = \beta$. The transformed macro-displacement is determined from Eq. (3.108) as

$$\hat{U}^M_\alpha(x_\beta) = \left(\frac{L_\beta}{2\pi}\right)^2 \frac{\hat{b}_\alpha}{s\hat{G}_{\alpha\beta\alpha\beta}\left[1 + \left(\frac{2\pi k}{L_\beta}\right)^2 \frac{\hat{S}^i_{\alpha\beta\beta\alpha\beta\beta}}{\hat{G}_{\alpha\beta\alpha\beta}}\right]}, \tag{3.109}$$

with $i = 1, 2$ and $k = 1, 2, ..$ The dimensionless transformed macro-displacement is written as

$$\tilde{\hat{U}}^M_\alpha = \frac{\hat{U}^M_\alpha \tilde{E}_1}{\Upsilon_\alpha \left(\frac{L_\beta}{2\pi}\right)^2}, \tag{3.110}$$

where $\tilde{E}_1$ is the Young's modulus related to the phase 1. In Figs. (23)-(25), the material is in plane stress condition, the sample has a length $L/\varepsilon = 11$, with amplitude $\Upsilon_\alpha = 1$ N/mm^3, the Poisson ratios are equal for both phases, $\tilde{\nu}_1 = \tilde{\nu}_2 = 0.2$, the ratio between the thicknesses is $\eta = 1$, the parameter γ is $\gamma = 1$, whereas the relaxation time is τ^i_ς, $i = 1, 2$, the ratio between the densities is r_ρ, the dimensionless complex frequency is

$s_\varsigma = ss_2/\sqrt{\frac{\hat{E}_2}{\rho_2}}$ and the ratio between the Young's moduli r_E are assumed to vary.

In Fig. (23) and (24), the relaxation times are assumed to be the same for both the phases, $\tau_\varsigma^1 = \tau_\varsigma^2 = 5$, the ratio between the densities and the ratio between the Young's moduli are $r_\rho = r_\rho = 10$ and the dimensionless complex frequency s_ς assumes different values.

In Fig. 23-(a) the magnitude of the dimensionless transformed macro-displacement (3.110), with $\alpha = 1$ along the direction x_1, is compared with the solution provided by a finite element analysis of the heterogeneous domain equipped with proper periodic boundary conditions on the displacement. The continuous curve stands for the analytical di-

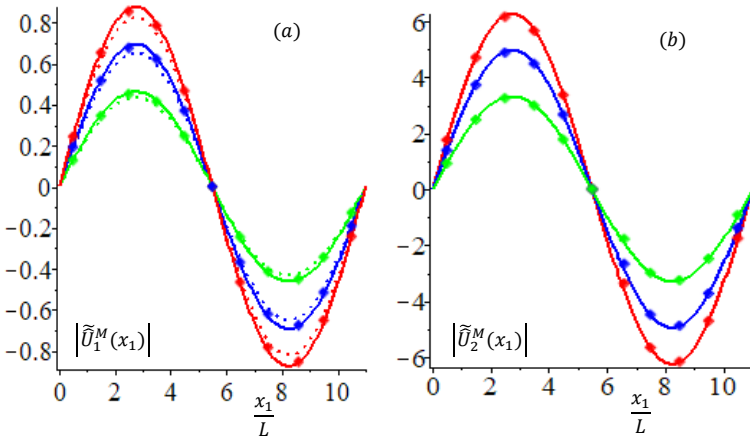

Figure 23: magnitude of the dimensionless macro-displacement component $\tilde{\tilde{U}}_1^M(x_1)$ induced by the harmonic body force $\hat{b}_1(x_1)$ (a) and $\tilde{\tilde{U}}_2^M(x_1)$ caused by $\hat{b}_2(x_1)$ (b) along direction x_1. The solution given by the homogenized model 1 (continuous curves) and model 2 (dotted curves) are compared with solution of the heterogeneous model (diamonds). The red curves are obtained by setting the dimensionless complex freqeuncy $s_\varsigma = -2$, the blue curves are obtained for $s_\varsigma = -0.5$ and the green ones are given for $s_\varsigma = -0.3$, with $\tau_\varsigma^i = 5$, $i \in 1, 2$, $r_E = r_\rho = 10$, $\tilde{\nu}_1 = \tilde{\nu}_2 = 0.2$, $\eta = 1$ and $\gamma = 1$.

mensionless transformed macro-displacement $\tilde{\hat{U}}_1^M(x_1)$, which is derived from the method 1 and provides the overall constitutive tensor $\hat{S}^1_{111111}$, Eq. (3.100). The dotted curve represents the analytical dimensionless transformed macro- displacement $\tilde{\hat{U}}_1^M(x_1)$ and derives from the alternative method 2, which provides the overall constitutive tensor $\hat{S}^2_{111111}$, Eq. (3.106). Finally the diamonds stand for the numerical results related to the heterogeneous model and obtained from the corresponding microscopic solution through the up-scaling relation (2.68) and considering the imaginary part of the body force $\hat{b}_1 = \Upsilon_1 \sin \frac{2\pi k}{L_1} x_1$, with $k = 1$. In Fig. 23-(a), three values for the dimensionless complex frequency $s_\varsigma = ss_2/\sqrt{\frac{\tilde{E}_2}{\rho_2}}$ are considered: the red curves and diamonds are obtained for $s_\varsigma = -2$,

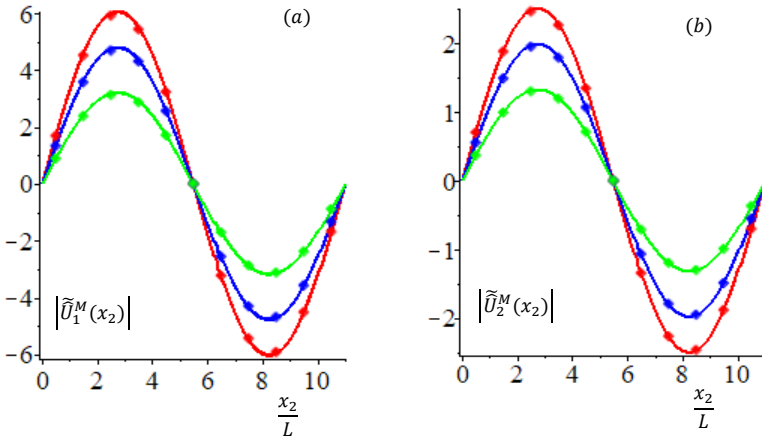

Figure 24: magnitude of the dimensionless macro-displacement component $\tilde{\hat{U}}_1^M(x_2)$ induced by the harmonic body force $\hat{b}_1(x_2)$ (a) and $\tilde{\hat{U}}_2^M(x_2)$ caused by $\hat{b}_2(x_2)$ (b) along direction x_2. The solution given by the homogenized model 1 (continuous curves) and model 2 (dotted curves) are compared with solution of the heterogeneous model (diamonds). The red curves are obtained by setting the dimensionless complex frequency $s_\varsigma = -2$, the blue curves are obtained for $s_\varsigma = -0.5$ and the green ones are given for $s_\varsigma = -0.3$, with $\tau_\varsigma^i = 5$, $i \in 1, 2$, $r_E = r_\rho = 10$, $\tilde{\nu}_1 = \tilde{\nu}_2 = 0.2$, $\eta = 1$ and $\gamma = 1$.

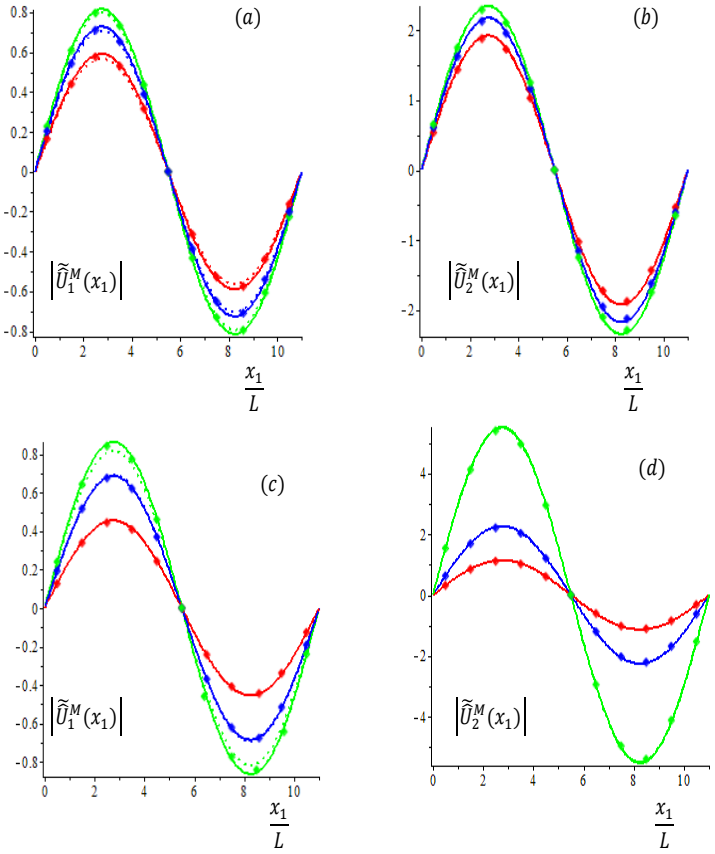

Figure 25: (a) magnitude of the dimensionless macro-displacement component $\hat{U}_1^M(x_1)$ induced by the harmonic body force $\hat{b}_1(x_1)$ along x_1. (b) Magnitude of the dimensionless macro-displacement component $\hat{U}_2^M(x_1)$ induced by the harmonic body force $\hat{b}_2(x_1)$ along x_1. The curves are obtained with different relaxation times related to phase 1 and phase 2: $\tau_\varsigma^1 = 1$, $\tau_\varsigma^2 = 2$ (red), $\tau_\varsigma^1 = 2$, $\tau_\varsigma^2 = 4$ (blue) and $\tau_\varsigma^1 = 10$, $\tau_\varsigma^2 = 20$ (green), with $r_E = r_\rho = 10$, $s_\varsigma = -0.5$, $\gamma = 1$ and $\eta = 1$. (c) Magnitude of the dimensionless macro-displacement component $\hat{U}_1^M(x_1)$ induced by the harmonic body force $\hat{b}_1(x_1)$ along x_1. (d) Magnitude of the dimensionless macro-displacement component $\hat{U}_2^M(x_1)$ induced by the harmonic body force $\hat{b}_2(x_1)$ along x_1. The curves are obtained as $r_E = 1$ (red), $r_E = 3$ (blue) and $r_E = 9$ (green), by considering $\tau_\varsigma^1 = 2$,$\tau_\varsigma^2 = 5$, $s_\varsigma = -0.5$, $\gamma = 1$ and $\eta = 1$.

the blue curves and diamonds are given for $s_\varsigma = -0.5$ and finally the green ones stand for $s_\varsigma = -0.3$. In Fig. 23-(b) the magnitude of the analytical dimensionless transformed macro-displacement $\tilde{\hat{U}}_2^M(x_1)$, which is obtained from the method 1 (continuous curve), and the transformed macro-displacement stemming from the method 2 (dotted curve) are put in relation with the heterogeneous solution (diamonds) for three increasing values of s_ς, which are $s_\varsigma = -2$ (red one), $s_\varsigma = -0.5$ (blue one) and $s_\varsigma = -0.3$ (green one). Both for the compressional and the shear problems 23-(a) and 23-(b), there is a very good agreement between the solution of the homogenized models and the numerical solution of the heterogeneous approach. Along the orthotropic direction x_2, the overall constitutive tensors $\hat{S}^i_{122122}$ and $\hat{S}^i_{222222}$, with $i = 1, 2$, are equal to zero and so the transformed macro-displacement (3.109) assumes the form

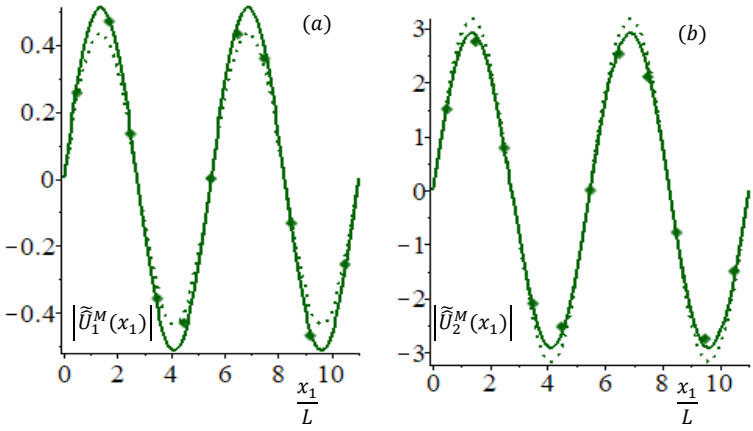

Figure 26: magnitude of the dimensionless macro-displacement component $\tilde{\hat{U}}_1^M(x_1)$ induced by the harmonic body force $\hat{b}_1(x_1)$ (a) and $\tilde{\hat{U}}_2^M(x_1)$ caused by $\hat{b}_2(x_1)$ (b) along direction x_1. The solution given by the homogenized model 1 (continuous curves) and model 2 (dotted curves) are compared with solution of the heterogeneous model (diamonds). The green curves are obtained for $s_\varsigma = -0.3$, with $\tau_\varsigma^i = 5$, $i \in 1, 2$, $r_E = r_\rho = 10$, $\tilde{\nu}_1 = \tilde{\nu}_2 = 0.2$, $\eta = 1$ and $\gamma = 1$.

$\hat{U}_{\alpha}^{M}(x_2) = \left(\frac{L_2}{2\pi}\right)^2 \frac{\Upsilon_\alpha \sin \frac{2\pi}{L_2} x_2}{s\hat{G}_{\alpha 2 \alpha 2}}$, with $\alpha = 1, 2$. Therefore, the magnitude of the dimensionless macro-displacement field $\tilde{\hat{U}}_1^M(x_2)$ (Fig. 24-(a)) and the magnitude of the dimensionless macro-displacement $\hat{U}_2^M(x_2)$ (Fig. 24-(b)), represented by continuous curves, are compared with the numerical macro-displacements associated with the heterogeneous model (diamonds), by varying the dimensionless complex frequency s_ς as: $s_\varsigma = -2$ (red one), $s_\varsigma = -0.5$ (blue one) and $s_\varsigma = -0.3$ (green one).
In Figs. (25)-(a) and (25)-(b), the magnitudes of the dimensionless transformed macro-displacement, $\tilde{\hat{U}}_j^M(x_1)$ $j = 1, 2$, along x_1 and deriving from method 1 (continuous curve) and method 2 (dotted curve) are compared with the numerical solution related to the heterogeneous domain (diamonds), by assuming different relaxation times for each phase, i.e.

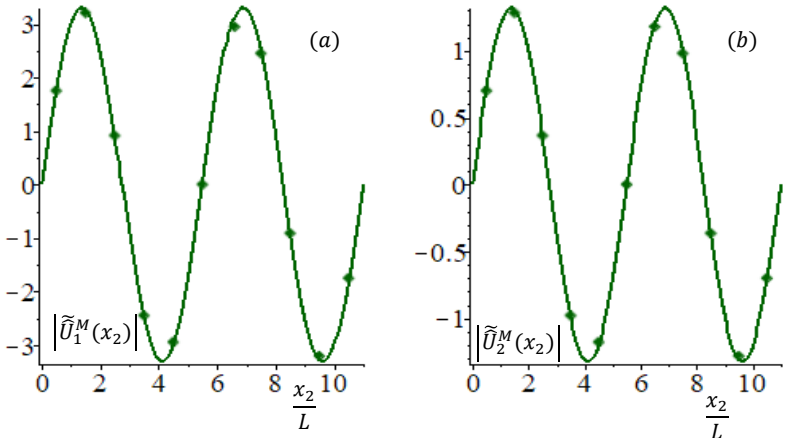

Figure 27: magnitude of the dimensionless macro-displacement component $\tilde{\hat{U}}_1^M(x_2)$ induced by the harmonic body force $\hat{b}_1(x_2)$ (a) and $\tilde{\hat{U}}_2^M(x_2)$ caused by $\hat{b}_2(x_2)$ (b) along direction x_2. The solution given by the homogenized model 1 (continuous curves) and model 2 (dotted curves) are compared with solution of the heterogeneous model (diamonds).The green curves are obtained by setting the dimensionless parameter $s_\varsigma = -0.3$, with $\tau_\varsigma^i = 5$, $i \in 1, 2$, $r_E = r_\rho = 10$, $\tilde{\nu}_1 = \tilde{\nu}_2 = 0.2$, $\eta = 1$ and $\gamma = 1$.

$\tau_\varsigma^1 \neq \tau_\varsigma^2$. In particular, in Figs. (25)-(a) and (25)-(b), the red curves are obtained for $\tau_\varsigma^1 = 1$, $\tau_\varsigma^2 = 2$, the blue curves for $\tau_\varsigma^1 = 2$, $\tau_\varsigma^2 = 4$ and the green ones for $\tau_\varsigma^1 = 10$, $\tau_\varsigma^2 = 20$. The magnitude of the dimensionless macro-displacement field $\tilde{\hat{U}}_1^M(x_1)$ (Fig. (25)-(c)) and the magnitude of the dimensionless macro-displacement $\hat{U}_2^M(x_1)$ (Fig. (25)-(d)) deriving from method 1 (continuous curve) and method 2 (dotted curve) are compared with the numerical macro-displacements corresponding with the heterogeneous model (diamonds), by varying the ratio between the Young's moduli r_E. The red curves are obtained by choosing $r_E = 1$, the blue curves for $r_E = 3$, and the green ones for $r_E = 9$, with two different and fixed relaxation times for each phase, $\tau_\varsigma^1 = 2$ and $\tau_\varsigma^2 = 5$. For the compressional problems ((25)-(a), (25)-(c)) and for the shear problems ((25)-(b), (25)-(d)), a good agreement is observed between the solution of

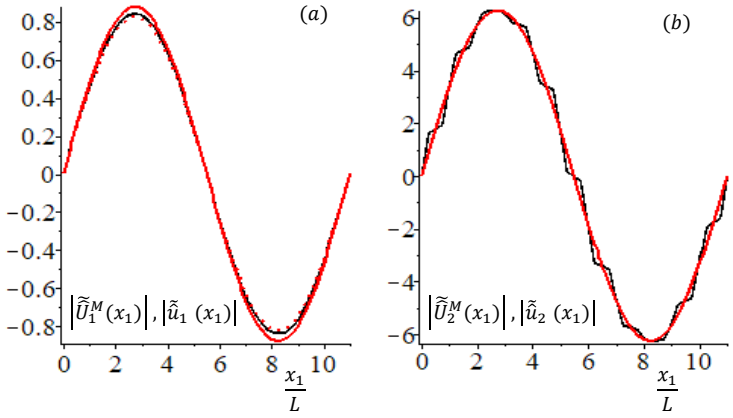

Figure 28: magnitude of the dimensionless macro-displacement component $\tilde{\hat{U}}_1^M$ (a) and $\tilde{\hat{U}}_2^M$ (b) caused by the harmonic body forces $\hat{b}_\alpha$ along direction x_1. The solution given by the homogeneous method 1 (continuous and red curves) and method 2 (dotted and red curves) are compared with the dimensionless transformed micro-displacement $\tilde{\hat{u}}_\alpha$ (black curves). The red curves are obtained by setting the dimensionless parameter $s_\varsigma = -2$, with $\tau_\varsigma^i = 5$, $i \in 1, 2$, $r_E = r_\rho = 10$, $\tilde{\nu}_1 = \tilde{\nu}_2 = 0.2$, $\eta = 1$ and $\gamma = 1$.

both homogenized models and the numerical solution of the heterogeneous method.

In Figs. (26)-(29), the material is in plane stress condition, the sample has a length $L/\varepsilon = 11$, with amplitude $\Upsilon_\alpha = 1$ N/mm^3, the Poisson ratios are equal for both phases, $\tilde{\nu}_1 = \tilde{\nu}_2 = 0.2$, the ratio between the thicknesses is $\eta = 1$, the parameter γ is $\gamma = 1$, the relaxation time is $\tau_\varsigma^i = 5$, $i = 1, 2$, the ratio between the densities is $r_\rho = 10$, the dimensionless complex frequency is $s_\varsigma = ss_2/\sqrt{\frac{\tilde{E}_2}{\rho_2}} = -0.3$ (for Figs. (26)-(27)) and $s_\varsigma = ss_2/\sqrt{\frac{\tilde{E}_2}{\rho_2}} = -2$ (for Figs. (28)-(29)) and the ratio between the Young's moduli is $r_E = 10$.

In Figs. 26 and 27, the harmonic body forces are supposed to be $\hat{b}_\alpha = \Upsilon_\alpha \sin \frac{4\pi}{L_\alpha} x_\alpha$. In Fig. 26-(a) a comparison between the magnitude of

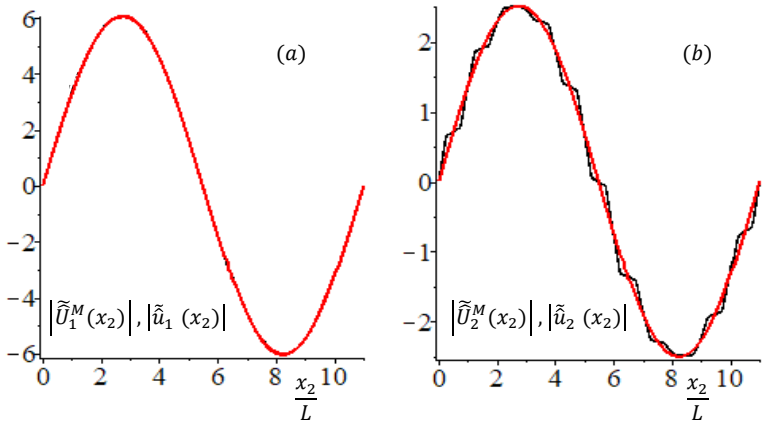

Figure 29: magnitude of the dimensionless macro-displacement component $\tilde{\hat{U}}_1^M$ (a) and $\tilde{\hat{U}}_2^M$ (b) caused by the harmonic body forces $\hat{b}_\alpha$ along direction x_2. The solution given by the homogeneous method 1 (continuous and red curves) and method 2 (dotted and red curves) are compared with the dimensionless transformed micro-displacement $\tilde{\hat{u}}_\alpha$ (black curves). The red curves are obtained for $s_\varsigma = -2$, with $\tau_\varsigma^i = 5$, $i \in 1, 2$, $r_E = r_\rho = 10$, $\tilde{\nu}_1 = \tilde{\nu}_2 = 0.2$, $\eta = 1$ and $\gamma = 1$.

the dimensionless macro-displacement $\tilde{\hat{U}}_1^M(x_1)$, derived from the approaches involving the overall constitutive tensors $\hat{S}^i_{111111}$, with $i = 1, 2$, and the solution of the heterogeneous problem is shown by setting $s_\varsigma = -0.3$. The continuous curve derives from the analytical solution, Eq. (3.109) with $i = 1$, and the dotted curve is related to the one with $i = 2$. In Fig 26-(b) the magnitude of the dimensionless macro-displacement $\tilde{\hat{U}}_2^M(x_1)$, derived from the approaches relying on the overall constitutive tensors $\hat{S}^i_{211211}$, $i = 1, 2$, and the heterogeneous solution (diamonds) are performed by imposing $s_\varsigma = -0.3$. The continuous curve is related to the analytical solution, Eq. (3.109) with $i = 2$, and the dotted curve stands for the one with $i = 1$.

The magnitude of the dimensionless macro-displacement field $\tilde{\hat{U}}_1^M(x_2)$ (Fig. 27-(a)) and the magnitude of the dimensionless macro-displacement $\hat{U}_2^M(x_2)$ (Fig. 27-(b)), represented by continuous curves, are compared with the numerical macro-displacements associated with the heterogeneous model (diamonds), by taking into account the dimensionless complex frequency $s_\varsigma = -0.3$. In Fig. 26 and 27, the effectiveness of the proposed homogenized models is well assessed because of the good agreement between the observed results.

In Fig 28-(a) the magnitudes of the dimensionless transformed macro-displacement $\tilde{\hat{U}}_1^M(x_1)$, obtained from approach 1 (continuous and red curve) and approach 2 (dotted and red curve), are compared with the magnitude of the dimensionless micro-displacement $\tilde{\hat{u}}_1(x_1)$, Eq. (2.67), represented by a continuous and a black curve and obtained by considering the mean line of the section. In Fig 28-(b) a comparison between the magnitudes of the dimensionless transformed macro-displacement $\tilde{\hat{U}}_2^M(x_1)$, from approach 1 (continuous and red curve) and from approach 2 (dotted and red curve), and the magnitude of the dimensionless micro-displacement $\tilde{\hat{u}}_2(x_1)$, obtained numerically, (continuous and black line) is performed, by setting the dimensionless complex frequency as $s_\varsigma = -2$.

Finally, the magnitude of the dimensionless macro-displacement field $\tilde{\hat{U}}_1^M(x_2)$ (Fig. 29-(a)) and the magnitude of the dimensionless macro-

displacement $\hat{U}_2^M(x_2)$ (Fig. 29-(b)), represented by red curve, are compared with the numerical micro-displacements $\tilde{\hat{u}}_1(x_2)$ and $\tilde{\hat{u}}_2(x_2)$, associated with the heterogeneous model (diamonds), by taking into account the dimensionless complex frequency $s_\varsigma = -2$.
In Figs. (23)-(a), (25)-(a), (25)-(c), (26)-(a), (26)-(b) and (28)-(a), it is clear to see a discrepancy between the two homogenized methods, represented by the continuous curves and the dotted curves. Such a discrepancy arises from Fig. (21)-(a) and (21)-(b).
Finally, the magnitudes of the transformed constitutive tensor $\hat{G}_{1111}$ (Fig. (30)-(a)) and $\hat{G}_{1212}$ (Fig. (30)-(b)), represented by the green line, are compared with the Voigt-Reuss bounds by varying the ratio related to phase 1, $\phi_1 = \frac{\eta}{\eta+1}$. It can be seen that $|\hat{G}_{1212}|$ coincides with the Voigt bound (red), thus the proposed method complies with the Voigt-Reuss bounds for viscoelastic materials through the corresponding principles, see Hashin and Shtrikman (1963); Hashin (1965); Hashin (1970); Chen and Lakes (1993); and Christensen (2012).

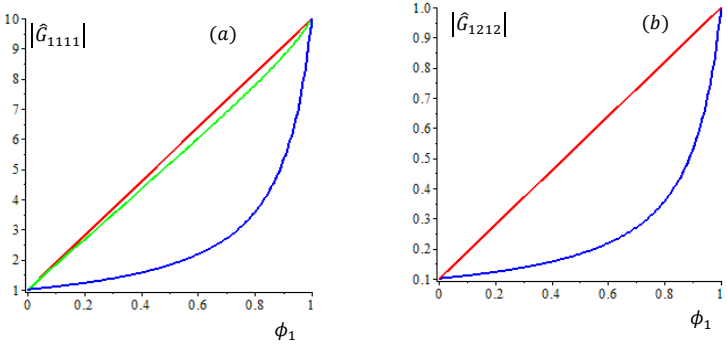

Figure 30: (a) magnitude of the constitutive tensor $\hat{G}_{1111}$, obtained with the homogenized method (green), is compared with the Voigt-Reuss bounds, with respect to $\phi_1 = \frac{\eta}{\eta+1}$. (b) The magnitude of the constitutive tensor $\hat{G}_{1212}$, obtained with the homogenized method (green), is compared with the Voigt-Reuss bounds, with respect to the volumetric ratio $\phi_1 = \frac{\eta}{\eta+1}$. The values are fixed as: $r_E = \tau_\varsigma^i = s_\varsigma = 10$, $i = 1, 2$, $\eta = 1$ and $\gamma = 1$.

The dispersion relation (2.147) is an implicit function depending on the real part of s, $\mathfrak{Re}(s)$, its imaginary part, $\mathfrak{Im}(s)$, and the wave number k_β, $\beta = 1, 2$, which have been non-dimensionalized as $\frac{\mathfrak{Re}(s)s_2}{\sqrt{\frac{\tilde{E}_2}{\rho_2}}}$, $\frac{\mathfrak{Im}(s)s_2}{\sqrt{\frac{\tilde{E}_2}{\rho_2}}}$ and $k_\beta\varepsilon$. Eq. (2.147) provides the dispersion curves related to the dynamic homogenization model and its simplified version presented in Sec. (2.7.2).

The dispersion curves obtained with two homogenized approaches are compared in Figs. (31), (32), (33), (34) and (35), where it is possible to observe the dual nature of the viscoelastic material that is reflected by the presence of the complex parameter s. Infact, its real part is related to the viscosity of the material whereas its imaginary part deals with its elastic behaviour. Therefore, the dispersion curves lay both on the real axis of s, which describes the wave propagation, and its imaginary axis, which characterizes the damping.

In Figs. (31) and (32), the dispersion curves, which are related to the compressional and the shear waves along the direction $\boldsymbol{e}_2$ and achieved with the homogenized models (dark line), are compared with the generalized dispersion function (light line) for longitudinal wave propagation in a periodic layered composite proposed by Rytov (1956), (see Appendix B). In Fig. (31)-(a), the parameter γ is chosen to assume different values, whereas the values of the dimensionless parameters are set as $\eta = 1$, $\tilde{\nu}_1 = \tilde{\nu}_2 = 0.2$, $r_\rho = r_E = 10$ and $\tau_\varsigma^i = 1$, $i = 1, 2$. In particular, Fig. (31)-(a) shows the curves related to the compressional waves as $\gamma = 1/10$ (red), $\gamma = 1/2$)blue and $\gamma = 1$ (green). When γ decreases the effect of the viscosity is less detectable because the curves approach the imaginary axes of the complex frequency. In Fig. (31)-(b), the dimensionless relaxation time τ_ς^i is supposed to vary, whereas the values of the dimensionless parameters are set as $\eta = 1$, $\tilde{\nu}_1 = \tilde{\nu}_2 = 0.2$, $r_\rho = r_E = 10$ and $\gamma = 1/10$. Fig. (31)-(b) shows that by increasing the relaxation time τ_ς^i up to high values ($\tau_\varsigma^i = \infty$) the green curve approaches the imaginary axes of the complex frequency. For low values ($\tau_\varsigma^i = 1$ and $\tau_\varsigma^i = 1/3$) the related curves (the red and the blue one) are strongly affected by the viscoelastic response.

In Fig. (31)-(c), the dimensionless ratio between the thicknesses of the material η is supposed to vary, whereas the values of the dimensionless parameters are set as $\tilde{\nu}_1 = \tilde{\nu}_2 = 0.2$, $r_\rho = r_E = 10$, $\tau_\varsigma^i = 1$ and $\gamma = 1/10$. Fig. (31)-(c) depicts three dispersion curves obtained for $\eta = 2$ (blue), for $\eta = 1$ (red) and for $\eta = 1/2$ (green). In Fig. (31)-(d), the ratio between the densities r_ρ and the ratio between the Young's moduli r_E are assumed to vary, whereas the values of the dimensionless parameters are set as $\tilde{\nu}_1 = \tilde{\nu}_2 = 0.2$, $\eta = 1$, $\tau_\varsigma^i = 1$ and $\gamma = 1/10$. Fig. (31)-(d) shows three dispersion curves derived for $r_\rho = r_E = 10$ (red), $r_\rho = r_E = 20$ (blue) and $r_\rho = r_E = 50$ (green). From the diagrams of Fig. (31), the dispersion curves derived from the proposed homogenized models are in good agreement with the ones related to the heterogeneous material obtained with the exact theory of Floquet–Bloch in the range of $[0, \pi/2]$.

Fig. (32) represents the dispersion curves related to the shear waves along the direction $\boldsymbol{e}_2$ normal to the layers in terms of the dimensionless wave number $k_2\varepsilon \in [0, 2\pi]$. In Fig. (32)-(a), the parameter γ is supposed to assume different values, whereas the values of the dimensionless parameters are set as $\eta = 1$, $\tilde{\nu}_1 = \tilde{\nu}_2 = 0.2$, $r_\rho = r_E = 10$ and $\tau_\varsigma^i = 2$, $i = 1, 2$. In Fig. (32)-(a), the red curve corresponds to $\gamma = 1/10$, the blue one to $\gamma = 1/5$ and the green one to $\gamma = 1/2$. In Fig. (32)-(b), the dimensionless relaxation time τ_ς^i, $i = 1, 2$, is supposed to vary, whereas the values of the dimensionless parameters are set as $\gamma = 1/10$, $\eta = 1$, $r_\rho = r_E = 10$, $\tilde{\nu}_1 = \tilde{\nu}_2 = 0.2$. In Fig. (32)-(b), the red curve is related to $\tau_\varsigma^i = 1/2$, the green one to $\tau_\varsigma^i = 1$ and the blue one to $\tau_\varsigma^i = 2$. By increasing the value of the dimensionless relaxation time, the viscosity effect becomes less evident. Fig. (32)-(c) is obtained by varying the dimensionless ratio between the thicknesses of the material η, with the following dimensionless parameters $\tau_\varsigma^i = 1$, $r_\rho = r_E = 10$, $\tilde{\nu}_1 = \tilde{\nu}_2 = 0.2$ and $\gamma = 1/10$. Fig. (32)-(c) shows three dispersion curves stemming from the heterogeneous and the homogenized models, where the blue curves are obtained for $\eta = 2$, the red oness for $\eta = 1$ and the green ones for $\eta = 1/2$. Fig. (32)-(d) is derived by varying the ratio between the densities and ratio between the Young's moduli $r_\rho = r_E$, with the following dimensionless parameters $\tau_\varsigma^i = 1$, $\eta = 1$, $\tilde{\nu}_1 = \tilde{\nu}_2 = 0.2$ and $\gamma = 1/10$. Fig. (32)-(d)

illustrates the dispersion curves obtained for $r_\rho = r_E = 10$ (red), the blue $r_\rho = r_E = 15$ (blue) and for $r_\rho = r_E = 20$ (green).
In Figs. (31) and (32), it is clear to see that the discrepancy between the phase velocity and the group velocity, which is noticeable in the heterogeneous model, generates dispersion phenomena that are well described by the proposed homogenized models at the second order in contrast with the first order homogenized model which is not able to capture the dispersion phenomena.
Fig. (33) and Fig. (34) show the behavior of the dimensionless real part of s in terms of the dimensionless imaginary part of s and the dimensionless wave number $k_1\varepsilon$. In case of dispersion curves related to compressional and shear waves along the layering axis $\boldsymbol{e}_1$, the wave number $k_1\varepsilon$ belongs to the interval $[0, \pi/2]$, where the dispersione curves derived from approach 1 (thicker line) and approach 2 (thinner line) are compared. Fig. (33)-(a) shows the dispersion curves obtained by varying the parameter γ, whereas the dimensionless parameters are assumed as $\tau_\varsigma^i = 2$, $i = 1, 2$, $\eta = 1$, $r_\rho = r_E = 10$ and $\tilde{\nu}_1 = \tilde{\nu}_2 = 0.2$. Fig. (33)-(a) shows the curves related to the compressional waves and corresponding to $\gamma = 1/20$ (red), $\gamma = 1/10$ (blue) and $\gamma = 1/5$ (green). As γ goes up the curves gradually increase. Fig. (33)-(b) depicts the dispersion curves obtained with different values of the relaxation time τ_ς^i, $i = 1, 2$, which is the same for both phases, whereas the dimensionless parameters are assumed as $\gamma = 1/10$, $\eta = 1$, $r_\rho = r_E = 10$ and $\tilde{\nu}_1 = \tilde{\nu}_2 = 0.2$. In particular, for low values of τ_ς^i, namely $\tau_\varsigma^i = 1/20$, which is represented by the red curve, and $\tau_\varsigma^i = 1/10$, identified by the blue curve, the viscoelasticity strongly affects the dispersion curves, which are enterely embedded in the real and the imaginary plane. By increasing the relaxation time $\tau_\varsigma^i = \infty$, the elastic behaviour is retrieved (green curve) and the curve is squeezed in the imaginary axes of the complex frequency. Fig. (33)-(c) highlights the trends of three curves developed by setting three different values of the ratio between the thicknesses of the material η and by assuming the dimensionless parameters as $r_E = r_\rho = 10$, $\tau_\varsigma^i = 2$ and $\gamma = 1/10$ and $\tilde{\nu}_1 = \tilde{\nu}_2 = 0.2$. The red curve is obtained for $\eta = 5$, the blue one for $\eta = 3$ and the green one for $\eta = 1/2$. Finally, Fig. (33)-(d)

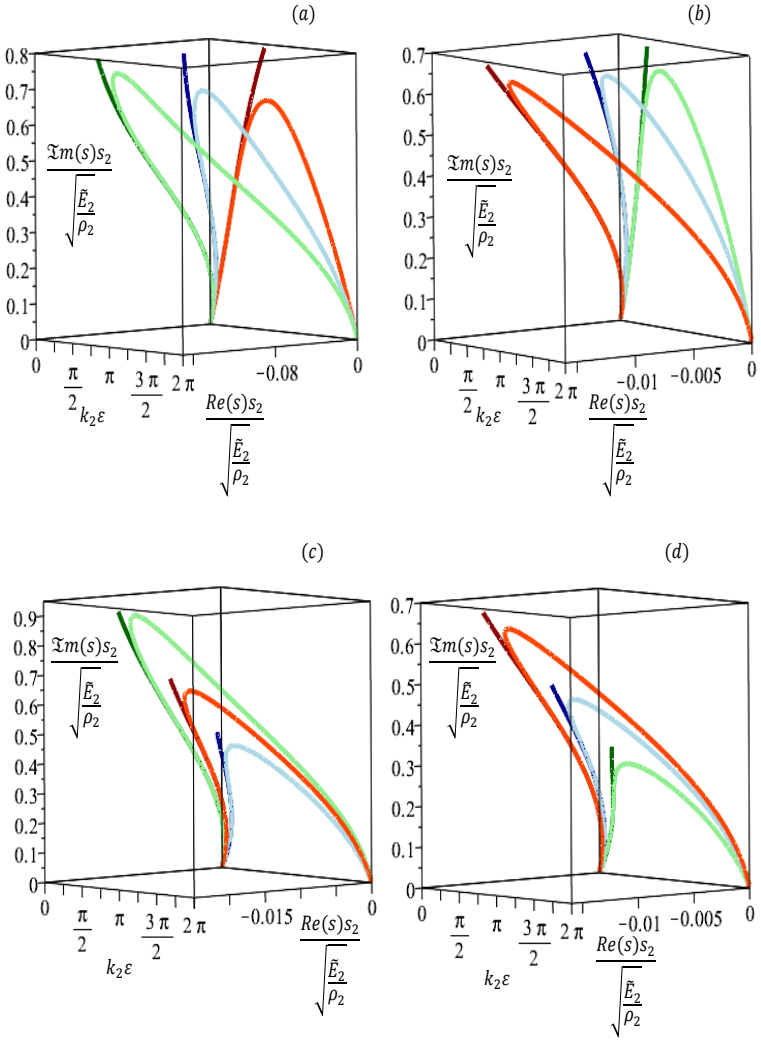

Figure 31: compressional waves along the normal direction $\boldsymbol{e}_2$ derived from two homogenized approaches (dark line) and from the heterogeneous one (light line) (a) for: $\gamma = 1/10$ (red curves), $\gamma = 1/5$ (blue curves) and $\gamma = 1$ (green curves), with $\tau_\varsigma^i = 2$, $i = 1, 2$, $\eta = 1$ and $r_\rho = r_E = 10$. (b) is obtained for: $\tau_\varsigma^i = 1/3$ (red), $\tau_\varsigma = 2$ (blue) and $\tau_\varsigma^i = \infty$ (green). (c) is derived for: $\eta = 2$ (blue), $\eta = 1$ (red), and $\eta = 1/2$ (green). (d) is derived for: $r_\rho = r_E = 10$ (red), $r_\rho = r_E = 20$ (blue) and $r_\rho = r_E = 50$ (green), with $\tilde{\nu}_1 = \tilde{\nu}_2 = 0.2$.

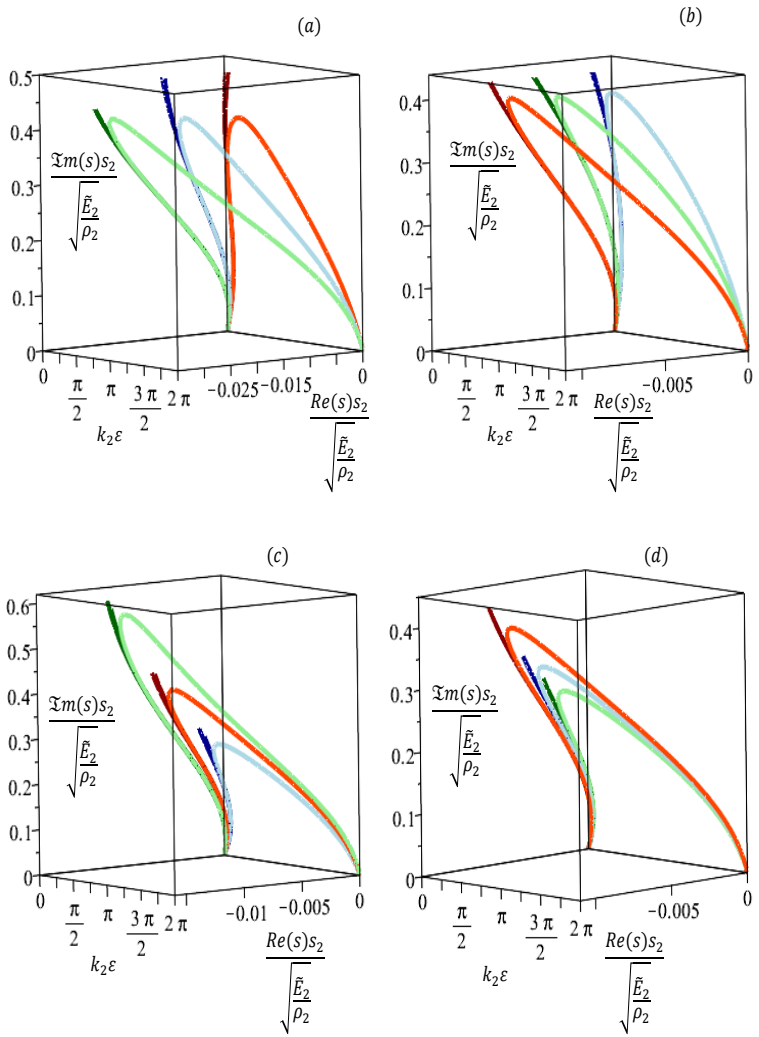

Figure 32: shear waves along the normal direction $\boldsymbol{e}_2$ derived from two homogenized approaches (dark line) and from the heterogeneous one (light line) (a) by varying γ as $\gamma = 1/10$ (red curves), $\gamma = 1/5$ (blue curves) and $\gamma = 1/2$ (green curves). (b) is obtained for: $\tau_\varsigma^i = 1/2$ (red), $\tau_\varsigma = 1$ (green) and $\tau_\varsigma^i = 2$ (blue). (c) is derived for: $\eta = 2$ (blue) $\eta = 1$ (red) and $\eta = 1/2$ (green). (d) is retrieved for: $r_\rho = r_E = 10$ (red), $r_\rho = r_E = 15$ (blue) and $r_\rho = r_E = 20$ (green), with $\tilde{\nu}_1 = \tilde{\nu}_2 = 0.2$.

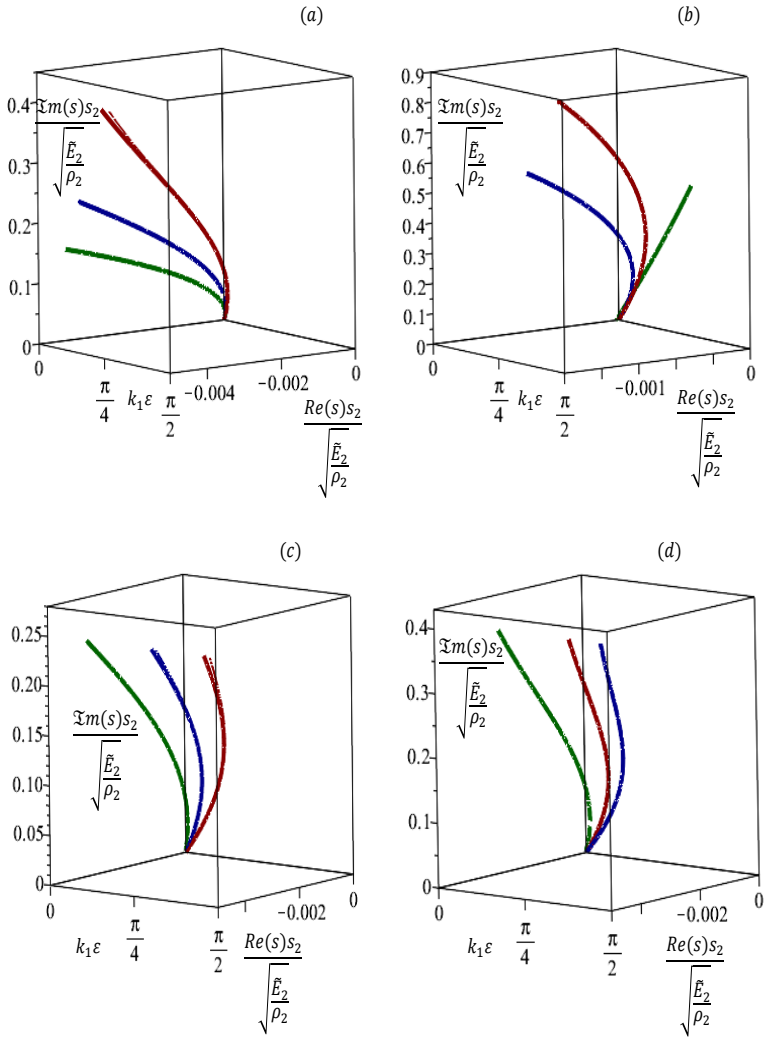

Figure 33: compressional waves along the layering direction $\boldsymbol{e}_1$ derived from two approaches (a) by varying γ as $\gamma = 1/20$ (red curves), $\gamma = 1/10$ (blue curves) and $\gamma = 1/5$ (green curves). (b) is obtained for: $\tau_\varsigma^i = 1/20$ (blue), $\tau_\varsigma^i = 1/10$ (red) and $\tau_\varsigma = \infty$ (green). (c) is derived for: $\eta = 5$ (red), $\eta = 3$ (blue) and $\eta = 1/2$ (green). (d) is retrieved for: $r_\rho = r_E = 50$ (blue), $r_\rho = r_E = 30$ (red) and $r_\rho = r_E = 5$ (green), with $\tilde{\nu}_1 = \tilde{\nu}_2 = 0.2$.

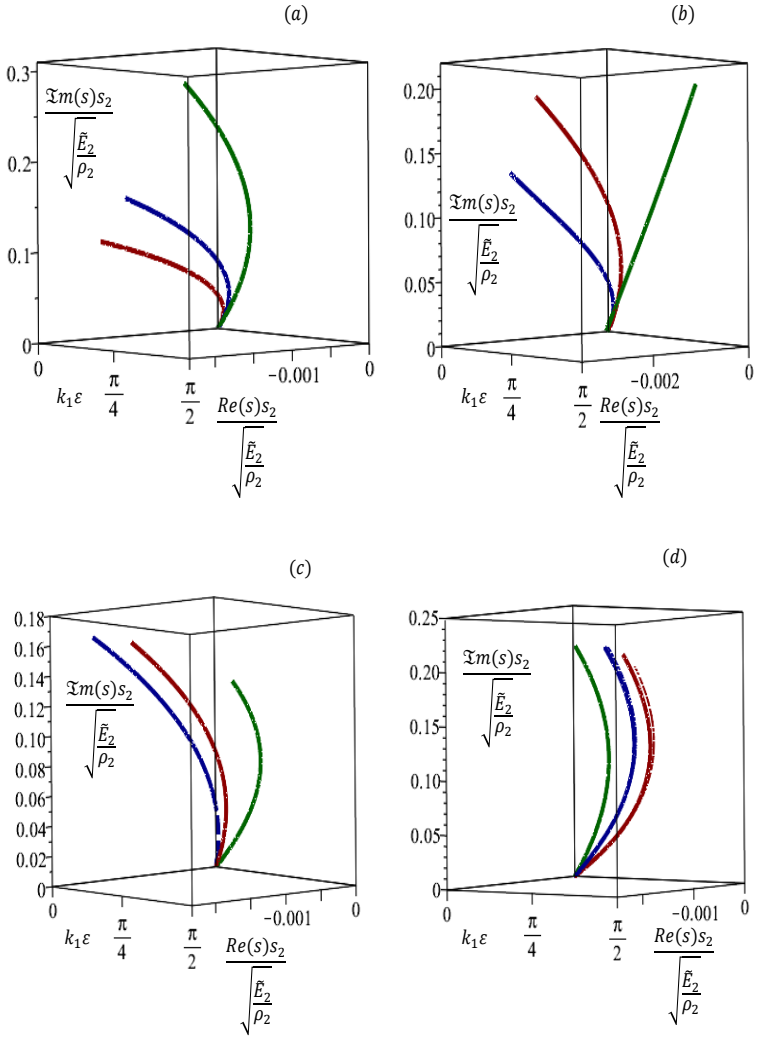

Figure 34: shear waves along the layering direction $\boldsymbol{e}_1$ derived from two approaches (a) by modifying γ as $\gamma = 1/5$ (red curves), $\gamma = 1/10$ (blue curves) and $\gamma = 1/30$ (green curves). (b) is obtained for: $\tau_\varsigma^i = 2$ (blue), $\tau_\varsigma^i = 5$ (red) and $\tau_\varsigma = \infty$ (green). (c) is derived for: $\eta = 1/5$ (blue), $\eta = 1$ (red) and $\eta = 4$ (green). (d) is obtained for: $r_\rho = r_E = 50$ (red), $r_\rho = r_E = 25$ (blue), and $r_\rho = r_E = 10$ (green), with $\tilde{\nu}_1 = \tilde{\nu}_2 = 0.2$.

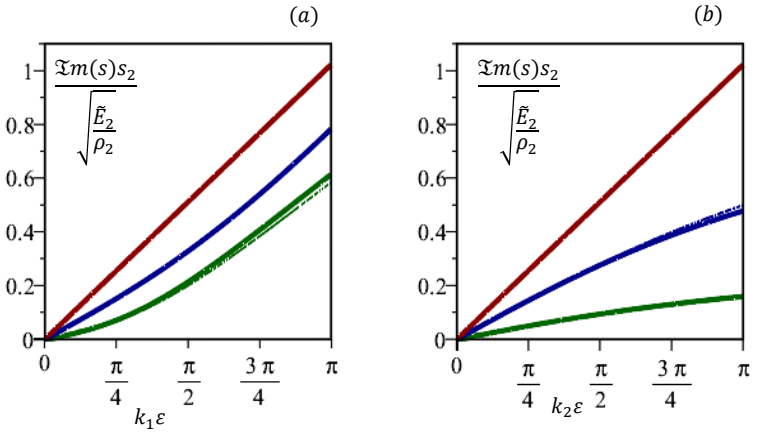

Figure 35: shear waves along the layering direction $\boldsymbol{e}_1$ (a) and the normal direction $\boldsymbol{e}_2$ (b) deriving from the homogenized method 1 (thicker line) and the homogenized method 2 (thinner line) for different values of the ratio between the densities and ratio between the Young's moduli: $r_\rho = r_E = 1$ (red), $r_\rho = r_E = 10$ (blue) and $r_\rho = r_E = 100$ (green), by fixing the dimensionless relaxation time as $\tau_\varsigma^i = \infty$ with $\tilde{\nu}_1 = \tilde{\nu}_2 = 0.2$, $\eta = 1$ and $\gamma = 1/10$.

represents how for three increasing values of the ratio between the densities and ratio between the Young's moduli, $r_\rho = r_E$, the related curves are influenced, by fixing $\gamma = 1/10$, $\tau_\varsigma^i = 2$ and $\eta = 1$. The green curve is given with $r_\rho = r_E = 5$, the red one with $r_\rho = r_E = 30$ and the blue one corresponds to $r_\rho = r_E = 50$.

In Fig. (34) dispersion curves related to the shear waves along the axes $\boldsymbol{e}_1$ are taken into account and the curves achieved from approach 1 and approach 2 are compared. Fig. (34)-(a) shows the dispersion curves obtained by varying the parameter γ, whereas the dimensionless parameters are set as $\tau_\varsigma^i = 2$, $\eta = 1$ and $r_\rho = r_E = 10$ and $\tilde{\nu}_1 = \tilde{\nu}_2 = 0.2$. In Fig. (34)-(a), the red curve corresponds to $\gamma = 1/5$, the blue one to $\gamma = 1/10$ and the green one to $\gamma = 1/30$. As γ goes up the curves steadily decrease. Fig. (34)-(b) is obtained by varying the relaxation time τ_ς^i, $i \in 1, 2$, by taking into account the dimensionless parameters as $\eta = 1$, $r_\rho = r_E = 10$,

$\gamma = 1/10$ and $\tilde{\nu}_1 = \tilde{\nu}_2 = 0.2$. In particular, Fig. (34)-(b) shows that by increasing the relaxation time τ_ς^i up to high values ($\tau_\varsigma^i = \infty$) the green curve is achieved and so the viscoelastic effect is negligible. As the relaxation time assumes low values ($\tau_\varsigma^i = 2$ and $\tau_\varsigma^i = 5$) the corresponding curves (the red and the blue one) are strongly influenced by the viscoelastic response. In Fig. (34)-(c), by setting three values for the dimensionless ratio between the thicknesses of the material η, the following curves are obtained: the blue curve stems from $\eta = 1/5$, the red one from $\eta = 1$ and the green one from $\eta = 4$, with fixed values of the dimensionless parameters $\gamma = 1/10$, $\tau_\varsigma^i = 2$, $r_\rho = r_E = 10$ and $\tilde{\nu}_1 = \tilde{\nu}_2 = 0.2$. Fig. (34)-(d) shows the curves obtained for three values of the ratio between the densities and ratio between the Young's moduli, $r_\rho = r_E$. The green one relates to $r_\rho = r_E = 10$, the blue curve corresponds with the value $r_\rho = r_E = 25$ and the red one $r_\rho = r_E = 50$, with the fixed parameters $\gamma = 1/10$, $\tau_\varsigma^i = 2$, $\eta = 1$ and $\tilde{\nu}_1 = \tilde{\nu}_2 = 0.2$. From Figs. (33)-(a), (33)-(c) and (34)-(d), it is clear that there is a slight difference between the dispersion curves obtained from the two homogenized models in the range of the considered dimensionless wave number $k_1\varepsilon$.

Fig. (35)-(a) and (35)-(b) show the dispersion curves related to the shear waves along the direction $\boldsymbol{e}_1$ and $\boldsymbol{e}_2$, respectively. The dimensionless parameters are set as $\gamma = 1/10$, $\eta = 1$ and $\tilde{\nu}_1 = \tilde{\nu}_2 = 0.2$. The dispersion curves are obtained from the homogenized method 1 (thicker line) and method 2 (thinner line) by varying the ratio between the densities and ratio between the Young's moduli and by fixing the dimensionless relaxation time as $\tau_\varsigma^i = \infty$ to retrieve the elasic case. The red lines are obtained for $r_\rho = r_E = 1$, the blue one for $r_\rho = r_E = 10$ and the green one for $r_\rho = r_E = 100$. The green curve of Fig. (35)-(a) and the blue curve of Fig. (35)-(b) show an appreciable difference between the two homogenized models. In Fig. (35), there is point in observing that the dispersion phenomenon is emphasized by the non-linearity of the dispersion curves as a consequence of the variation of the ratio between the densities and ratio between the Young's moduli. Moreover, in Fig. (35)-(a), it is clear that the group velocity, which describes the velocity at which the wave envelope propagates, is greater than the velocity phase, describing the velocity of

the individual harmonic contribution. Such an issue is emphasized in the the green curve. Finally, in Fig. (35)-(b) the phase velocity is greater than the group velocity and so the individual harmonic contribution has a speed of travel greater than the wave envelope, which ca be observed in the blue curve.

Chapter 4

Conclusions

The thesis proposed a variational-asymptotic homogenization model for viscoelastic materials having a periodic microstructure. Specifically, the field equations at the micro-scale have been derived and transposed into the Laplace domain to treat viscoelasticity, relying on the complex frequency and the micro-relaxation tensor. Next, the down-scaling relation and the up-scaling relation have been detailed. In particular, the down-scaling relation relates the transformed micro-displacement field to the transformed macro-displacement field and its gradients by means of the perturbation functions, which are the solutions of the cell problems defined over the unit cell $\mathcal{Q}$. Perturbation functions are $\mathcal{Q}$-periodic and have vanishing mean values over the unit cell. On the other hand, the up-scaling relation defines the transformed macro-displacement field as the mean value of the transformed micro-displacement field over the unit cell $\mathcal{Q}$. By introducing the down-scaling relation into the field equations at the micro-scale of the viscoelastic material, the average field equations of infinite order have been determined. Their truncation at an arbitrary order could not ensure the ellipticity of the differential problem. To avoid such an issue, two methods, based on a variational-asymptotic approach, have been invoked. According to the first method, the down-scaling relation is replaced into the transformed energy-like functional, which is truncated at the second order. By imposing the first variation of the

truncated energy-like functional equal to zero, the field equation at the macro-scale and the overall inertial and constitutive tensors have been determined. In the second method, the gradient related to the down-scaling relation has been approximated at the first order and the transformed micro-displacement has been truncated at second order. Both are introduced into the transformed energy-like functional and, from its first variation, the field equation at the macro-scale and the corresponding overall inertial and constitutive tensors have been derived. In both methods, the overall constitutive tensors depend on the localization functions, whereas the overall inertial tensors are expressed through the perturbation functions. In the limit case of an homogeneous material without heterogeneities, the perturbation functions consistently become identically equal to zero, the components of the localization tensors vanish and the equation of motion of the classical continuum has been retrieved.
To assess the accuracy of the homogenized model herein analysed and its validity limits, a bimaterial periodically-layered composite with orthotropic phases endowed with an orthotropy axis parallel to the layer direction has been considered. In this case, the micro-fluctuation functions and the components of the overall inertial and constitutive tensors have been derived in an analytic way and their dependence on the real part and on the imaginary part of the complex frequency has been emphasized. Without loss of generality, it is specialized in case of isotropic phases. Moreover, a detailed study of the dispersion function, deriving from the generalized Christoffel equation for shear and compressional waves along two orthogonal axis, is performed. A good agreement has been pointed out between the dispersion curves derived from the homogenized methods and those retrieved from the heterogeneous material with the Floquet-Bloch approach. Finally, the analytical solutions for the transformed macro-displacement field derived from the two homogenized models and subjected to $\mathcal{L}-$periodic forces have been compared with the reference numerical solution obtained from a finite element analysis of the heterogeneous model in order to evaluate the forced response in the transformed domain. A good agreement between the three models has been achieved, proving the validity of the proposed

homogenized methods.
The variational-asymptotic homogenization method herein proposed is helpful to describe the dispersive properties of a viscoelastic material and to detect the effective viscoelastic properties of many composite materials and it may be adopted for the manufacture and the design of more efficient and sophisticated devices, for a large spectra of applications.

REFERENCES

Addessi D., De Bellis M. L. and Sacco E., (2013). *Micromechanical analysis of heterogeneous materials subjected to overall cosserat strains.* Mech. Res. Commun. 54, 27–34.

Aifantis E.C., (2003). *Update on a class of gradient theories.* Mechanics of materials. 35(3-6), 259-280.

Allaire G., (1992). *Homogenization and two-scale convergence*. SIAM Journal of Mathematical Analisys. 23, 1482-1518.

Andrianov I.V., Bolshakov V.I., Danishevskyy V.V. and Weichert D., (2008). *Higher order asymptotic homogenization and wave propagation in periodic composite materials.* Proceedings of the Royal Society of London A: Mathematical, Physical and Engineering Sciences. 464(2093), 1181-1201.

Azar K. and Graebner J.E., (1996). *Experimental determination of thermal conductivity of printed wiring boards.* SEMI-THERM XII Proceedings, Twelfth Annual IEEE. 123(3), 169-182.

Bacca M., Bigoni D., Dal Corso F. and Veber D., (2007). *Anisotropic effective higher-order response of heterogeneous Cauchy elastic materials* Mechanics Research Communications. 54, 63-71.

Bacca M., Bigoni D., Dal Corso F. and Veber D., (2013a). *Mindlin second-gradient elastic properties from dilute two-phase cauchy-elastic composites. part I: closed form expression for the effective higher-order constitutive tensor.* Int. J. Solids Struct. 50 (24), 4010–4019.

Bacca M. , Bigoni D. , Dal Corso F. , Veber D., (2013b). *Mindlin second-gradient elastic properties from dilute two-phase cauchy-elastic composites. part II: Higher-order constitutive properties and application cases.* Int. J. Solids Struct. 50 (24), 4020–4029.

Bacigalupo A. and Gambarotta L., (2010). *Second-order computational homogenization of heterogeneous materials with periodic microstructure.* J. Appl. Math. Mech./Z. Angew. Math. Mech. 90, 796–811.

Bacigalupo A. and Gambarotta L., (2010). *Micro-polar and second order homogenization of periodic masonry.* In Materials Science Forum,Trans Tech Publications. 638, 2561-2566

Bacigalupo A. and Gambarotta L., (2011). *Non-local computational homogenization of periodic masonry.* International Journal for Multiscale Computational Engineering. 9(5), Begel House Inc.

Bacigalupo A. and Gambarotta L., (2013). *A multi-scale strain-localization analysis of a layered strip with debonding interfaces.* International Journal of Solids and Structures. 50(13) 2061–2077, Elsevier.

Bacigalupo A., (2014). *Second-order homogenization of periodic materials based on asymptotic approximation of the strain energy: formulation and validity limits.* Meccanica 49 (6), 1407–1425.

Bacigalupo A. and Gambarotta L., (2014a). *Computational dynamic homogenization for the analysis of dispersive waves in layered rock masses with periodic fractures.* Comput. Geotech. 56, 61–68.

Bacigalupo A. and Gambarotta L. , (2014b). *Second-gradient homogenized model for wave propagation in heterogeneous periodic media.* Int. J. Solids Struct. 51 (5), 1052–1065.

Bacigalupo A., Morini L., Piccolroaz A., (2014). *Effective elastic properties of planar sofcs: a non-local dynamic homogenization approach.* Int. J. Hydrogen Energy 39 (27), 15017–15030 .

Bacigalupo A. and De Bellis M.L., (2015). *Auxetic anti-tetrachiral materials:*

equivalent elastic properties and frequency band-gaps. Composite Structures. 131, 530-544.

Bacigalupo A., Morini L. and Piccolroaz A., (2016a). *Multiscale asymptotic homogenization analysis of thermo-diffusive composite materials.* Int. J. Solids Struct. 85–86, 15–33.

Bacigalupo A., Morini L., Piccolroaz A., (2016b). *Overall thermomechanical properties of layered materials for energy devices applications.* Compos. Struct. 157, 366–385.

Bakhvalov N. and Panasenko G., (1984). *Homogenization: Averaging Processes in Periodic Media.* Kluwer Academic Publishers, Dordrecht-Boston-London.

Bensoussan A., Lions J. and Papanicolaou, G., (1978). *Asymptotic Analysis for Periodic Structures.* North-Holland, Amsterdam.

Beurthey S. and Zaoui A., (2000) *Structural morphology and relaxation spectra of viscoelastic heterogeneous materials.* European Journal of Mechanics-A/Solids, 19(1):1–16.

Bigoni D. and Drugan W., (2007). *Analytical derivation of cosserat moduli via homogenization of heterogeneous elastic materials.* J. Appl. Mech. 74 (4), 741–753, American Society of Mechanical Engineers.

Bourdin B., Francfort G. and Marigo J.J., (2008). *The variational approach to fracture.* Springer.

Boutin C. and Auriault J.L., (1993). *Rayleigh scattering in elastic compisite materials.* International Journal of Solids and Structures. 31, 1669-1689.

Boutin C., (1996). *Microstructural effects in elastic composites.* International Journal of Solids and Structures. 33, 1023-1051.

Chen C. and Lakes R., (1993). *Analysis of high-loss viscoelastic composites.* Journal of materials science, 28(16):4299–4304.

Chen Q., Wang G., Chen X. and Geng J., (2017). *Finite-volume homogenization of elastic/viscoelastic periodic materials.* Composite Structures. 182, 457-470.

Christensen R., (2012). *Theory of viscoelasticity: an introduction.* Elsevier.

Colinas-Armijo N., Di Paola M. and Pinnola F.P., (2016). *Fractional characteristic times and dissipated energy in fractional linear viscoelasticity.* Communications in Nonlinear Science and Numerical Simulation, 37, pp.14-30.

Davies B. and Martin B., (1979). *Numerical inversion of the laplace transform: a survey and comparison of methods*. Journal of computational physics, 33(1):1–32.

De Bellis M.L. and Bacigalupo A., (2017). *Auxetic behavior and acoustic properties of microstructured piezoelectric strain sensors*. Smart Materials and Structures. 26(8), 741–753, IOP Publishing.

Dhakal H. N., Ismail S. O., Ojo S. O., Paggi M. and Smith J. R., (2018). *Abrasive water jet drilling of advanced sustainable bio-fibre-reinforced polymer/hybrid composites: a comprehensive analysis of machining-induced damage responses.* The International Journal of Advanced Manufacturing Technology. 1-15.

Di Paola M. and Pinnola F. P., *Calcolo Frazionario e Viscoelasticità*, Dipartimento di Ingegneria Civile Ambientale e Aerospaziale, Universita degli Studi di Palermo, Palermo, Italy.

Di Paola M., Pirrotta A. and Valenza A., (2011). *Visco-elastic behavior through fractional calculus: an easier method for best fitting experimental re-*

sults. Mechanics of Materials, 43(12), pp.799-806.

Di Paola M., Fiore V., Pinnola, F.P. and Valenza, A., (2014). *On the influence of the initial ramp for a correct definition of the parameters of fractional viscoelastic materials.* Mechanics of Materials, 69(1), pp.63-70.

Donolato C., (2002). *Analytical and numerical inversion of the laplace–carson transform by a differential method.* Computer Physics Communications, 145(2):298–309.

Drugan W.J. and Willis J.S., (1996). *A micromechanics-based nonlocal constitutive equation and estimates of representative volume element size for elastic composites.* Journal of the Mechanics and Physics of Solids. 44(4), 497-524.

Einstein A., (1906). *A new determination of molecular dimensions.* Annalen der Physik. 19, 289-306.

Eringen A.C., Suhubi E.S., (1964). *Nonlinear theory of simple micro-elastic solids.* International Journal of Engineering Science. 2(2), 189-203.

Eringen A.C., (1995). *Balance laws of micromorphic continua revisited.* International Journal of Engineering Science. 30(6), 805-810.

Eringen A.C. , Maugin G.A., (2012). *Electrodynamics of Continua I: Foundations and Solid Media.* Springer Science Business Media.

Ezzat M.A., El-Karamany A.S. and El-Bary A.A., (2015). *Thermo-viscoelastic materials with fractional relaxation operators.* Applied Mathematical Modelling, 39(23-24), pp.7499-7512.

Fantoni F., Bacigalupo A. and Paggi M., (2017). *Multi-field asymptotic homogenization of thermo-piezoelectric materials with periodic microstructure.* International Journal of Solids and Structures. 120, 31-56, Elsevier.

Fleck N.A., and Hutchinson J.W., (2001). *A reformulation of strain gradient plasticity.* Journal of the Mechanics and Physics of Solids. 49(10), 245-2271.

Forest S., (2002). *Homogenization methods and mechanics of generalized continua-part 2.* Theoretical and applied mechanics, (28-29):113–144.

Forest S. and Sab K., (1998). *Cosserat overall modeling of heterogeneous materials.* Mech. Res. Commun. 25 (4), 449–454.

Forest S. and Aifantis E.C., (2010). *Some links between recent gradient thermoelasto-plasticity theories and the thermomechanics of generalized continua.* Int. J. Solids Struct. 47 (25), 3367–3376.

Forest S. and Trinh D., (2011). *Generalized continua and nonhomogeneous boundary conditions in homogenisation methods.* J. Appl. Math. Mech./Z. Angew. Math. Mech. 91 (2), 90–109.

Francfort G., Leguillon D. and Suquet P., (1983). *Homogenization for linearly viscoelastic bodies.* Comptes rendus de l'academie des sciences serie mathematiques,296(5):287–290.

Francfort G. and Suquet P. M., (1986). *Homogenization and mechanical dissipation in thermoviscoelasticity.* Archive for Rational Mechanics and Analysis, 96(3):265–293.

Gambin B. and Kroner E., (1989). *Higher Order Terms in the Homogenized Stress-Strain Relation of Periodic Elastic Media. physica status solidi (b).* International Journal of Engineering Science. 151(2) 513-519.

Gerasik V. and Stastna M.,(2010). *Complex group velocity and energy transport in absorbing media.* Physical Review E, 81(5):056602.

Germain P. (1973). *The method of virtual power in continuum mechanics. Part*

2: Microstructure. SIAM Journal on Applied Mathematics, 25(3), 556-575.

Green A.E. and Rivlin R.S., (1964). *Multipolar continuum mechanics.* Archive for Rational Mechanics and Analysis. 17 (2), 113–147.

Green A.E. and Lindsay K.A., (1972). *Thermoelasticity.* J. Elast. 2 (1), 1–7.

Haasemann G. and Ulbricht V., (2010). *Numerical evaluation of the viscoelastic and viscoplastic behavior of composites.* Technische Mechanik. 30(1-4), 122-135.

Hashin Z. and Shtrikman S., (1963). *A variational approach to the theory of the elastic behaviour of multiphase materials.* Journal of the Mechanics and Physics of Solids, 11(2):127–140.

Hashin Z.,(1965). *Viscoelastic behavior of heterogeneous media.* Journal of Applied Mechanics, 32(3):630–636.

Hashin Z., (1970). *Complex moduli of viscoelastic composites—i. general theory and application to particulate composites.* International Journal of Solids and Structures, 6(5):539–552.

Hoang-Duc H., Bonnet G., and Meftah F., (2013). *Generalized self-consistent scheme for the effective behavior of viscoelastic heterogeneous media: a simple approximate solution.* European Journal of Mechanics-A/Solids, 39:35–49.

Hui T. and Oskay C., (2013). *A nonlocal homogenization model for wave dispersion in dissipative composite materials.* International Journal of Solids and Structures.50(1), 38-48.

Kaczmarczyk L., Pearce C.J.,and Bicanic N., (2008). *Scale transition and enforcement of rve boundary conditions in second-order computational homogenization.* International Journal for Numerical Methods in Engineering,

74(3): 506–522.

Kanoute P., Boso D., Chaboche J. and Schrefler B., (2009). *Multiscale methods for composites: a review.* Archives of Computational Methods in Engineering, 16(1):31–75.

Kleinert H., (1989). *Gauge Fields in Condensed Matter: Vol. 1: Superflow and Vortex Lines (Disorder Fields, Phase Transitions.* 2. Stresses and Defects (Differential Geometry, Crystal Melting).

Koiter W.T., (1964). *Couple-stress in the theory of elasticity.* Proc. K. Ned. Akad. Wet. 67, 17-44, North Holland Pub.

Kouznetsova V.G., Brekelmans W.A.M. and Baaijens F.P.T., (2001). *An approach to micro-macro modeling of heterogeneous materials.* Computational Mechanics. 27, 37-48.

Kouznetsova V. , Geers M. and Brekelmans W., (2002). *Multi-scale constitutive modelling of heterogeneous materials with a gradient-enhanced computational homogenization scheme.* International Journal for Numerical Methods in Engineering. 54(8), 1235-1260.

Kouznetsova V., Geers M. and Brekelmans W., (2004). *Multi-scale second-order computational homogenization of multi-phase materials: a nested finite element solution strategy.* Comput. Methods Appl. Mech. Eng. 193 (48), 5525–5550.

Martinez-Boza F., Partal P., Navarro F. and Gallegos C., (2001). *Rheology and microstructure of asphalt binders.* Rheologica acta. 40(2), 135-141.

Masson R. and Zaoui A., (1999). *Self-consistent estimates for the rate dependent elastoplastic behaviour of polycrystalline materials.* Journal of the Mechanics and Physics of Solids, 47(7):1543–1568.

Masson R., Brenner R. and Castelnau O., (2012). *Incremental homogenization approach for ageing viscoelastic polycrystals.* Comptes Rendus Mecanique, 340(4-5):378–386.

Maugin G.A., (2013). *The principle of virtual power: from eliminating metaphysical forces to providing an efficient modelling tool.* Continuum Mechanics and Thermodynamics. 25(2-4), 127-146.

Maxwel J.C., (1954) *Treatise on Electricity and Magnetism.* International Journal of Photoenergy.

Meaud J. and Hulbert G. M., (2013). *Dependence of the dynamic properties of voigt and reuss composites on the poisson's ratios and bulk loss factors of the constituent materials.* Journal of Composite Materials, 47(26):3237–3247.

Meguid S. and Kalamkarov A., (1994). *Asymptotic homogenization of elastic composite materials with a regular structure.* International Journal of Solids and Structures, 31(3), 303-316.

Miehe C., Schroder J. and Schotte J., (1999). *Computational homogenization analysis in finite plasticity simulation of texture development in polycrystalline materials.* Computer methods in applied mechanics and engineering. 171(3-4), 387-418.

Mindlin R.D., (1964). *Micro-structure in linear elasticity.* Archive for Rational Mechanics and Analysis 16, 51-78.

Mindlin R.D. and Eshel N.N., (1968). *On first strain-gradient theories in linear elasticity.* International Journal of Solids and Structures. 4, 109-124.

Mindlin R. D., (1974). *Equations of high frequency vibrations of thermopiezoelectric crystal plates.* International Journal of Solids and Structures, 10, 625-637.

Fabrizio M. and Morro A., (1992). *Mathematical problems in linear viscoelasticity.* 12, Siam.

Lakshmikantham V., Leela S. and Vasundhara Devi J., (2009). *Theory of fractional dynamic systems*, Cambridge scientific publishers.

Lahellec N. and Suquet P., (2007). *Effective behavior of linear viscoelastic composites: a time-integration approach.* International Journal of Solids and Structures, 44(2):507–529.

Leitman J., (1966). *Variational principles in the linear dynamic theory of viscoelasticity.* Quarterly of Applied Mathematics. 24(1), 36-46.

Ohno N., X. Wu, and Matsuda T., (2000). *Homogenized properties of elastic viscoplastic composites with periodic internal structures.* International Journal of Mechanical Sciences. 42, 1519-1536.

Paggi M., Corrado M., and Berardone I., (2016). *A global/local approach for the prediction of the electric response of cracked solar cells in photovoltaic modules under the action of mechanical loads.* Engineering Fracture Mechanics. 168, 40-57.

Paley R.E.A.C. and Wiener N., (1934). *Fourier transforms in the complex domain.* 19, American Mathematical Soc.

Panasenko G., (2009). *Boundary conditions for the high order homogenized equation: laminated rods, plates and composites.* Comptes Rendus Mecanique, 337(1):8–14.

Peerlings R.H.J and Fleck N.A., (2004). *Computational evaluation of strain gradient elasticity constants.* International Journal for Multiscale Computational Engineering. 2(4).

Phillips C.L., Parr J.M. and Riskin E.A, (1995), *Signals, systems, and trans-*

forms. Prentice Hall Upper Saddle River, NJ.

Rayleigh Lord J.W.S., (1871). *On the scattering of light by small particles.* Phil. Mag. 41 (447-454).

Reuss A., (1929). *Calculation of the flow limits of mixed crystals on the basis of the plasticity of mono-crystals.* Z. Angew. Math. Mech. 9, 49-58.

Rytov S., (1956). *Acoustical properties of a thinly laminated medium.* Sov. Phys. Acoust, 2(1):68–80.

Sanchez–Palencia E., (1974). *Comportements local et macroscopique d'un type de milieux physiques heterogenes.* International Journal of Engineering Science. 12(4), 331-351.

Selivanov M. F. and Chernoivan Y. A., (2007). *A combined approach of the laplace transform and pade approximation solving viscoelasticity problems.* International journal of solids and structures, 44(1):66–76.

Sharma M., (2008). *Wave propagation in thermoelastic saturated porous medium.* Journal of earth system science, 117(6): 951.

Skrzypek J.J. and Ganczarski A.W., (2015). *Introduction to mechanics of anisotropic materials.* Engineering Materials, Springer.

Smyshlyaev V.P. and Fleck N.A., (1994). *Bounds and estimates for linear composites with strain gradient effects.* Journal of the Mechanics and Physics of Solids. 42(12), 1851-1882.

Smyshlyaev V.P., Fleck N.A. and Norman A., (1995). *Bounds and estimates for the overall plastic behaviour of composites with strain gradient effects.* Proc. R. Soc. Lond. A. 451(1943), 795-810.

Smyshlyaev V.P. and Fleck N.A., (1996). *The role of strain gradients in the*

grain size effect for polycrystals. Journal of the Mechanics and Physics of Solids. 44(4), 465-496.

Smyshlyaev V.P., (2009). *Propagation and localization of elastic waves in highly anisotropic periodic composites via two-scale homogenization.* Mechanics of Materials. 434-447.

Smyshlyaev V.P. and Cherednichenko K.D., (2000). *On rigorous derivation of strain gradient effects in the overall behaviour of periodic heterogeneous media.* Journal of the Mechanics and Physics of Solids. 48(6), 1325-1357.

Srivastava A. and Nemat-Nasser S., (2014). *On the limit and applicability of dynamic homogenization.* Wave Motion, 51(7), pp.1045-1054.

Suquet P., (2012). *Four exact relations for the effective relaxation function of linear viscoelastic composites.* Comptes Rendus Mecanique, 340(4-5):387–399.

Toupin R.A., (1964). *Elastic materials with couple-stresse.* Archive for Rational Mechanics and Analysis. 11 385-414.

Tran T.H., Monchiet V. and Bonnet G., (2012). *A micromechanics-based approach for the derivation of constitutive elastic coefficients of strain-gradient media.* International Journal of Solids and Structures. 49(5), 783-792.

Truesdell C. and Toupin R., (1960). *The Classical Field Theories.* Handbuch der Physik. III.

Wolff C., Busch K. and Mortensen N. A., (2018). *Modal expansions in periodic photonic systems with material loss and dispersion.* Physical Review B, 97(10):104203.

Voigt W., (1889). *Ueber die Beziehung zwischeden beiden Elasticit tsconstanten.* Annalen der Physik. 38, (573-587).

Yang F., Chong A.C.M., Lam D.C.C. and Tong P., (2002). *Couple stress based strain gradient theory for elasticity.* International Journal of Solids and Structures. 39(10), 2731-2743.

Yi Y., Park S. and Youn S., (1998). *Asymptotic homogenization of viscoelastic composites with periodic microstructures.* International Journal of Solids and Structures. 35(17), 2039-2055.

Yuan X., Tomita Y. and Andou T., (2008). *A micromechanical approach of nonlocal modeling for media with periodic microstructures.* Mechanics Research Communications, 35(1-2):126–133.

Zah D. and Miehe C., (2013). *Computational homogenization in dissipative electro-mechanics of functional materials.* Computer Methods in Applied Mechanics and Engineering.267, (487-510).

Appendix A

Symmetrization of the localization tensors

In order to perform the symmetrization of a tensor $Z_{hkpq_1...q_n}$ with respect to the indices $q_1...q_n$, the set $P^*(q)$, which consists of all permutations with no fixed indices, is considered. For instance, if $|q| = n$, it results that $P^*(q) = \Big\{ f_1 = \Big(q_1 \to q_1, q_2 \to q_2, ..., q_n \to q_n\Big), ..., f_n = \Big(q_1 \to q_n, q_2 \to q_1, ..., q_n \to q_2\Big) \Big\}$ and the tensor $Z_{hkpq_1...q_n}$ is symmetrized with respect to $q_1, ..., q_n$ as

$$\frac{1}{n} \sum_{P^*(q)} Z_{hkpq_1...q_n} = \frac{1}{n} \Big(Z_{hkpq_1...q_n} + ... + Z_{hkpq_nq_1..q_2} \Big).$$

In particular, if $|q| = 2$ then the permutations set $P^*(q)$ with no fixed points is $P^*(q) = \Big\{ f_1 = \Big(q_1 \to q_1, q_2 \to q_2\Big), f_2 = \Big(q_1 \to q_2, q_2 \to q_1\Big) \Big\}$ and the symmetrization with respect to q_1 and q_2 of the localization tensor $\tilde{B}^{(2,0)}_{hkpq_1q_2} = \Big(\delta_{kq_2} N^{(1,0)}_{hpq_1} + N^{(2,0)}_{hpq_1q_2,k} \Big)$ results

$$B^{(2,0)}_{hkpq_1q_2} = \frac{1}{2} \Big(\delta_{kq_2} N^{(1,0)}_{hpq_1} + \delta_{kq_1} N^{(1,0)}_{hpq_2} + N^{(2,0)}_{hpq_1q_2,k} + N^{(2,0)}_{hpq_2q_1,k} \Big) =$$

$$= \frac{1}{2} \Big(\delta_{kq_2} N^{(1,0)}_{hpq_1} + \delta_{kq_1} N^{(1,0)}_{hpq_2} \Big) + N^{(2,0)}_{hpq_1q_2,k}. \tag{A.1}$$

In case of $|q| = 3$, the permutations set $P^*(q)$ having no fixed points is $P^*(q) = \Big\{f_1 = \Big(q_1 \to q_1, q_2 \to q_2, q_3 \to q_3\Big), f_2 = \Big(q_1 \to q_2, q_2 \to q_3, q_3 \to q_1\Big), f_3 = \Big(q_1 \to q_3, q_2 \to q_1, q_3 \to q_2\Big)\Big\}$ and the localization tensor $\tilde{B}^{(3,0)}_{hkpq_1q_2q_3} = \Big(\delta_{kq_3} N^{(2,0)}_{hpq_1q_2} + N^{(3,0)}_{hpq_1q_2q_3,k}\Big)$ is symmetrized with respect to q_1, q_2 and q_3 as

$$B^{(3,0)}_{hkpq_1q_2q_3} = \frac{1}{3}\Big(\delta_{kq_3} N^{(2,0)}_{hpq_1q_2} + \delta_{kq_1} N^{(2,0)}_{hpq_2q_3} + \delta_{kq_2} N^{(2,0)}_{hpq_3q_1} +$$

$$+ N^{(3,0)}_{hpq_1q_2q_3,k} + N^{(3,0)}_{hpq_2q_3q_1,k} + N^{(3,0)}_{hpq_3q_1q_2,k}\Big) =$$

$$= \frac{1}{3}\Big(\delta_{kq_3} N^{(2,0)}_{hpq_1q_2} + \delta_{kq_1} N^{(2,0)}_{hpq_2q_3} + \delta_{kq_2} N^{(2,0)}_{hpq_3q_1}\Big) + N^{(3,0)}_{hpq_1q_2q_3,k}, \tag{A.2}$$

as it appears in Eq. (2.94).

Appendix B

Generalized dispersion function

Rytov (1956) proposed the exact dispersion relation for wave propagating in a periodic layered composite transversal to the layers. In the present paper the dispersion relation has been generalized by considering complex frequency modulus and evaluated via the correspondence principle as follows

$$cos(k_2\varepsilon) = cos\Big(\omega\frac{s_1}{c_1}\Big)cos\Big(\omega\frac{s_2}{c_2}\Big) + \frac{1}{2}\Big(\frac{\rho_1 c_1}{\rho_2 c_2} + \frac{\rho_2 c_2}{\rho_1 c_1}\Big)sin\Big(\omega\frac{s_1}{c_1}\Big)cos\Big(\omega\frac{s_2}{c_2}\Big),$$

where $\omega = \frac{s}{\imath}$, $s = \Re e(s) + \Im m(s)$ and $c_i = \sqrt{\frac{\hat{C}^i_{\alpha\beta\alpha\beta}}{\rho_i}}$ is the velocity of the compressional $\alpha = \beta$ and shear $\alpha \neq \beta$ waves along the direction $\boldsymbol{e}_2$ and referred to the i-th layer $i = 1, 2$.